

Spectroscopic Investigation of Tooth Caries and Demineralization

Doctoral Thesis

submitted to

Cochin University of Science and Technology

for the award of the degree of

Doctor of Philosophy

by

Shiny Sara Thomas

Biophotonics Laboratory

Atmospheric Sciences Division

Centre for Earth Science Studies

Thiruvananthapuram

India



May 2009

DECLARATION

I hereby declare that the thesis entitled “**Spectroscopic Investigation of Tooth Caries and Demineralization**” is an authentic record of research work carried out by me under the supervision and guidance of **Dr. N. Subhash**, Scientist F, Biophotonics Laboratory & Head, Atmospheric Sciences Division, Centre for Earth Science Studies, Thiruvananthapuram, in the partial fulfilment of the requirement for the Ph.D degree under the Faculty of Science, Cochin University of Science and Technology, and no part of it has previously formed the basis of the award of any degree, diploma, associateship, fellowship or any other similar title or recognition.



Shiny Sara Thomas

Thiruvananthapuram

May 20, 2009



CENTRE FOR EARTH SCIENCE STUDIES

An Institution under the Kerala State Council for Science Technology & Environment

P.B. 7250, Akkulam, Trivandrum - 695 031, India

Tel: 91-471-2511638; Fax: 91-471-2442280 e-mail: subhashn@cessind.org

May 20, 2009

Dr. N. Subhash
Scientist F, Biophotonics Laboratory &
Head, Atmospheric Sciences Division

CERTIFICATE

This is to certify that the thesis entitled “***Spectroscopic Investigation of Tooth Caries and Demineralization***” is an authentic record of the research work carried out by **Mrs. Shiny Sara Thomas** under my direct supervision and guidance in partial fulfillment of the requirements for the Ph. D degree of Cochin University of Science and Technology, under the Faculty of Science and no part thereof has been presented for the award for any degree in any University.

A handwritten signature in black ink, appearing to read 'N. Subhash', is written over a horizontal line. There are some small marks below the line.

N. Subhash

“Do not despise the day of small beginnings”

Acknowledgements

Oh what a journey it has been, there were times when I thought I will never make it, to other times when the advice and help made me feel that this is what I was supposed to do. It's now time to recognize all those who made this piece of work, possible.

This work could not have been possible to perform without the support and encouragement of many people and I take this occasion to express my warmest gratitude. In particular:

My research guide, Dr. N. Subhash, for giving me the opportunity to learn, perform research under his excellent scientific guidance and for always being accessible and lending me an ear when things did not go right. Humble thanks for his encouragement throughout the duration of my study. His support made me achieve my goal. I am also grateful for his nice and warm friendship.

I express my gratitude to the members of the Ethics Committee of the Government Dental College, Thiruvananthapuram for their approval of my application for conducting clinical trials. I extend my thanks especially to Dr Beena VT for her friendliness and support during clinical trials. I am also grateful for the nice collaboration with Dr. Jolly Mary Varughese, Head of the Department of Conservative Dentistry and Endodontics, who supported me in carrying out the clinical trials. I also extend my gratitude to Dr. Anitha Balan, Head of the Department of Oral Medicine and Radiology, for her support.

It has been a pleasure and really exciting to be working in a hospital atmosphere. I am wordless to express my gratefulness to Dr. Soumyakant Mohanty of the Department of Conservative Dentistry for his support and understanding during clinical trials. I am also thankful to Dr. Anulekh Babu of the Department of Conservative Dentistry, Dr. Akhilanand Chaurasia, Dr. Satheesh, Dr. Ranimol P and Dr. Nithya of the Department of Oral Medicine and Radiology for their help and support. They have all shown amazing enthusiasm for our joint projects, for which I am very grateful. All the patients who have given their time to participate in measurements are also deeply appreciated.

This study was fully supported by my colleague Miss. Jayanthi JL especially during clinical trials. I appreciate you and am grateful to your friendship and support throughout the tough times. I express my sincere gratitude to Mr. Rupananda J Mallia for helping me during in vitro studies and also for his support and assistance in my studies. I also extend my gratitude to Miss Aparna GN and Mr Prasanth CS for their support. I am grateful to all the postgraduate students who assisted me in this study especially Miss Renji, Miss. Sapna, Miss. Kavitha and Miss. Mrinalini.

I would like to appreciate the support I received from Dr Mini Jose and Dr. Joji Thomas during in vitro studies. I would also extend my gratitude to the Ph.D programme review committee (CUSAT) and Dr. C. S. Paulose, member of the doctoral committee, for his valuable suggestions. Thanks to all the staff in the Atmospheric Science Division, CESS, especially to Mr. T. K. Krishnachandran and Mr. M. Ismail for their assistance and help. I am also extending my sincere thanks to the administrative staff of CESS for all their support. Finally, I would like to thank Dr. M. Baba, Director and Mr. P. Sudeep, Registrar, CESS for their support and encouragement during the course of the study. I would like to extend my sincere gratitude to Kerala State Council for Science, Technology and Environment (KSCSTE) for their financial support.

I would like to take this time to extend my sincere thanks to all my friends especially Vishnu who was always there to lend a hand or support. I am also grateful to Anjali, Chitra for being always there for me. I express my thanks to Hari, Sinoosh and Prasanth for their support. The rest of my friends are fortunately too many to mention by name and too good to blame me for not doing so. Thank you!

I am especially grateful to my parents and all my family members. Without your massive support behind me nothing would have been possible.

Last but never the least, I would like to thank my husband Varghese for making my life so sweet and the motivation and support he has given me to complete this work.

SHINY SARA THOMAS

CESS, THIRUVANANTHAPURAM

“To my dear ones”

Table of Contents

| | |
|---|--------|
| Abstract | xxi |
| List of Publications | xxiii |
| Preface | xxvii |
| Abbreviations and Acronyms | xxxiii |
| | |
| Chapter 1 | |
| | |
| Background, Intention and Description of the Problem | |
| 1.1 Background and Intention | 3 |
| 1.2 Objectives of the Study | 5 |
| 1.3 Some Facts About Dental Caries | 6 |
| 1.3.1 Carious Process | 6 |
| 1.3.2 Etiology of Caries | 7 |
| 1.3.3 Clinical Presentation of Caries | 7 |
| 1.3.3.1 Pit and Fissure Caries/Occlusal Caries | 7 |
| 1.3.3.2 Smooth Surface Caries | 7 |
| 1.3.3.3 Root Surface Caries | 8 |
| 1.3.4 Histopathology of Caries | 8 |
| 1.3.4.1 Caries of Enamel | 8 |
| 1.3.4.2 Caries of Dentin | 9 |
| 1.3.5 Diagnosis of Caries | 10 |
| 1.3.5.1 Visual Examination | 11 |

| | |
|---|----|
| 1.3.5.2 Visual-Tactile Techniques | 11 |
| 1.3.5.3 Radiographic Examination | 12 |
| 1.3.5.4 Alternative Caries Detection Methods | 13 |
| 1.3.5.4.1 Diagnostic Method Based on X-rays: Digital and Subtraction Radiography | 14 |
| 1.3.5.4.2 Diagnostic Systems Based on Electrical Current: ECM/EIM | 14 |
| 1.3.5.4.3 Transillumination: FOTI and DIFOTI | 15 |
| 1.3.5.4.4 Quantitative Laser/Light-Induced Fluorescence (QLF) | 16 |
| 1.3.5.4.5 DIAGNOdent- Infrared Fluorescence | 17 |
| 1.3.5.4.6 Diagnostic Based on Ultrasound Measurements | 18 |
| 1.3.5.4.7 Optical Coherence Tomography (OCT) | 18 |
| 1.3.6 Prevention of Caries | 19 |
| 1.3.6.1 Oral Hygiene | 19 |
| 1.3.6.2 Dietary Modification | 19 |
| 1.3.6.3 Other Preventive Measures | 20 |
| 1.4 Conclusions | 20 |

Chapter 2

Tooth Anatomy and its Interaction with Light

| | |
|------------------|----|
| 2.1 Introduction | 25 |
|------------------|----|

| | | |
|---------|--|----|
| 2.2 | Tooth: An Overview | 26 |
| 2.3 | Tooth Development | 27 |
| 2.3.1 | Developmental Stages | 27 |
| 2.4 | Tooth Structure | 30 |
| 2.4.1 | Enamel | 30 |
| 2.4.2 | Dentin | 32 |
| 2.4.3 | Pulp | 34 |
| 2.4.4 | Supporting Structures | 35 |
| 2.5 | Light | 36 |
| 2.5.1 | Basic Aspects of Light-Tissue Interaction | 37 |
| 2.5.2 | Optical Properties of Hard Tissues | 38 |
| 2.5.2.1 | Spectral Properties of Enamel and Dentin | 38 |
| 2.5.2.2 | Waveguide Effects | 42 |
| 2.6 | Optical Spectroscopy | 44 |
| 2.6.1 | Fluorescence Spectroscopy | 44 |
| 2.6.1.1 | Basic Principles | 44 |
| 2.6.1.2 | Autofluorescence and Endogenous Fluorophores | 45 |
| 2.6.1.3 | Detection Principle | 48 |
| 2.6.2 | Diffuse Reflectance Spectroscopy | 49 |
| 2.6.3 | LIF and DR Spectroscopy in Caries Research: | |
| | Current Status | 50 |
| 2.7 | Conclusions | 54 |

Chapter 3

Experimental Methods

| | | |
|-----|--|----|
| 3.1 | Introduction | 57 |
| 3.2 | Point Monitoring System | 58 |
| 3.3 | Development of LIFRS System for Caries Detection | 59 |
| | 3.3.1 Compact LIFRS System for Clinical Trials | 61 |
| 3.4 | Data Acquisition and Analysis | 62 |
| | 3.4.1 Data Acquisition using OOI Base32 Software | 62 |
| | 3.4.2 Curve-Fitting of LIF Spectra | 63 |
| | 3.4.3 Statistical Analysis | 63 |
| | 3.4.3.1 Sensitivity and Specificity | 63 |
| | 3.4.3.2 Positive and Negative Predictive Values | 64 |
| | 3.4.3.3 Receiver Operating Characteristic Analysis | 66 |
| | 3.4.3.3.1 Area Under the Curve | 67 |
| 3.5 | <i>In vitro</i> Studies | 67 |
| 3.6 | <i>In vivo</i> Studies | 68 |
| | 3.6.1 Ethical Clearance for the Study | 68 |
| | 3.6.2 Inclusion and Exclusion Criteria for the Study | 68 |
| | 3.6.3 Conduct of Clinical Trials | 69 |
| | 3.6.4 Validation Studies | 70 |
| 3.7 | Conclusions | 70 |

Chapter 4

Tooth Caries Detection by Curve-Fitting of Laser-Induced Fluorescence Emission: A Comparative Evaluation with DR Spectroscopy

| | | |
|-------|--|----|
| 4.1 | Introduction | 73 |
| 4.2 | Study Material and Protocol | 73 |
| 4.3 | Results | 74 |
| 4.3.1 | Fluorescence Measurements | 74 |
| 4.3.2 | Curve-Fitting Analysis | 75 |
| 4.3.3 | Gaussian Curve-Fitted and Raw LIF Ratios | 77 |
| 4.3.4 | Diffuse Reflectance Measurements | 78 |
| 4.3.5 | Lesion Profiling | 79 |
| 4.4 | Discussion | 80 |
| 4.5 | Conclusions | 83 |

Chapter 5

Investigation of *in vitro* Dental Erosion by Optical Techniques

| | | |
|---------|---------------------------------|----|
| 5.1 | Introduction | 87 |
| 5.2 | Study Material and Protocol | 87 |
| 5.3 | Results | 88 |
| 5.3.1 | LIF Spectral Features | 88 |
| 5.3.1.1 | Tooth Enamel and Dentin Spectra | 88 |
| 5.3.1.2 | Tooth Demineralization | 89 |

| | | |
|---------|-------------------------------------|----|
| 5.3.2 | Diffuse Reflectance Characteristics | 92 |
| 5.3.2.1 | Reflectance Spectral Features | 92 |
| 5.3.2.2 | Tooth Demineralization | 93 |
| 5.4 | Discussion | 94 |
| 5.5 | Conclusions | 99 |

Chapter 6

Spectroscopic Investigation of De- and Re-mineralization of Tooth Enamel *in vitro*

| | | |
|-------|---|-----|
| 6.1 | Introduction | 102 |
| 6.2 | Study Material and Protocol | 102 |
| 6.2.1 | Visual Assessment of Lesions | 104 |
| 6.3 | Results | 105 |
| 6.3.1 | LIF Spectral Features | 105 |
| 6.3.2 | Diffuse Reflectance Spectral Features | 106 |
| 6.3.3 | Spectral Intensity and Curve Area Plots | 106 |
| 6.4 | Discussion | 108 |
| 6.5 | Conclusions | 112 |

Chapter 7

Characterization of Dental Caries by LIF Spectroscopy with 404 nm Excitation

| | | |
|-----|-----------------------------|-----|
| 7.1 | Introduction | 115 |
| 7.2 | Study Material and Protocol | 115 |

| | | |
|-------|--|-----|
| 7.2.1 | Experimental Methods | 115 |
| 7.3 | Results | 116 |
| 7.3.1 | LIF Spectral Features | 116 |
| 7.3.2 | LIF Intensity Ratios | 117 |
| 7.3.3 | Diagnostic Performance of LIF Spectroscopy | 118 |
| 7.4 | Discussion | 119 |
| 7.5 | Conclusions | 122 |

Chapter 8

Clinical Trial for Early Detection of Tooth Caries using a Fluorescence Ratio Reference Standard

| | | |
|-------|--|-----|
| 8.1 | Introduction | 125 |
| 8.2 | Study Material, Protocol and Ethical Issues | 125 |
| 8.3 | Results | 127 |
| 8.3.1 | LIF Spectral Features | 127 |
| 8.3.2 | LIF Intensity Ratios | 128 |
| 8.3.3 | Discrimination using FRS Ratio Scatter Plots | 128 |
| 8.4 | Discussion | 130 |
| 8.4.1 | LIF Spectral Features | 130 |
| 8.4.2 | LIF Intensity Ratios | 131 |
| 8.4.3 | Validation of FRS Ratio | 132 |
| 8.5 | Conclusions | 134 |

Chapter 9

Application of Curve-Fitting to Diagnose Dental Caries *in vivo*

| | | |
|-----|--|-----|
| 9.1 | Introduction | 137 |
| 9.2 | Study Material, Protocol and Data Processing | 137 |
| 9.3 | Results | 139 |
| | 9.3.1 LIF Spectral Features | 139 |
| | 9.3.2 Curve-Fitting Analysis | 139 |
| | 9.3.3 Curve-Fitted and Raw LIF Ratios | 140 |
| | 9.3.4 Diagnostic Performance of LIF Spectroscopy | 142 |
| 9.4 | Discussion | 142 |
| 9.5 | Conclusions | 146 |

Chapter 10

Diffuse Reflectance Spectroscopy for *in vivo* Caries Detection

| | | |
|------|--|-----|
| 10.1 | Introduction | 147 |
| 10.2 | Study Material and Protocol | 149 |
| 10.3 | Results | 150 |
| | 10.3.1 DR Spectral Features | 150 |
| | 10.3.2 Discrimination with DRRS Ratio | 151 |
| | 10.3.3 Caries Discrimination using ROC Curve | 151 |
| 10.4 | Discussion | 152 |
| 10.5 | Conclusions | 154 |

Chapter 11

| | |
|----------------------------------|-----|
| Discussion and Conclusion | 157 |
|----------------------------------|-----|

| | |
|-------------------|-----|
| References | 167 |
|-------------------|-----|

Abstract

Dental caries persists to be the most predominant oral disease in spite of remarkable progress made during the past half-century to reduce its prevalence. Early diagnosis of carious lesions is an important factor in the prevention and management of dental caries. Conventional procedures for caries detection involve visual-tactile and radiographic examination, which is considered as “gold standard”. These techniques are subjective and are unable to detect the lesions until they are well advanced and involve about one-third of the thickness of enamel. Therefore, all these factors necessitate the need for the development of new techniques for early diagnosis of carious lesions. Researchers have been trying to develop various instruments based on optical spectroscopic techniques for detection of dental caries during the last two decades. These optical spectroscopic techniques facilitate non-invasive and real-time tissue characterization with reduced radiation exposure to patient, thereby improving the management of dental caries. Nonetheless, a cost-effective optical system with adequate sensitivity and specificity for clinical use is still not realized and development of such a system is a challenging task.

Two key techniques based on the optical properties of dental hard tissues are discussed in this current thesis, namely laser-induced fluorescence (LIF) and diffuse reflectance (DR) spectroscopy for detection of tooth caries and demineralization. The work described in this thesis is mainly of applied nature, focusing on the analysis of data from in vitro tooth samples and extending these results to diagnose dental caries in a clinical environment. The work mainly aims to improve and contribute to the contemporary research on fluorescence and diffuse reflectance for discriminating different stages of carious lesions. Towards this, a portable and compact laser-induced fluorescence and reflectance spectroscopic system (LIFRS) was developed for point monitoring of fluorescence and diffuse reflectance spectra from tooth samples. The LIFRS system uses either a 337 nm nitrogen laser or a 404 nm diode laser for the excitation of tooth autofluorescence and a white light source (tungsten halogen lamp) for measuring diffuse reflectance.

Extensive in vitro studies were carried out on extracted tooth samples to test the applicability of LIFRS system for detecting dental caries, before being tested in a clinical environment. Both LIF and DR studies were performed for diagnosis of dental caries, but special emphasis was given for early detection and also to discriminate between different stages of carious lesions. Further the potential of

LIFRS system in detecting demineralization and remineralization were also assessed.

In the clinical trial on 105 patients, fluorescence reference standard (FRS) criteria was developed based on LIF spectral ratios (F500/F635 and F500/F680) to discriminate different stages of caries and for early detection of dental caries. The FRS ratio scatter plots developed showed better sensitivity and specificity as compared to clinical and radiographic examination, and the results were validated with the blind-tests. Moreover, the LIF spectra were analyzed by curve-fitting using Gaussian spectral functions and the derived curve-fitted parameters such as peak position, Gaussian curve area, amplitude and width were found to be useful for distinguishing different stages of caries. In DR studies, a novel method was established based on DR ratios (R500/R700, R600/R700 and R650/R700) to detect dental caries with improved accuracy. Further the diagnostic accuracy of LIFRS system was evaluated in terms of sensitivity, specificity and area under the ROC curve. On the basis of these results, the LIFRS system was found useful as a valuable adjunct to the clinicians for detecting carious lesions.

List of Publications

The study mentioned in this thesis is mainly based on the following scientific papers.

A. International Journals:

Subhash N, **Shiny Sara Thomas**, Rupananda Mallia J, Mini Jose, (2005). Tooth caries detection by curve fitting of laser-induced fluorescence emission: A comparative evaluation with reflectance spectroscopy. *Lasers in Surgery and Medicine* 37: 320–328.

Shiny Sara Thomas, Rupananda Mallia J, Mini Jose, Subhash N (2008). Investigation of *in vitro* dental erosion by optical techniques. *Lasers in medical Sciences* 23: 319-329.

Shiny Sara Thomas, Subhash N., Rupananda Mallia J, Mini Jose (2008). Spectroscopic investigation of de- and re-mineralization of tooth enamel *in vitro*. *Applied Spectroscopy* (under preparation).

Shiny Sara Thomas, Jayanthi JL, Subhash N, Joji Thomas, Rupananda Mallia J, Aparna GN (2009). Characterization of dental caries by LIF spectroscopy with 404 nm excitation. *Lasers in medical Science* (under review).

Shiny Sara Thomas, Jayanthi JL, Soumyakant M, Subhash N, Jolly Mary Varughese, Anitha Balan (2009). Clinical Trial for early detection of tooth caries using a fluorescence ratio reference standard. *European Journal of Oral Sciences* (under review).

Shiny Sara Thomas, Jayanthi JL, Soumyakant M, Subhash N, Jolly Mary Varughese, Anitha Balan (2009). Application of curve-fitting to diagnose dental caries *in vivo*. *Caries Research* (under preparation).

Shiny Sara Thomas, Jayanthi JL, Soumyakant M, Subhash N, Jolly Mary Varughese, Anitha Balan (2009). Diffuse reflectance spectroscopy for *in vivo* caries detection. *Journal of Biophotonics* (under preparation).

B. Patent Pending:

Subhash N, **Shiny Sara Thomas**, Rupananda Mallia J, Mini Jose. Tooth caries detection by curve fitting of UV laser induced fluorescence emission. New Provisional

Indian Patent Application No.: 1919/VHE/2005, Filed on: December 12, 2005.

Subhash N, Rupananda Mallia J, **Shiny Sara Thomas**, Jayaprakash Madhavan, Anitha Mathews, Paul Sebastian. A low cost device for detecting neoplastic changes in tissue. Indian Patent Application No.: 265/CHE/2006, Filed on: February 20, 2006.

C. Conference Proceedings:

Shiny Sara Thomas, Jayanthi J L, Joji Thomas, Rupananda J. Mallia, Aparna G N, Subhash N (2008). Characterization of dental caries by fluorescence spectroscopy, Swadeshi Science Congress 2008, Trivandrum (Presented).

D. Publications from other fields:

1. International Journals:

Subhash N, Rupananda Mallia J, **Shiny Sara Thomas**, Anitha Mathews, Paul Sebastian, Jayaprakash Madhavan (2006). Oral cancer detection using diffuse reflectance spectral ratio R540/R575 of oxygenated hemoglobin bands. *Journal of Biomedical Optics* 11(1): 014018 (1–6).

Rupananda Mallia J, Subhash N, **Shiny Sara Thomas**, Rejnish Kumar, Anitha Mathews Jayaprakash Madhavan, Paul Sebastian (2007). Oral Pre-malignancy detection using autofluorescence spectral ratios. *Oral Oncology (S)* 2(1): 259–260.

Rupananda Mallia J, **Shiny Sara Thomas**, Anitha Mathews, Rejnish Kumar, Paul Sebastian, Jayaprakash Madhavan, Subhash, N (2008). Laser-induced autofluorescence spectral ratio reference standard for early discrimination of oral cancer. *Cancer* 112 (7): 1503-1512.

Rupananda Mallia J, **Shiny Sara Thomas**, Anitha Mathews, Rejnish Kumar, Paul Sebastian, Jayaprakash Madhavan, Subhash N (2008). Oxygenated hemoglobin diffuse reflectance ratio for *in vivo* detection of oral pre-cancer. *Journal of Biomedical Optics* 13 (4): 041306 (1-10).

Rupananda Mallia J, **Shiny Sara Thomas**, Paul Sebastian, Rejnish Kumar, Anitha Mathews, Jayaprakash Madhavan, Subhash N (2008). Grading of oral mucosa by curve fitting of corrected autofluorescence spectra. *Head and Neck* (under review).

Jayanthi JL, Rupananda Mallia J, **Shiny Sara Thomas**, Baiju KV, Anitha Mathews, Rejnish Kumar, Paul Sebastian, Jayaprakash Madhavan, Aparna GN, Subhash N

(2009). Discrimination analysis of autofluorescence spectra for classification of oral lesions *in vivo*. *Lasers in Surgery and Medicine* (accepted).

2. Conference Proceedings:

Subhash N, Rupananda Mallia J, **Shiny Sara Thomas**, Anitha Mathews, Paul Sebastian,, Jayaprakash Madhavan, (2004). Discrimination of malignant oral cavity lesions using R540/R575 reflectance spectral ratio. *Proceedings of the International PHOTONICS 2004 Conference*, Kochi, December 2004.

Rupananda Mallia J, **Shiny Sara Thomas**, Rejnish Kumar, Anitha Mathews, Paul Sebastian Jayaprakash Madhavan, Subhash N (2006). Diagnosis of oral cavity neoplasms with fluorescence spectroscopy. *Kerala Science Congress 2006*, CESS, Trivandrum, 458-461.

Rupananda Mallia J, **Shiny Sara Thomas**, Rejnish Kumar, Anitha Mathews, Paul Sebastian, Jayaprakash Madhavan, Gigi Thomas, Subhash N (2007). Photodiagnosis of oral cancer detection *in vivo* using diffuse reflectance spectral ratios. *National Laser Symposium*, Ahemadabad, Gujarat, Dec. 17-20, (Presented).

Jayanthi J L, Rupananda J. Mallia, **Shiny Sara Thomas**, Aparna G N, Baiju K V, Rejnish Kumar, Anitha Mathews, Subhash N (2008). Applicability of discriminant analysis in the grading of oral mucosa, *Swadeshi Science Congress 2008*, Trivandrum (Presented).

Preface

This study is a multidisciplinary research intended to contribute to improved management of dental caries. One of the significant aspects in dental caries diagnosis is that if early changes are not detected, lesion would continue to demineralise leading to cavity formation. Once cavitation occurs, the lost tooth structure cannot be regenerated. Further, tooth demineralization is difficult to diagnose in the early stages of development with the existing detection methods. Therefore, the main focus of the study is to explore the potential of laser-induced fluorescence (LIF) and diffuse reflectance (DR) spectroscopy techniques to identify incipient changes in tooth enamel, which is crucial for decisions on treatment modalities in operative dentistry.

Chapter 1 gives a brief insight into dental caries and demineralization that leads to mineral loss in tooth, current methods of detection and their limitations in a clinical setting, and also on disease management. It is intended as a brief survey of the tools that are available to the dentists for diagnosis and should not be considered as a comprehensive review. Finally, the significance of early detection of dental caries and the need to develop new techniques for detecting early changes in tooth enamel are presented.

Basic knowledge on the development and structure of the teeth is essential to understand the various diseases affecting teeth as well as for the exploitation of optical techniques for diagnostic applications. In addition, a practical understanding of the biologic processes of tissue and the physical properties of light would help to comprehend and control the outcome of its interaction for the detection of dental caries. **Chapter 2** details the basic anatomy of the tooth and its interaction with light, with special emphasis on the basic concepts of tissue fluorescence and diffuse reflectance, which form the basis of the work presented in this thesis. In addition, different types of endogenous fluorophores and their absorption and emission characteristics are also described in this chapter.

In the past decade, key technologies such as (a) compact lasers, (b) CCD detectors and (c) easy-to-use computing platforms combined with fiber-optic coupled instrumentation has lead to the development of many photonics based diagnostic and therapeutic methods in dentistry. The use of optical spectroscopy in dentistry is crucial for early detection of dental caries, to carry out more effective but, minimally-invasive targeted-therapies and to restore diseased tissues functionally

and aesthetically. Among the various non-invasive optical techniques, those relying on tooth autofluorescence and diffuse reflectance are most promising in the diagnosis of dental caries. **Chapter 3** presents details of a compact, non-invasive, laser-induced fluorescence and reflectance spectroscopic system (LIFRS) developed for detection and point monitoring of caries progression. Details on data acquisition using LIFRS and the various statistical methods adopted for data analysis are also given in this chapter. Further, this chapter describes the ethical issues, the protocol adopted for clinical studies, and patient inclusion/exclusion criteria.

Chapter 4 examines the potential of LIFRS system for distinguishing different stages of caries. Towards this, nitrogen laser (337.1 nm) excited fluorescence and white light illuminated DR spectra of extracted tooth samples belonging to different categories were measured. The caries tooth showed lower fluorescence and reflectance intensities in the 350 to 700 nm region as compared to sound tooth. The LIF spectra were analyzed by curve fitting to determine the peak position of the various bands present and their relative contribution to the overall spectra. The deconvoluted peaks in the LIF spectra were found centered at 403.8, 434.2, 486.9 and 522.5 nm in sound tooth, whereas a new peak was observed at 636.8 nm in pulp level caries. Curve-fitted parameters such as peak center, Gaussian curve area and full width at half intensity maximum (FWHM) and their ratios were found to vary with the stage of tooth caries. The intensity and Gaussian curve area ratios of the peaks at 405, 435 and 490 nm were found to be sensitive to discriminate between sound, dentin and pulp level caries. Among the diffuse reflectance spectral ratios studied, the R500/R700 was found to be most sensitive to distinguish between pulp and dentin level caries. The LIF measurement with spectral analysis done by curve fitting outscores DR spectroscopy and shows potential to screen different levels of tooth decay in a clinical setting.

Chapter 5 explores the application of tissue fluorescence and DR to detect tooth demineralization and evaluates their applicability in a clinical setting. The LIFRS system was used to measure LIF and DR spectra from *in vitro* premolar tooth during various stages of artificial erosion. It was observed that both LIF and DR spectral intensity increases gradually during tooth erosion. With curve fitting carried out using Gaussian spectral functions, broad-bands seen at 440 and 490 nm in sectioned sound enamel were resolved into four peaks centered at 409.1, 438.1, 492.4 and 523.1 nm, whereas in sound dentin slices the peaks were observed at 412.0, 440.1, 487.8 and 523.4 nm. The fluorescence spectral ratio, F410/F525, derived from curve-fitted Gaussian peak amplitudes and curve areas were found to

be more sensitive to erosion as compared to the DR ratio R500/R700 and the raw LIF spectral ratio F440/F490.

Further, in **Chapter 6**, the results of a study conducted to compare the capability of LIF and diffuse reflectance (DR) spectral data to detect de- and re-mineralization changes on *in vitro* tooth samples are presented. Towards this, nitrogen laser-induced fluorescence and tungsten halogen lamp-induced DR spectra were recorded on a miniature fiber-optic spectrometer from a set of premolar tooth samples subjected to cyclic de- and re-mineralization (CDR) for 10 days, followed by continuous remineralization (CR) for 14 days to enhance the effect of remineralization. The LIF and DR spectral intensities were found to decrease with CDR, but get reversed during CR. Significant differences ($p < 0.05$) were noticed in spectral features between sound, demineralized and remineralized tooth with one-way ANOVA. The constituent peaks in sound tooth LIF spectra deconvoluted by curve fitting were found centered at 411.32, 440.08, 484.37 and 521.98 nm. Spectral features like peak center, full width at half intensity maximum (FWHM), Gaussian amplitude and curve area derived by curve fitting were found to vary with de- and re-mineralization. However, the characteristics of LIF peaks at 410 and 525 nm were found to be more suited for detecting tooth mineralization changes as compared to the raw LIF and DR spectral signatures.

Chapter 7 explains the potential of fluorescence spectroscopy (LIF) to characterize different stages of dental caries with 404 nm diode laser excitation. *In vitro* spectra were recorded on a miniature fibre-optic spectrometer from 16 sound, 10 non-cavitated and 10 cavitated molar teeth. The area under curve of the receiver operating characteristics (ROC-AUCs) and one way variance analysis (ANOVA) were calculated. Autofluorescence spectral intensity of carious lesions were found lower than that of sound tooth and decreased with the extent of caries. The LIF spectra of caries tooth showed two peaks at 635 and 680 nm in addition to a broad band seen at 500 nm in sound tooth. It was observed that fluorescence intensity ratios, F500/F635 and F500/F680, of caries tooth are always lower than that of sound tooth. The ROC-AUC for discriminating caries from sound tooth was 0.94, whereas for distinguishing non-cavitated lesions the ROC-AUC was 0.87. Statistically significant differences ($p < 0.001$) were seen between sound, non-cavitated and cavitated caries lesions. These results show that LIF spectroscopy could be utilized for characterizing different stages of caries in a clinical setting.

Chapter 8 examines the clinical applicability of a diagnostic algorithm or the fluorescence reference standard (FRS) developed based on LIF spectral ratios

to discriminate different stages of caries. Towards this, LIF emission spectra were recorded in the 400-800 nm spectral range on a miniature fiber optic spectrometer from 105 patients, with excitation at 404 nm from a diode laser. The spectral results were correlated with visual-tactile and radiographic examinations. The LIF emission of sound tooth shows a broad emission at 500 nm that is characteristic of natural enamel whereas in carious tooth, additional peaks were seen at 635 and 680 nm, due to emission from porphyrins linked to oral bacteria. In order to discriminate different stages of tooth caries, FRS ratio scatter plots of the fluorescence intensity ratios $F500/F635$ and $F500/F680$ were developed to differentiate sound from incipient, sound from advanced and incipient from advanced caries using the spectral data obtained from 65 carious sites and 25 sites of sound tooth in 65 patients. The sensitivity, specificity, PPV and NPV of the developed algorithm to detect tooth caries were calculated and presented. Sequentially, a blind-test was carried out in 15 sound and 40 carious sites of 40 patients to check the accuracy of the developed standard for early detection of tooth caries.

Chapter 9 presents the application of LIF spectral ratios and curve-fitting for distinguishing different stages of tooth caries in a clinical setting with 404 nm excitation. The LIF spectra show a broad emission around 500nm for sound tooth, whereas additional peaks were seen at 635 and 680 nm in carious tooth. Curve-fitted parameters such as peak center, peak amplitude, Gaussian curve area and FWHM were found vary with the different stages of tooth caries. Fluorescence intensity ratios, $F490/F635$ and $F490/F675$, derived from the raw spectral intensities, curve-fitted peak amplitudes and Gaussian curve areas were higher for sound tooth as compared to caries lesions and tend to decrease with the progression of caries. The Gaussian curve ratios, $F490/F635$ and $F490/F675$ were found to be more sensitive for discriminating different stages of caries as compared to raw LIF ratios. Finally, the diagnostic performance of LIF spectroscopy in a clinical settling was evaluated in terms of receiver operating characteristic (ROC) curves.

The potential of DR spectroscopy for detecting tooth caries *in vivo* are presented in **Chapter 10**. A clinical study conducted on patients has shown that *in vivo* DR spectral intensity decreases in caries tooth. Diffuse reflectance reference standard (DRRS) scatter plots of the DR ratios $R500/R700$, $R600/R700$ and $R650/R700$ were developed to differentiate sound from caries tooth using spectral data from 24 patients. The sensitivity, specificity, PPV and NPV of these DRRS ratios to detect tooth caries are calculated and presented. The diagnostic performance of DR spectroscopy was also evaluated in terms of receiver operating characteristic (ROC)

curve. Among the various ratios studied, R600/R700 ratio gave comparatively higher sensitivity and specificity. In this study, DR ratios were able to discriminate sound from non-cavitated caries lesions with an average sensitivity of 88% and specificity of 100%.

Chapter 11 is the wrapping up section, which discusses the merits of the LIFRS system and this doctoral thesis, its future perspectives in the detection of dental caries and the limitations of the optical spectroscopy techniques utilized in this study. This section also reviews the diagnostic accuracies of LIF and DR modalities by comparing the present results with those obtained by other research groups using optical techniques for early detection of caries lesions.

As stated above, the common thread in the studies presented is the use of optical spectroscopy to detect tissue transformations. A fiber-optic LIFRS system was developed in our laboratory to perform autofluorescence and diffuse reflectance measurements. It has therefore been the fundamental device in the course of this work. Its flexibility allowed us to sequentially probe the fluorescence and diffuse reflectance spectra from same sample in real-time. The instrument sensitivity allowed us to detect very faint autofluorescence signals of biological tissues and the fact that the unit was fabricated in-house allowed us to suitably adapt and modify it whenever necessary.

Abbreviations and Acronyms

| | |
|---------------|--|
| <i>ANOVA</i> | <i>Analysis of variance</i> |
| <i>AUC</i> | <i>Area under the curve</i> |
| <i>CCD</i> | <i>Charge Coupled Device</i> |
| <i>CDR</i> | <i>Cyclic de- and re-mineralization</i> |
| <i>CI</i> | <i>Confidence interval</i> |
| <i>CR</i> | <i>Continuous remineralization</i> |
| <i>DCJ</i> | <i>Dentino-cemental junction</i> |
| <i>DEJ</i> | <i>Dentino-enamel junction</i> |
| <i>DIFOTI</i> | <i>Digital imaging fiber-optic transillumination</i> |
| <i>DR</i> | <i>Diffuse reflectance</i> |
| <i>DRRS</i> | <i>Diffuse reflectance reference standard</i> |
| <i>DRS</i> | <i>Diffuse reflectance spectroscopy</i> |
| <i>ECM</i> | <i>Electrical conductance measurement</i> |
| <i>EIM</i> | <i>Electrical impedance measurement</i> |
| <i>FAD</i> | <i>Flavin Adenine Dinucleotide</i> |
| <i>FN</i> | <i>False negative</i> |
| <i>FOTI</i> | <i>Fiber-optic transillumination</i> |
| <i>FP</i> | <i>False positive</i> |
| <i>FPF</i> | <i>False-positive fraction</i> |
| <i>FRS</i> | <i>Fluorescence reference standard</i> |
| <i>FWHM</i> | <i>Full width at half maximum</i> |
| <i>HA</i> | <i>Hydroxyapatite</i> |

| | |
|------------------------|--|
| <i>Hb</i> | <i>Deoxygenated Hemoglobin</i> |
| <i>HbO₂</i> | <i>Oxygenated Hemoglobin</i> |
| <i>IR</i> | <i>Infrared</i> |
| <i>LF</i> | <i>laser fluorescence</i> |
| <i>LIF</i> | <i>Laser-induced fluorescence</i> |
| <i>LIFRS</i> | <i>Laser-induced fluorescence reflectance spectroscopy</i> |
| <i>LIFS</i> | <i>Laser-induced fluorescence spectroscopy</i> |
| <i>LOO</i> | <i>Leave-one-out</i> |
| <i>NADH</i> | <i>Reduced Nicotinamide Adenine Dinucleotide</i> |
| <i>NADPH</i> | <i>Nicotinamide Adenine Dinucleotide phosphate</i> |
| <i>NPV</i> | <i>Negative predictive value</i> |
| <i>OCT</i> | <i>Optical coherence tomography</i> |
| <i>PpIX</i> | <i>Protoporphyrin IX</i> |
| <i>PPV</i> | <i>Positive predictive value</i> |
| <i>PS-OCT</i> | <i>Polarization sensitive-optical coherence tomography</i> |
| <i>QLF</i> | <i>Quantitative laser/light-induced fluorescence</i> |
| <i>ROC</i> | <i>Receiver operating characteristic</i> |
| <i>TN</i> | <i>True negative</i> |
| <i>TP</i> | <i>True positive</i> |
| <i>TPF</i> | <i>True-positive fraction</i> |
| <i>UV</i> | <i>Ultraviolet</i> |
| <i>VIS</i> | <i>Visible</i> |

Chapter 1

Background, Intention and Description of the Problem

1.1 BACKGROUND AND INTENTION

Dental caries is an important Dental-Public-Health dilemma and it is the most widespread oral disease in the world. The prevalence of dental caries has been of great concern for long and is a principal subject of many epidemiological researches carried out in India and abroad. This disease not only causes damage to the tooth, but is also responsible for several morbid conditions of the oral cavity and other systems of the body (WHO 1981). The prevalence pattern of dental caries not only varies with age, sex, socio economic status, race, geographical location, food habits and oral hygiene practices but also within the oral cavity. All the teeth and all the surfaces are not equally susceptible to caries. Factors contributing to the progression of the disease include diet (mainly fermentable carbohydrates), microbes, and the host (amount and constituents of the saliva, habits). The progression of dental caries lesions needs time. Fluoride protects the teeth from dental caries by influencing the tooth structure.

Over the last decades, a remarkable decline in caries prevalence has been noticed in the world population, primarily due to the increase in scientific knowledge on the etiology, initiation, progression and prevention of the disease coupled with the wide scope of preventive measures and fluoride therapy (Elderton, 1983; Kidd et al, 1987; Newbrun, 1993; Ekstrand et al, 2001). However, it is still a major oral health concern in developing countries, affecting 60-90% of the school children and the vast majority of adults (World Oral Health Report, 2003). On the other hand, dental caries is highly prevalent in India, which is influenced by the lack of dental awareness among the public at large and is reported to be about 50-60% in India (Naseem, 2005). The dramatic improvements in the prevalence and incidence of dental caries and the changes in the epidemiology and pattern of disease over the past thirty years is well documented (Marthaler 1990, 2004). Most notably, the rate of progression through the teeth has slowed. This reduction in prevalence has not occurred uniformly for all dental surfaces. The utmost reduction was seen at smooth surfaces lesions, followed by proximal surfaces, so that occlusal surfaces are now the most probable sites for development of caries. Nevertheless, the disease has not been eradicated and although less widely distributed in the dentition and less acute in terms of lesion progression, caries persists in the general population.

In addition to the drastic changes in the disease manifestation itself, in recent years there has also been major progress in our understanding of the mechanisms underlying the development of clinical stages of the disease. In clinical dentistry, this new knowledge has led to an evident change in the interpretation of signs of possible hard tissue damage due to caries at individual tooth sites. Thus the initial effect of the disease on the enamel is clinically undetectable subsurface demineralization and net loss of tooth mineral as the result of a mineral imbalance between plaque fluid and tooth surface (Fejerskov, 1997). At this stage, the damage is reversible and the affected site can be remineralized. Factors that determine the balance of the reactions and thus the likelihood of mineral loss or gain and the rate at which it occurs, are composition and thickness of the biofilm covering tooth surfaces, the diet, the fluoride ion concentration, and the salivary secretion rate (Kidd & Fejerskov, 2004).

In clinical dental practice, the decrease in the rate of lesion progression has led to the modification of thresholds for restorative intervention and a change towards a less invasive approach to the management of the disease. Despite our improved understanding of the caries process and the availability of effective intervention, caries lesions still progress to the stage where tooth structure is compromised and invasive intervention and restoration are required. On the basis of these concepts of the disease process, lesion detection and early intervention, the goals of caries management are to inhibit the initiation of new lesions, to arrest the progression of established lesions and to enhance the natural process of lesion repair by remineralization (Featherstone, 2004).

For decades, dentists have relied on visual inspection, tactile examination with probe and X-rays to identify dental caries and early-stage cavitation sites. Among these, visual inspection is the favoured choice to diagnose dental caries because it is non-destructive as compared to mechanical methods such as probing, which can damage tooth structure and X-rays, which are ionizing and hazardous in nature. All of these methods have limitations affecting either their diagnostic ability or their practicality in a clinical setting. Once the caries cavity is detected by conventional techniques, tooth demineralization has usually progressed through approximately one-third to one-half of the enamel's total thickness (Angmar-Mansson and ten Bosch, 1993; Schneiderman et al, 1997; Ashley et al, 1998; Hintze et al, 1998; Ross, 1999; Young, 2002). Because X-rays only show good contrast when considerable mineral loss has already taken place, this technique allows detection only of already well-advanced caries. At this stage, the treatment option is drilling and filling with restorative material. Thus there is an emerging need for sensitive, clinically relevant methods for early

detection and quantification of caries lesions. The development of new techniques could improve the accuracy of detection and especially could create the possibility of early caries detection and helps to apply suitable preventive measures or operative procedures.

1.2 OBJECTIVES OF THE STUDY

Detection of dental caries using optical techniques is receiving a lot of attention these days. Several, published data demonstrate the potential of optical spectroscopy to characterize caries lesions. Diagnostic techniques based on optical spectroscopy allow non-invasive and real-time characterisation of tissue. In particular, these techniques are fast, quantitative and can be easily automated. As well as, they also elucidate the chemical composition and morphology of the tissue which in turn help in monitoring metabolic parameters of the tissue and also distinguish sound from carious tooth. Among them, the potential of laser-induced fluorescence (LIF) and diffuse reflectance (DR) is enormous and yet, is not fully explored for early detection of dental caries *in vivo*. The hypothesis of present work is that these optical techniques will help to discriminate different stages of caries with good sensitivity and specificity. This thesis mainly aims at testing the applicability of LIF and DR spectroscopic techniques for detecting caries in its early stage. As part of this work, the applicability of LIF and DR spectroscopy in detecting early demineralization and remineralization is also tested.

In this current thesis, autofluorescence and diffuse reflectance spectra were obtained from sound and caries tooth belonging to different categories, with the intention of early detection of tooth caries. The major objectives of the study are:

1. Development of a compact, non-invasive, point monitoring laser-induced fluorescence reflectance spectroscopy (LIFRS) system for simultaneous measurement of laser-induced fluorescence and diffuse reflectance spectra from the same tooth samples, to detect dental caries or discriminate different stages of caries.

2. Standardization of measurement parameters and study protocol through *in vitro* studies

3. To test the applicability of the developed LIFRS system to detect dental erosion.
4. To test the ability of the device to detect early demineralization changes in tooth.

5. To study the effects of remineralization treatment on demineralized tooth.

6. Modification of the device based on the *in vitro* results, for clinical studies at the Department of Conservative Dentistry and Endodontics of Government Dental College Thiruvananthapuram and to measure LIF and DR spectra in patient and correlate with visual-tactile and radiographic findings.

7. To check the diagnostic accuracy of LIFRS system with visual-tactile and radiographic examination, in terms of sensitivity, specificity and ROC analysis for detection of dental caries both *in vitro* and *in vivo* conditions.

1.3 SOME FACTS ABOUT DENTAL CARIES

Dental caries is a dynamic process, taking place in the microbial deposits (dental plaque on the tooth surfaces), which results in a disturbance of the equilibrium between tooth substance and the surrounding plaque fluid so that, over time, the end result is the loss of mineral from the tooth surface (Thylstrup and Fejerskov, 1994).

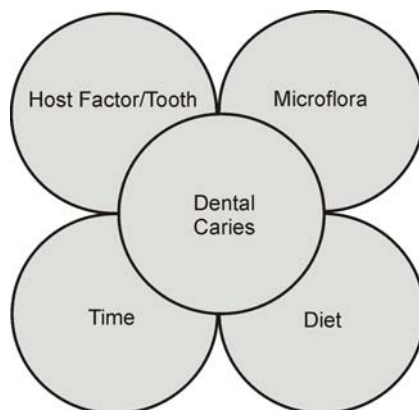


Fig. 1.1 Etiology of dental caries.

1.3.1 Carious process

The carious process affects the mineralized tissues of the teeth mainly enamel, dentin and cementum, which is caused by the action of microorganisms on fermentable carbohydrates in the diet. It can eventually lead to the demineralization of mineral portion of these tissues, followed by the disintegration of the organic material. At the crystal level, onset of carious process may be expected, but progression of a microscopic lesion to clinically detectable lesion is not a certainty because in its initial stage, the process can be arrested and a carious lesion may become inactive. Nevertheless, progression of the lesion into dentin can finally result

in bacterial invasion and death of the pulp and spread of infection into periapical tissues, producing pain.

1.3.2 Etiology of Caries

Dental caries is a multi-factorial disease. Many variations are seen in the incidence of caries due to the complex interplay of several factors. Basically, caries occurs when there is interaction of four principal factors; the host i.e., tooth, the microflora, the substrate and the time. For caries to occur all the four factors should be favourable- it means caries requires a susceptible tooth surface, cariogenic oral flora and a suitable substrate for a sufficient length of time (Fig. 1.1).

1.3.3 Clinical presentation of caries

The characteristics of carious lesions vary according to the surface on which they develop (Fig. 1.2).

1.3.3.1 Pit and fissure caries/occlusal caries

Pit and fissure caries “fans out” as it penetrates into enamel. The entry is over a small region but the occlusal enamel rods bend down and terminate on the dentin immediately below the developmental fault. This makes the carious lesion occupy a broad area of enamel after penetrating through a small opening on the pit or fissure. It is primary type and develops in the occlusal surface of molars and premolars. It appears brown or black and will feel slightly soft. In longitudinal sections of teeth, pit and fissure caries can be seen as a cone-shaped defect with its base towards the dentino-enamel junction (DEJ) and apex towards the pit. At the DEJ, the caries spreads laterally, rather than pulpally. So the carious lesion in dentin also appears cone-shaped with the base at the DEJ and apex towards the pulp.

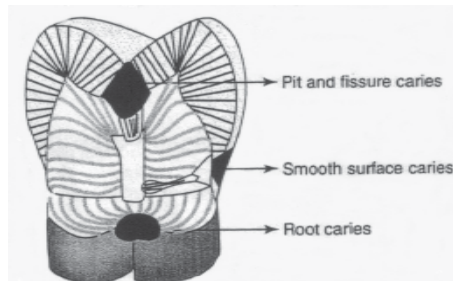


Fig.1.2. Clinical presentation of caries.

1.3.3.2 Smooth surface caries

Caries starting on smooth surfaces has a broad area of origin and a conical extension towards the pulp. The path of origin is roughly parallel to the long axis of the

enamel rods in the region. It develops on the proximal surfaces of the teeth or on the gingival third of buccal and lingual surfaces. In longitudinal section, the caries process is seen as cone-shaped area, with its base towards the enamel surface and its apex towards the DEJ. At DEJ, it spreads laterally along the junction, rather than pulpally. The base of the cone in dentin is again at the DEJ and its apex is toward the dental pulp.

1.3.3.3 Root surface caries

The cementum covering root surfaces is relatively thin and provides little resistance to caries attack. Root surface caries begins directly on dentin. It is U-shaped in cross section and spreads more rapidly because dentin is less resistant to caries attack.

1.3.4 Histopathology of caries

1.3.4.1 Caries of enamel

Enamel is highly mineralized tissue and forms an effective barrier to bacterial attack. However, its organic substance and water content make enamel act like a molecular sieve allowing free movement of small molecules and blocking the passage of larger molecules and ions. Caries in enamel preferentially attacks the interprismatic areas and the more permeable Striae of Retzius, because these regions have more organic content, followed by prism cores. As caries progresses in enamel along these regions, it spreads laterally thereby undermining enamel.

The first sign of enamel caries is seen as white spot. It appears opaque on drying the tooth surface and translucent on wetting the surface. If the enamel lesion is allowed to develop, demineralization becomes more predominant, which in turn cause a break in the enamel surface, producing cavity. Once cavity is formed, bacteria gains entry into the surface and progress deeper into the tooth.

An early enamel lesion seen under polarized light reveals four distinct zones of mineralization. These zones include,

a) *Surface Zone*: This outermost zone is relatively unaffected by caries attack. It is well mineralized by replacement ions from plaque and saliva.

b) *Body of the lesion*: This is the major portion of enamel caries. It is poorly mineralized. Caries spreads along the Striae of Retzius and interprismatic areas

and then attacks the prism cores. Bacteria are present in this zone.

c) *Dark zone*: This lies deeper to the body of the lesion and represents some remineralization.

d) *Translucent zone*: This is the deepest zone which represents the advancing front of the enamel caries. This is translucent due to demineralization which creates a structureless appearance of the enamel.

These zones represent the dynamic series of events taking place in early enamel caries. The early enamel caries can be reversed and remineralized if plaque is removed.

1.3.4.2 Caries of dentin

Caries progression in dentin is different from that of enamel. Dentin has lesser mineral content and microscopic dentinal tubules provide a pathway for the spread of caries. Thus caries progresses more rapidly in dentin than in enamel. The DEJ is less resistant to caries attack and allows lateral spread of caries. Dentinal caries is V-shaped in cross-section with its base at the DEJ and apex towards the pulp. Changes seen as caries spread in dentin:

- i) Weak organic acids demineralize the dentin.
- ii) The organic content of dentin especially collagen undergoes degeneration and dissolution.
- iii) Breakdown of the structural integrity and bacterial invasion.

Pathological changes seen in carious dentin is divided into various zones. They are

a) *Zone 1, Normal dentin*: The deepest zone of carious dentin is normal with normal collagen, odontoblastic processes and intertubular dentin.

b) *Zone 2, Sub-transparent dentin*: Here the intertubular dentin is demineralized, odontoblast processes are damaged and fine crystals are seen in the lumen of the dentinal tubules. But no bacteria are present.

c) *Zone 3, Transparent dentin*: This is superficial to the subtransparent dentin. It is softer than normal dentin and exhibits mineral loss in intertubular dentin. No bacteria are present and collagen cross-linking is intact. So this layer is capable of remineralization.

d) *Zone 4, Turbid dentin:* Here dentinal tubules are widened and distorted due to bacterial invasion. There is considerable demineralization and collagen is irreversibly denatured.

e) *Zone 5, Infected dentin:* This is the outermost zone. It has decomposed dentin with destruction of dentinal tubules and collagen. A high concentration of bacteria is present. This zone has to be removed to avoid the spread of infection.

Since dentin and pulp are intimately related, once caries attack dentin the dentin-pulp complex produces a protective response by blocking the open dentinal tubules. This response depends on the severity of the caries attack.

1.3.5 Diagnosis of dental caries

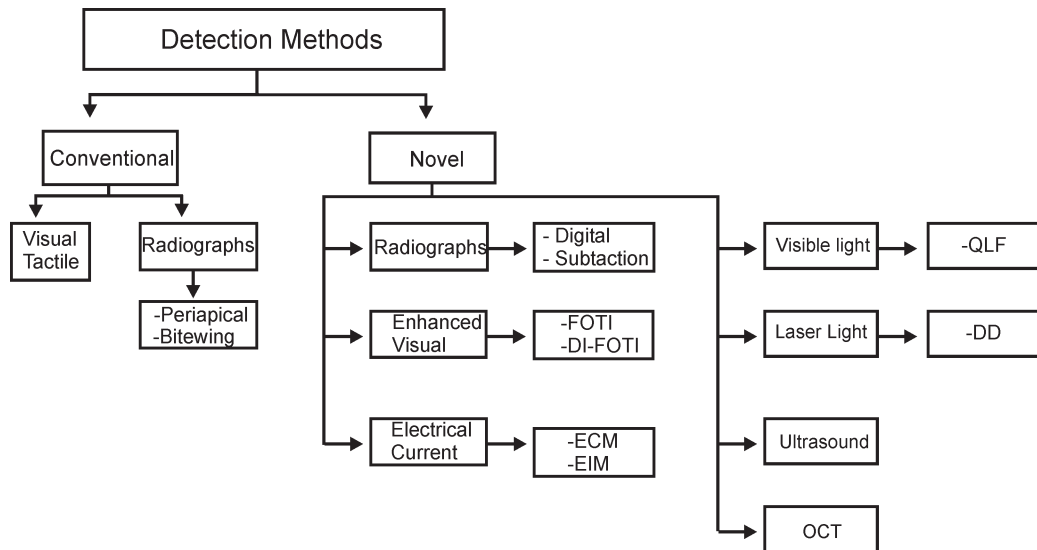


Fig.1.3. Diagnostic methods for dental caries.

Early diagnosis of carious lesion is essential because the carious process can be modified by preventive measures so that the lesion does not advance. The search for an ideal caries diagnostic method continues as such technique must be accurate, sensitive, specific, reproducible and reliable. Traditional methods of caries detection include visual inspection, tactile examination with an explorer and radiographic examination. These traditional techniques are still used in contemporary dental

practices; nevertheless some practices have been altered due to paradigm shift or new diagnostic equipment (Fig. 1.3).

1.3.5.1 Visual examination

Visual inspection is best performed in a well lit, clean, dry field, with the aid of magnification. The first step in assessing the caries status of a patient is to visually inspect all tooth surfaces, including root surfaces (Baysan, 2007). Visual data of caries is a good indicator of the degree of caries penetration within tooth tissues. 'Sharp eyes', with or without the aid of x2-4 loupes, in combination with good illumination and drying with a three-in-one syringe, termed as detection triangle (Fig. 1.4), may offer more information than the use of a mirror and a sharp probe.

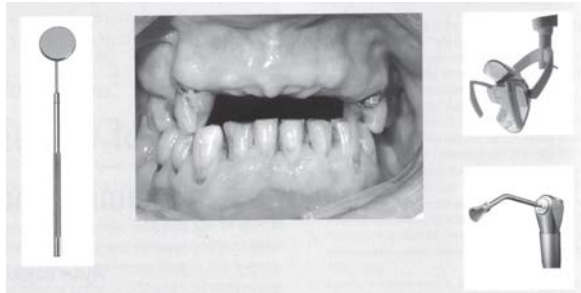


Fig.1.4. Detection triangle.

The procedure for initial visual inspection, with or without the help of loupes is as follows:

- a) Clean the tooth surface
- b) Place cotton rolls and saliva ejector
- c) With the surface wet, examine the suspected white or brown spot lesions.
- d) Dry the tooth using the three-in-one syringe.
- e) Confirm the presence of any white or brown spot lesions.
- f) If there is any obvious cavitation, then visual-tactile examination can be considered to determine if there is any exposed dentin (Ekstrand et al, 2001).

1.3.5.2 Visual-Tactile Techniques

At present, most caries tends to be detected using visual-tactile criteria, based on the presence or absence of cavitation and the surface texture of lesions. Usually curved explorers are used for examining occlusal pits and fissures while interproximal explorers

are used to detect proximal caries. The use of dental explorers may not improve the accuracy of diagnosis; indeed, it may increase the number of false positive diagnoses. Probing can also transfer infective microorganisms from one site to another and disrupt tooth surfaces prone to cavitation (Kidd et al, 1993). It has also been observed that excessive pressure with a sharp explorer tip can convert initial lesions into cavitation (Yassin, 1995). Therefore it is advised to use only blunt probes to remove debris and confirm frank cavitation.

1.3.5.3 Radiographic examination

The use of radiographs to scrutinize teeth and other oral structures for the presence of oral disease remains the 'gold standard' (Barnes, 2005). Conventional, intraoral periapical and bitewing radiographs are used to diagnose dental caries. Of the two, bitewing radiographs have more diagnostic value. Bitewing radiographs has been used for the detection of occlusal and proximal surface caries as well as caries adjacent to the margins of restorations (secondary caries) in posterior teeth in both adults and children (Fig. 1.5). Periapical radiographs are used for detecting early proximal surface caries in anterior teeth. Characteristics of acceptable radiographs are shown in Table 1.1.

Table 1.1 *Characteristics of acceptable radiographs.*

| Characteristics | Appearance |
|--------------------------|---|
| Image | All parts of teeth of interest must be shown close to natural size, with minimal overlap and minimal distortion |
| Area covered | Sufficient tissue surrounding tooth for diagnostic purposes |
| Density | Proper density for diagnosis |
| Contrast | Proper contrast for diagnosis |
| Definition and sharpness | Clear outline of objects, minimal penumbra |

Adapted from White and Pharoah. Oral radiology principles and interpretation. 5th edition. St Louis, Mosby, 2004

Initial enamel caries in the occlusal surfaces are difficult to detect using bitewing radiographs due to its complicated three dimensional shapes. Also caries involving the buccal or lingual grooves of molars may mimic occlusal lesions due to superimposition. Once caries has progressed into dentin, it appears as radiolucent zone.

Bitewing radiographs are very important in diagnosing proximal caries. Early

proximal enamel caries appear as a small radiolucent notch below the contact area in enamel. Advanced proximal caries is seen as dark triangular area in the proximal enamel with its base towards the external tooth surface. Proximal caries may be scored according to its progress through enamel and dentin towards the pulp.

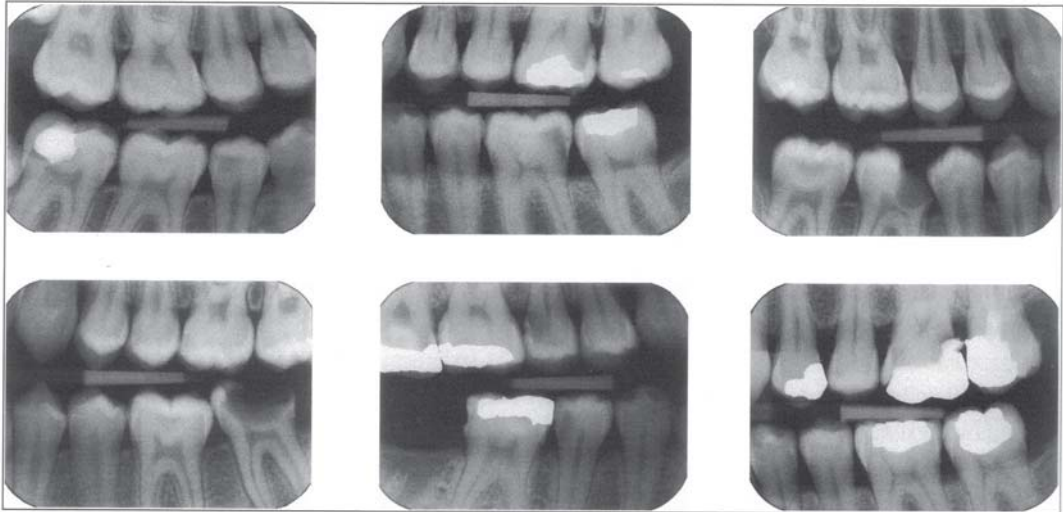


Fig.1.5. Bitewing radiographic image of different sized caries lesions in proximal and occlusal caries. (Adapted from Whaites, In Minimally Invasive Dentistry: The management of caries, Eds. Wilson NHF. Quintessence Publ. Co, Ltd, London, et al., 2007.

Diagnostic yield

Clinical examination only results typically in less than 50% of occlusal and proximal caries lesions present being detected. When clinical and appropriate radiographic diagnoses are combined, more than 90% of occlusal and proximal surface lesions may be detected, with cavitated lesions tending to be easier to diagnose correctly than non-cavitated lesions. Visual inspection and radiographs or bitewing x-rays, although effective in revealing advanced stages of caries (Kidd, 1994; Verdonschot et al, 1999) are unsuccessful in detecting early caries, especially in the complex anatomy of fissure areas (King and Shaw, 1979).

1.3.5.4 Alternative caries detection methods

In recent years, more than a few caries detection methods and devices have been developed. The advent of these detection techniques is welcomed as traditional caries detection methods do not allow for the detection of caries until they have progressed

through at least the thickness of enamel. Some of these new caries detection methods are so recent that they are not yet marketed to the dental profession and others have been found to be more practical for research purposes. These methods include:

1.3.5.4.1 Diagnostic method based on X-rays: Digital and subtraction radiography

Currently, digital radiographic methods offer a more superior means of detecting caries than conventional radiographs. Digital radiographic images are created by using the spatial distribution of pixels and the different shades of gray of each of the pixels. These radiographic devices interface with a computer to digitize the digital radiographic images into pixels that are then viewed on a computer. It offers several advantages over traditional dental radiography:

- i) Reduced radiation exposure to patient
- ii) Instant image visualization
- iii) Eliminates chemical processing and accompanying errors
- iv) Image enhancement, processing and magnification can be done

The most important advantage of digital imaging is that it can be used for subtraction purposes. Here images which are not of diagnostic value in a radiograph are reduced so that the changes in the radiograph can be precisely detected. Images taken over time are superimposed to check the differences between original and subsequent images.

1.3.5.4.2 Diagnostic systems based on electrical current: ECM/EIM

The theory behind the use of Electrical Conductance Measurement (ECM) is that sound tooth enamel is an insulator, due to its high inorganic content. On the other hand, carious or demineralized enamel has a measurable conductivity which increases with the degree of demineralization. On the basis of this difference, four coloured lights were used as indicator for caries.

- i) Green: no caries
- ii) Yellow: enamel caries
- iii) Orange: dentin caries
- iv) Red: pulpal involvement

Many researchers have used ECM for both *in vitro* (Verdonschot et al, 1993; Ashley et al, 1998) and *in vivo* studies (Rock and Kidd, 1988; Verdonschot et al, 1992a) and the reported sensitivities for diagnosing dentinal carious lesions of permanent molar and premolar ranged from 0.67 to 0.96, whereas the specificities ranged from 0.71 to 0.98. In addition, they are more accurate in diagnosing early occlusal caries than visual method, radiographs or fiber optic transillumination (FOTI). The major disadvantage of ECM method is the use of sharp metal explorers, which in turn cause traumatic defects in pits and fissures.

Cariouss tissues have much lower electrical impedance or much better electrical conductivity than sound tooth. This principal of electrical impedance has been used to detect caries lesions at approximal surfaces of teeth (Huysmans et al, 1996; Longbottom et al, 1996). Even though the results from these *in vitro* studies were very promising, no follow up results have been reported since.

1.3.5.4.3 Transillumination: FOTI and DIFOTI

Transillumination has been used as diagnostic tool in dentistry for over 30 years (Stokey, 2003). Caries detection using transillumination with a bright fiber-optic light depends on the light scattering by the lesion. Increased opacity of the enamel is the visual sign of early caries. Optical scattering can be used to quantify the degree of demineralization in enamel and dentin. In sound tooth, scattering is more prominent than absorption. Nevertheless, when light transmits through damaged tooth, light absorption increases. Dark shadowing indicates the presence of caries. It is especially useful in detecting proximal caries, with the added advantage over radiographic techniques that the patient is not exposed to ionizing radiation. It does not detect small carious lesions; hence its use is limited.

The Digital imaging fiber-optic transillumination (DIFOTI) is a relatively new technique that has developed in an attempt to decrease the short coming of FOTI, by combing FOTI and a digital CCD camera. Illumination is delivered to the tooth surface by means of fibre-optic light source. The resultant change in light distribution is captured by the camera and is sent to the computer for analysis. It is non-invasive and can detect incipient and recurrent caries very early. But it does not measure the depth of the lesion and are not able to discriminate between deep fissure, stain and dental caries. Nevertheless, these techniques have lower sensitivities for caries detection when compared with radiologic images and poor reliability as compared to visual inspection and bitewing radiography (Hintze et al, 1998; Schneiderman et al, 1997).

1.3.5.4.4 Quantitative laser/light-induced fluorescence (QLF)-yellow/orange fluorescence

As the name of the method implies, QLF is based on fluorescent light. In QLF this light is not induced by X-rays or other ionizing radiation but by visible or near ultraviolet radiation. The fluorescence of tooth tissue has been known for a very long time. Three types of fluorescence have to be distinguished. The first is the blue fluorescence that is excited in the near ultraviolet. The second is the yellow and orange fluorescence excited in the blue and green. The third is the fluorescence in the far red and near infrared that has recently received much attention for quantitative non-image diagnosis of caries lesions. Initially the technique was developed using lasers and was demonstrated by Bjelkhan (1982). With concerns existing over the intra oral use of lasers, de Josselin de Jong (1995) developed a system using filtered visible light, QLF. The experimental method involves quantification of the light-induced fluorescence level of enamel. Sound, healthy enamel shows a higher fluorescence than demineralized enamel; demineralized areas appear relatively darker under light that excites the fluorescence.

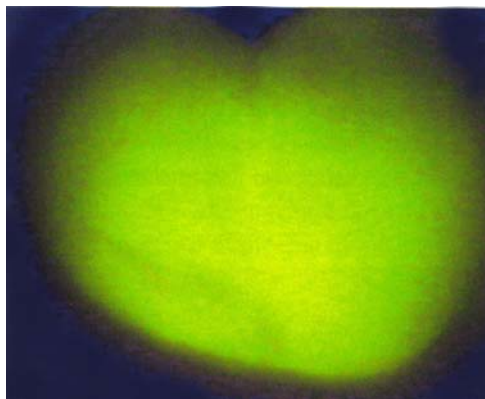


Fig.1.6. QLF image.

The teeth are illuminated with a broad beam of blue-green light from an argon ion laser (488 nm) or blue light from a xenon arc lamp, equipped with a band pass filter with peak transmission at 370 nm. A yellow high pass filter (520nm) is placed in front of the CCD micro camera which captures the tooth image. Image of the tooth under examination is displayed on a PC screen (Fig. 1.6). The absolute decrease in fluorescence is determined by calculating the percentage loss between actual and reconstructed fluorescence and is expressed as F value.

The QLF has been tested in several *in vitro* and *in vivo* studies for smooth surface, occlusal and secondary caries (Al-Khateeb et al, 1997a; Emami et al, 1996; Pretty et al, 2002, 2003; Ferreira Zandona et al, 2000, Heinrich-Weltzein et al, 2005; Ando et al, 2000, Kuhnisch et al, 2006, Hall et al, 1997). It has shown that QLF is a sensitive, reproducible method for the quantification of enamel lesions on smooth surfaces. Nevertheless, its application seems to be restricted to a lesion depth of about 500 μ m.

Also, QLF cannot discriminate between active and inactive lesions and between caries, hypoplasia, stain and calculus.

1.3.5.4.5 DIAGNOdent-infrared fluorescence

The DIAGNOdent device (KaVo, Biberach, Germany) was introduced in 1998 by Hibst and Gall (1998) to help in the diagnosis of occlusal caries as an adjunct to visual inspection and radiographic examination (Fig.1.7). It operates with light from a diode laser with a wavelength of 655 nm and 1mW peak power, which is transported through a fibre bundle to the tip of a hand piece. The tip is placed in contact with tooth surface and laser light will penetrate the tooth. Both organic and inorganic molecules in the tooth absorb light. Fluorescence occurs within the infrared spectrum. The fluorescence as well as backscattered light is collected through the tip and passed in ascending fibres to a photodiode detector. The fluorescence light is measured and its intensity is an indication of the size and depth of the caries lesion. The fluorescence intensity is displayed as a number ranging from 0 to 99, with 0 indicating a minimum and 99 a maximum of fluorescence light.



Fig.1.7. DIAGNOdent.

In the presence of carious tooth substance, fluorescence increases. The cause of fluorescence is due to the presence of protoporphyrins and mesoporphyrins, by-products of bacteria (Hibst and Paulus, 1999, 2000). DIAGNOdent has been used widely for detecting occlusal and smooth surface caries (Aljehani et al, 2006, 2007; Antonnen et al, 2003; Bamzahim et al, 2004, 2005; Lussi et al, 2003, 2006). *In vitro* validity studies showed that the sensitivity of DIAGNOdent caries diagnoses ranged from 0.17 to 0.87, whereas specificity ranged from 0.72 to 0.98 (Lussi et al, 1999; Shi et al, 2000). Regarding the reliability of this method, good to excellent observer agreement were reported (Attrill and Ashley, 2001; Lussi et al, 2001). Majority of works indicate that DIAGNOdent is clearly more sensitive than traditional methods;

nevertheless, the increased likelihood of false positive diagnoses limits its usefulness as a principle diagnostic tool (Bader et al, 2004). It is therefore recommended that the DIAGNOdent readings should serve as guidelines and a treatment choice should never be based on its value alone.

1.3.5.4.6 Diagnostic based on ultrasound measurements

Ultrasonic imaging can be used to detect early caries on smooth surfaces (Ng et al, 1988). Here an ultrasonic probe is used to send and receive sound waves from the tooth surfaces. Sound enamel produces no echoes while, initial white spot produce weak surface echoes and cavitated areas produce echoes of higher amplitude. This method is inappropriate to apply in patients and also could not detect shallow caries lesions.

1.3.5.4.7 Optical coherence tomography (OCT)

Optical coherence Tomography (OCT) that uses low coherence interferometry, has found broad applications in the cross sectional imaging of biological structures, including dental hard and soft tissue. Polarization sensitive (PS) OCT systems that utilize polarized incident light (1310 nm) and measure the polarization information from the backscattered signal in two separate channels, have been used for imaging of birefringent tissues.

Due to the rod-like organization of hydroxyapatite crystals, dental enamel is usually birefringent, and initial measurement of tooth enamel with PS-OCT emphasized characterization of the tissue birefringence. PS-OCT images resolved enamel demineralization through an increasing backscattered intensity and changes in the enamel birefringence. If the incident illuminating light is linearly polarized, the light scattered from the demineralized lesion area will rapidly depolarize. Since carious enamel depolarizes incident polarized light, PS-OCT images both the surface and subsurface enamel by recording changes in the magnitude of scattering and depolarization without interference from the strong surface reflection. Several studies have demonstrated that remineralization has a significant effect on the mineral volume on the outer perimeter of the lesion, near the enamel surface. This suggests that PS-OCT could be valuable in imaging the remineralization of caries lesions. Demineralization in the enamel was resolvable to a depth of 2-3 mm into the tooth. Moreover, OCT is not well suited for imaging entire tooth surfaces or interproximal surfaces in between teeth due to time restraints and the enormous quantity of data that would be collected.

1.3.6 Prevention of dental caries

1.3.6.1 Oral hygiene

Plaque control is essential in caries prevention because caries does not occur in the absence of plaque. Personal hygiene care consists of proper brushing and flossing daily. The purpose of oral hygiene is to minimize any etiologic agents of disease in the mouth. The primary focus of brushing and flossing is to remove and prevent the formation of plaque. As the amount of bacterial plaque increases, the tooth is more vulnerable to dental caries. A toothbrush can be used to remove plaque on most surfaces of the teeth except for areas between teeth. When used correctly, dental floss removes plaque from areas, which could otherwise develop proximal caries.

Professional hygiene care consists of regular dental examinations and cleanings. Sometimes, complete plaque removal is difficult, and a dentist or dental hygienist may be needed. Along with oral hygiene, radiographs may be taken at dental visits to detect possible dental caries development in high-risk areas of the mouth.

1.3.6.2 Dietary modification

Dietary modification is recommended to patients with active caries and those who are at high risk for caries development. For dental health, the frequency of sugar intake is more important than the amount of sugar consumed. In the presence of sugar and other carbohydrates, bacteria in the mouth produce acids, which can demineralize enamel, dentin, and cementum. The more frequently teeth are exposed to this environment; the more likely dental caries are to occur. Therefore, minimizing snacking is recommended, since snacking creates a continual supply of nutrition for acid-creating bacteria in the mouth. Also, chewy and sticky foods tend to adhere to teeth longer, and consequently are best eaten as part of a meal. Brushing the teeth after meals is recommended. Mothers are also recommended to avoid sharing utensils and cups with their infants to prevent transferring bacteria from the mother's mouth. It has been found that milk and certain kinds of cheese can help counter tooth decay if eaten soon after the consumption of foods potentially harmful to teeth. Also, chewing gum containing xylitol (wood sugar) is widely used to protect teeth. Xylitol's effect on reducing plaque is probably due to bacteria's inability to utilize it like other sugars. Chewing and stimulation of flavour receptors on the tongue are also known to increase the production and release of saliva, which contains natural buffers to prevent the lowering of pH in the mouth to the point where enamel may become demineralized.

1.3.6.3 Other preventive measures

The use of dental sealants is a good means of prevention. Sealants are thin plastic-like coating applied to the chewing surfaces of the molars. This coating prevents the accumulation of plaque in the deep grooves and thus prevents the formation of pit and fissure caries, the most common form of dental caries. Sealants are usually applied on the teeth of children, shortly after the molars erupt. Older people may also benefit from the use of tooth sealants, but usually their dental history and likelihood of caries formation are taken into consideration.

Fluoride therapy is often recommended to protect against dental caries. It has been demonstrated that water fluoridation and fluoride supplements decrease the incidence of dental caries. Fluoride helps prevent decay of a tooth by binding to the hydroxyapatite crystals in enamel. The incorporated fluoride makes enamel more resistant to demineralization and, thus, resistant to decay. Topical fluoride is also recommended to protect the surface of the teeth. This may include a fluoride toothpaste or mouthwash. Many dentists include application of topical fluoride solutions as part of routine visits.

1.4 CONCLUSIONS

Caries diagnosis in its early stage is often difficult. Accurate diagnosis is required in order to apply appropriate preventive measures or operative procedures. Recently, several techniques have been introduced to aid dentists in accomplishing this task. Exploration of the potential of new techniques in the biomedical field is always challenging. Conventional diagnostic methods to detect demineralization or dental caries have limitations affecting either their diagnostic ability or feasibility in a clinical setting. Therefore, there is a need to develop diagnostic methods that can accurately screen dental caries at an earlier stage.

Currently, radiographic examination is widely used as a diagnostic test adjunct to visual-tactile techniques. In view of the possible hazardous effects of ionizing radiation and the shortcomings in its performance in detecting small lesions, a search for alternatives to radiography has resulted in a number of advanced methods for the detection of caries lesions. The development of new methods could increase the accuracy of detection and in particular generate the likelihood of early caries detection. In this context, if applied effectively, optical spectroscopy has enormous potential to represent the main forward step towards advances in diagnostic applications. For the development of such optimized optical systems, there is a need

to understand the structure of tooth and its interaction with light. The next chapter throws light on different aspects of optical spectroscopy and basic concepts of interaction of light with dental hard tissue.

Chapter 2

Tooth Anatomy and its Interaction with Light

2.1 INTRODUCTION

The oral cavity is a unique and complex environment, where hard and soft tissues exist in close proximity, within bacteria laden saliva. Moreover, teeth are complex anatomical units consisting of four types of tissues, each with its own structure and properties. A basic knowledge of the development and structure of the teeth is essential to clearly understand the various defects and diseases affecting teeth as well as for the use of optical techniques for diagnostic applications.

All oral tissues are receptive to photonics based applications. Many of the fundamental principles governing light-tissue interactions are rather simple. The effects of light irradiation on dental hard tissues to some extent can be assessed in terms of what happens when light interacts with tissue. These involve biologic and physiologic processes of tissue, which are more complex in nature and reflect a more intricate interrelationship. Therefore, a practical understanding of the biologic processes of tissue and the physical properties of light will provide the clinician with the ability to comprehend and control the outcome of its interaction for a multitude of clinical applications.

The nature of tissue response to light interaction is both wavelength and time/rate dependent. Optical spectroscopic techniques involve the interaction of light with tissues, offer high intrinsic sensitivity and the use of non-ionizing radiation makes it more suited for mass screening and repeated use without any adverse effects. Light radiation in the UV-visible region is the preferred wavelength for this purpose. Important aspects for tissue diagnostics are based on light scattering and emission properties. By analyzing the features of scattered and re-emitted light in terms of wavelength, indirect information on tissue characteristics can be achieved.

As compared to current clinical diagnosis, optical spectroscopic techniques are fast, non-invasive, quantitative and provide real-time information about the extent of disease in a highly sensitive manner. Further, these systems can be easily be automated, facilitating use by even less-skilled personnel. Fluorescence spectroscopy, Raman spectroscopy, diffuse reflectance spectroscopy and optical coherence tomography are emerging techniques in the field of dentistry. Among them, the potential of laser-induced fluorescence and diffuse reflectance is enormous

and yet, is not fully explored for early detection of demineralization or dental caries.

This chapter details the basic anatomy of the tooth and its interaction with light, with emphasis on the basic concepts of tissue fluorescence and diffuse reflectance, and this forms the basis of the work presented in this thesis. In addition, different types of endogenous fluorophores and their absorption and emission characteristics are described in this chapter.

2.2 TOOTH: An Overview

Teeth constitute approximately 20% of the surface area of the mouth, the upper

teeth significantly more than the lower teeth. They are both ectodermal and mesodermal in origin and are derived from the primitive oral mucous membrane. Humans usually have 20 primary teeth (also called deciduous, baby, or milk teeth) and 32 permanent teeth. Among primary teeth, 10 are found in the (upper) maxilla and the other 10 in the (lower) mandible. Teeth are classified as incisors, canines and molars. In the primary set of teeth, there are two types of incisors - centrals and laterals, and two types of molars - first and second. All primary teeth are replaced with permanent counterparts except for molars which are replaced by permanent premolars. Among permanent teeth, 16 are found in the maxilla with the other 16 in the mandible

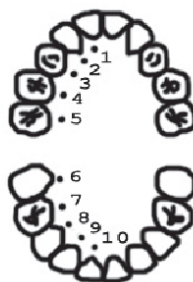
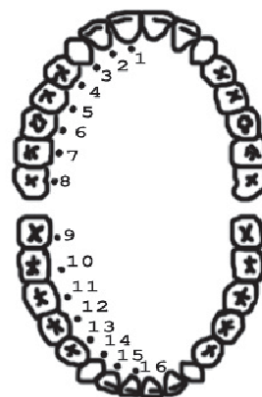
Adult Teeth

Upper Teeth

1. Central Incisor
2. Lateral Incisor
3. Canine (cuspid)
4. First Premolar (first bicuspid)
5. Second Premolar (second bicuspid)
6. First Molar
7. Second Molar
8. Third Molar (wisdom tooth)

Lower Teeth

9. Third Molar (wisdom tooth)
10. Second Molar
11. First Molar
12. Second Premolar (second bicuspid)
13. First Premolar (first bicuspid)
14. Canine (cuspid)
15. Lateral Incisor
16. Central Incisor



Baby Teeth

Upper Teeth

1. Central Incisor
2. Lateral Incisor
3. Canine (cuspid)
4. First Molar
5. Second Molar

Lower Teeth

6. Second Molar
7. First Molar
8. Canine (cuspid)
9. Lateral Incisor
10. Central Incisor

Fig.2.1. Human dental formulae.

(Fig.2.1). The maxillary teeth are the maxillary central incisor, maxillary lateral incisor, maxillary canine, maxillary first premolar, maxillary second premolar, maxillary first molar, maxillary second molar and maxillary third molar. The mandibular teeth are the mandibular central incisor, mandibular lateral incisor, mandibular canine,

mandibular first premolar, mandibular second premolar, mandibular first molar, mandibular second molar and mandibular third molar. Third molars are commonly called “wisdom teeth” and may never erupt into the mouth or form at all.

2.3 TOOTH DEVELOPMENT

The development of tooth is a complex process by which teeth form from embryonic cells, grow and erupt into the mouth. For human teeth to have a healthy oral environment, enamel, dentin, cementum, and the periodontium, must all develop during appropriate stages of tooth development. Primary (baby) teeth start to form between the sixth and eighth week in-utero, and permanent teeth begin to form in the twentieth week in-utero. If teeth do not start to develop at or near these times, they will not develop at all.

Tooth development/ odontogenesis begins by the localised proliferation of epithelial cells of the primitive oral mucosa, which give rise to a thickened ridge of epithelium extending around the dental arch of each jaw known as dental lamina. At certain points along the dental lamina, proliferation takes place at an increased rates and epithelium grows more deeply to form enamel organ, which eventually forms the enamel. At the same time proliferative changes occurs in the ectomesenchyme and forms the dental papilla, which eventually forms the dentin and dental pulp. The mesodermal tissue surrounding the enamel organ later forms the dental follicle or dental sac, which finally forms the cementum, periodontal membrane and bony crypt. The enamel organ, dental papilla and the dental follicle together form the tooth bud or tooth germ (Fig.2.2).

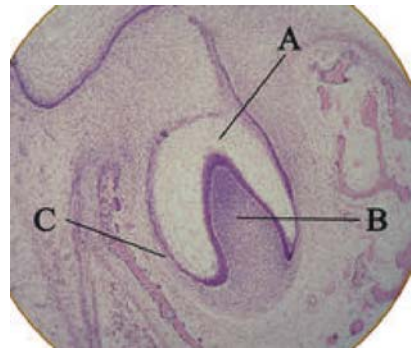


Fig.2. 2. Histology slide showing a tooth bud **a)** enamel organ, **b)** dental papilla and **c)** dental follicle.

2.3.1 Development Stages

Tooth develops as a result of interaction between oral epithelium and underlying mesenchymal tissue. The ectoderm lining stomodeum begins to develop during the third week in-utero as an invagination of the tissues underlying the forebrain. Subsequent to 37 days of development, a continuous band of epithelium forms around the oral cavity in the maxillary and mandibular processes. This epithelial band gives rise to the vestibular and dental lamina. The vestibular lamina continues to proliferate and then

degenerates to form a cleft that becomes the vestibule between the cheek and the dental arch. The dental lamina proliferates to form a series of invaginations into the underlying mesenchyme at the sites of the future primary teeth. Tooth development occurs in many stages, which is similar for both primary and permanent dentition (Table 2.1). These stages depend on the appearance of developing tooth structures. Subsequent to the initiation of tooth development, each tooth develops through the bud stage, the cap and the bell stages. Tooth development then progresses to the apposition and maturation stages, with the formation and mineralization of the hard dental structures (Fig. 2.3). During the early stages (A to C), the tooth germs grow and expand, and the cells that forms the dental hard-tissues differentiate. Differentiation takes place in the bell stage, setting the stage for formation of enamel and dentin (D and E). When the

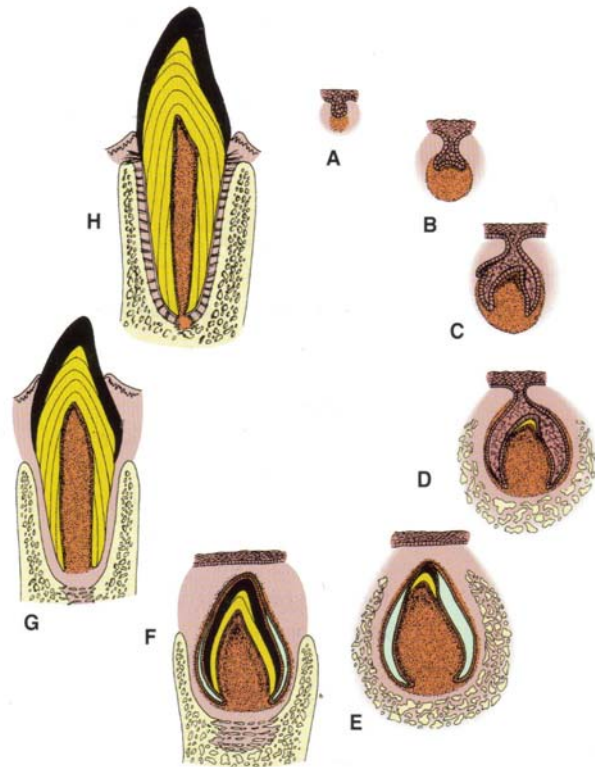
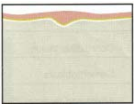
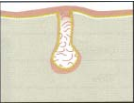
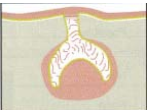
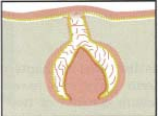
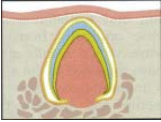
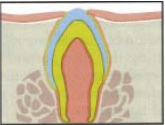


Fig.2.3. Tooth development stages. **A)** Bud, **B)** Cap, **C)** Bell, **D)** and **E)** Dentinogenesis and Amelogenesis, **F)** Crown formation, **G)** Root formation and eruption, **H)** Function (Adapted from Avery and Chiego, In *Essentials of Oral Histology and Embryology: A clinical approach*. Mosby, Canada, 2006).

crowns are formed and mineralized, the roots of the teeth begin to form. After the calcification of root, supporting structures of the teeth - cementum, periodontal ligament and alveolar bone, begins to develop (F and G). This formation occurs even if it is an incisor with a single root, a premolar with several roots or a molar with multiple roots. Subsequently, the completed tooth crown erupts into the oral cavity (G). Root formation and cementogenesis continue until a functional tooth and its supporting tissues are fully developed (G and H).

Table 2.1 Developmental Stages of Tooth.

| Stage/Time span* | Microscopic appearance | Main processes involved | Description |
|---|---|---|--|
| Initiation stage/6 th to 7 th weeks |  | Induction | Ectoderm lining stomodeum gives rise to oral epithelium and then to dental lamina, adjacent to deeper ectomesenchyme, which is influenced by the neural crest cells. These tissues are separated by a basement membrane. |
| Bud stage/8 th week |  | Proliferation | Growth of dental lamina into bud that penetrates growing ectomesenchyme. |
| Cap stage/ 9 th to 10 th weeks |  | Proliferation, differentiation, morphogenesis | Enamel organ forms into cap, surrounding mass of dental papilla from the ectomesenchyme and surrounded by mass of dental sac also from the ectomesenchyme. Formation of the tooth germ. |
| Bell stage/ 11 th to 12 th weeks |  | Proliferation, differentiation, morphogenesis | Differentiation of enamel organ into bell with four cell types and dental papilla into two cell types. |
| Apposition stage/ varies per tooth |  | Induction, proliferation | Dental tissues secreted as matrix in successive layers. |
| Maturation stage/varies per tooth |  | Maturation | Dental tissues fully mineralized to their mature levels. |

*These are ~ prenatal time spans for development of the primary dentition.

(Adapted from Bath-Balogh, M and Fehrenbach, MJ, In Dental Embryology, Histology, and Anatomy. Philadelphia, PA: WB Saunders, 2006.

2.4 TOOTH STRUCTURE

Structurally tooth consists of a hard, inert, acellular *enamel* formed by epithelial cells supported by the less mineralized, more resilient and vital hard connective tissue *dentin*, which is formed and supported by the dental *pulp*, a soft connective tissue. Teeth are attached to the bones of the jaw by supporting tissues consisting of cementum, periodontal ligament and alveolar bone, which provide an attachment with adequate flexibility to withstand the forces of mastication (Fig. 2.4).

2.4.1 Enamel

Enamel covers the anatomic crown of the tooth and is the hardest and most highly mineralized substance in the human body. It is responsible for the aesthetic colour and translucency of the tooth. Ninety six percent of enamel consists of inorganic material in the form of hydroxyapatite crystals with water and organic material forming the rest (Hunt, 1959). The large amount of minerals in enamel accounts not only for its strength but also for its brittleness. Enamel is ectodermal in origin and is formed by cells called ameloblasts.

The normal colour of enamel varies from light-yellow to greyish white. It varies in thickness over the surface of the tooth and is often thickest at the cusp, up to 2.5mm and thinnest at its border.

Enamel is composed of millions of enamel rods or prisms covered by rod sheaths and cementing inter-rod substances. The rods are densely packed and are oriented perpendicular to the dentinoenamel junction (DEJ) and the tooth surface except in the cervical margin of permanent teeth where they are oriented outward in a slightly apical direction. In cross section, it is best compared to a keyhole, with the top, or head, oriented toward the crown of the tooth, and the bottom, or tail, oriented toward the root of the tooth (Fig. 2.5). Each rod has a sheath and core. The rod sheath surrounds rod head and tail. The number of rods per tooth varies from approximately

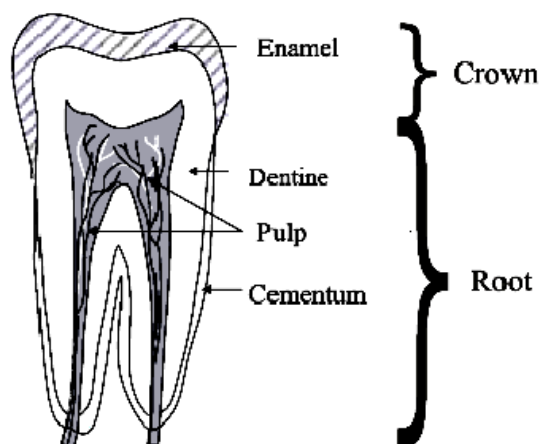


Fig.2.4. Structure of a tooth

five to twelve million. Some of the specialized structural components seen in some areas of enamel are

a) Gnarled enamel: This consists of a group of enamel rods which entangle with adjoining groups of rods and taking a curving, irregular path toward the tooth surface. It is seen in the cervical, incisal and occlusal areas.

b) Enamel tufts: These are hypomineralized structures of enamel rods and inter-rod substance. They arise from the DEJ and extend into the enamel along the long axis of the crown, which may have a role in the spread of dental caries.

c) Enamel lamellae: These are thin, leafy like faults between normal groups of enamel rods, start at the enamel surface and extend up to the DEJ. It contains mostly organic material and serves as entry regions for bacteria causing dental caries.

d) Enamel spindles: Odontoblastic processes of dentin may cross DEJ and extend into the enamel, called enamel spindles. They are formed during the formative period of enamel when they insinuate themselves between ameloblasts. They may be pain receptors in the enamel responsible for the enamel sensitivity.

e) Hunter-Schreger bands: Changes in the direction of enamel rods that minimize cleavage in the axial direction produce an optical appearance called Hunter-Schreger bands. They have alternate light and dark zones, which have slightly different permeability and organic content.

f) Incremental Straie of Retzius: They represent the successive apposition of enamel in the form of discrete increments.

g) Prismless enamel: This is a structure less outer layer of enamel seen in the cervical areas of teeth. It is heavily mineralized.

h) Dentino-enamel junction (DEJ): This is the interface of enamel and dentin.

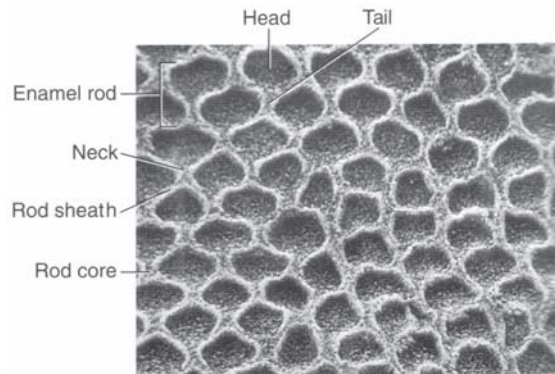


Fig.2.5. Cross section of enamel rods. (Adapted from Avery and Chiego, In *Essentials of Oral Histology and Embryology: A clinical approach*. Mosby, Canada, 2006).

It is 30µm thick and hypermineralized. The DEJ is scalloped or wavy in outline as the rounded projections of enamel fit into the shallow depressions of the dentin.

i) Nasmyth membrane/primary enamel cuticle: This is a membrane secreted by the ameloblast cell after completion of enamel formation. It covers the newly erupted tooth.

j) Pellicle: This is a membrane formed by the precipitation of salivary proteins, which covers the enamel surface after the removal of nasmyth membrane. It can be invaded by bacteria to form plaque which initiates dental caries or periodontal disease.

k) Occlusal pits and fissures: Macroscopically, the occlusal enamel surface of molars and premolars show grooves, pits and fissures. They form at the junction of the developmental lobes of the enamel.

2.4.2 Dentin

The dentin is a specialized connective tissue of mesodermal origin, formed from the dental papilla of the tooth bud. It forms the largest portion of the tooth and gives the basic shape to it. It is covered by the enamel in the crown and by the cementum in the root. Internally, dentin forms the boundary of the pulp. Dentin is considered as a living tissue and reacts to physiological and pathological stimuli. It is normally yellow white in colour and is more opaque. It is softer than enamel but harder than bone or cementum. Dentin is composed of mainly inorganic material (75%) with some amount of organic matter (20%) and water (5%). The mineral phase of dentin is mainly hydroxyapatite while the organic phase is composed of collagen.

Structurally, dentin consists of dentinal tubules extending throughout the dentin. Each tubule is lined by peritubular dentin and surrounded by intertubular dentin (Fig. 2.6).

a) Dentin tubules: These are small channels extending throughout the width of the dentin from DEJ or dentino cemental junction (DCJ) to the pulp. It carries the odontoblastic processes, which are the cytoplasmic extensions that line the pulp. They contain the dentinal fluid and are wavy or S- shaped; are perpendicular to the DEJ or DCJ. They are more closely packed near the pulp than near enamel or cementum.

b) Canaliculi: These are small lateral openings along the dentin tubule wall, through which odontoblastic processes convey lateral communications to the lateral branches of adjacent odontoblastic processes.

c) Peritubular dentin: This is a hyper-mineralized area around odontoblast process and forms the wall of the dentin tubule. It is composed of inorganic apatite crystals with a small amount of organic substance.

d) Intertubular dentin: This is the hypo-mineralized dentin which is present between the tubules.

e) Pre-dentin: This is an un-mineralized area, which is found immediately above the odontoblastic layer.

f) Primary dentin: This is the dentin that is formed initially till the root formation is completed.

g) Secondary dentin: This is the dentin which forms after root formation is completed, which occurs at a slow rate and the tubules are irregular in shape. The dentin tubules curve more sharply as they move from primary to secondary dentin.

h) Reparative or tertiary dentin: This is the dentin which is formed in response to external irritants like attrition, abrasion, erosion, trauma, caries or restorative procedures. This is localized to the area of irritation, and is formed either by existing odontoblasts or by secondary odontoblasts formed from the undifferentiated mesenchymal cells of the pulp.

i) Schlerotic dentin: This is formed as a result of change in structure of primary dentin. These are hypercalcified areas, found due to aging or as a result of erosion or caries as a protective phenomenon. They forms from the DEJ and proceeds towards the pulp.

j) Dead tracts: With moderate level of injury to dentin like caries, the odontoblast cells along with their processes die leaving empty dentinal tubules. Under transmitted

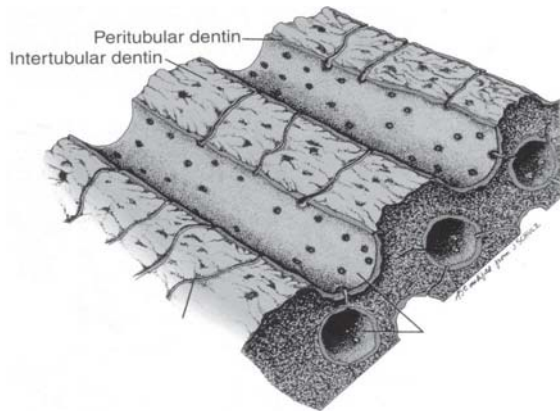


Fig.2.6 Image of Dentin tubules (Adapted from Bhaskar, In Orban's oral histology and embryology. Mosby, 2000).

light, these tubules appear as dark when viewed through microscope, called dead tracts.

2.4.3 Pulp

The pulp is a mesenchymal connective tissue that occupies pulp cavity in the central part of the tooth. It is formed of 75% water and 25% organic matter. It consists of collagen fibres, ground substance, vital cells, blood vessels and nerves of the tooth. It is surrounded by dentin on all sides except at the apical foramen and accessory pulp canal opening where it is in communication with periodontal tissue. Morphologically the pulp is divided into two parts namely

1. Pulp chamber/Coronal pulp: This occupies the pulp chamber in the crown portion of the tooth. The extension of pulp chamber into the cusps of tooth, called pulp horns, that project towards the incisal ridges.

2. Root canal/radicular pulp: This is located in the root portion of the tooth in the pulp canal. It is continuous with the periapical tissues via apical foramen.

Structurally the dental pulp contains myelinated and unmyelinated nerves, arteries, veins, lymph channels, connective tissue cells, intercellular substance, odontoblasts, fibroblasts, macrophages, collagen and fine fibres (Fig. 2.7) as described below:

a) Cells: The cells of pulp are of three types namely odontoblasts, fibroblasts and defence cells. The outermost layer of the pulp is made of *odontoblasts*. They are highly differentiated connective tissue cells, which have a nucleus. Each cell extends into one main (Tome's process) and several small cytoplasmic processes. They are responsible for the formation, nutrition and sensitivity of dentin. Inner to that, is the cell free zone, which is filled with both nerve and vascular plexuses. Adjacent to cell free zone is the cell rich zone composed of fibroblasts and undifferentiated mesenchymal cells. Fibroblasts are flat and have an oval nucleus and elongated processes.

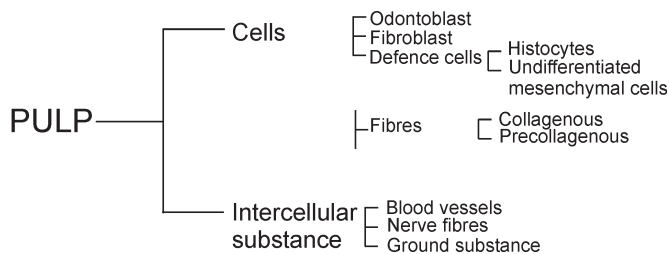


Fig.2.7. Flow chart showing the composition of pulp

b) Intercellular substance: They consist of ground substance and fibres. The ground substance is gelatinous. The fibres are of two types namely precollagenous or Korffs and collagenous. The pulp core contains the large blood vessels and nerve trunks, which exit via apical foramen.

2.4.4 Supporting structures

The periodontium is the supporting structure of a tooth, serving to attach the tooth to surrounding tissues and to permit sensations of touch and pressure. It consists of the cementum, periodontal ligaments, alveolar bone and gingiva. Of these, cementum is the only one that is a part of a tooth. Periodontal ligaments connect the alveolar bone to the cementum. Alveolar bone surrounds the roots of teeth to provide support and creates what is commonly called an alveolus. Lying over the bone is the gingival or gum, which is readily visible in the mouth.

1. **Cementum**: This is a hard tissue formed by the specialized cells called cementoblasts, derived from the undifferentiated mesenchymal cells of the dental follicle. It covers the radicular portion of the dentin. It consists of 45% of hydroxyapatite, 33% of organic material mainly collagen and protein polysaccharides and 22% water. This is light yellow in colour and is slightly softer than dentin. Cementum most often joins with enamel forming cemento-enamel junction. The principal role of cementum is to serve as a medium by which periodontal ligaments can attach to the tooth for stability. Structurally cementum consists of two layers namely acellular cementum, which is seen on the coronal half of the root and does not have cells in their structure and cellular cementum, predominates on the apical half and has cementoblasts.

2. **Periodontal ligament**: This is a connective tissue with stratified squamous epithelial lining that attaches the cementum of the tooth to the alveolar bone. It contains blood vessels, nerves and extracellular substance mainly of collagen fibres and ground substance. The function of periodontal ligaments is to provide attachment of the tooth to the bone, support for the tooth, formation and resorption of bone during tooth movement, sensation and eruption.

3. **Alveolar process**: This is a thin, compact bone which is a part of the maxilla and mandible. It forms the socket into which the tooth root fits. It is composed mainly of inorganic material (hydroxyapatite) and some organic matrix (Type I collagen, glycoproteins and proteoglycans). Alveolar bone consists of three parts mainly:

a) Inner and outer cortical plates: These form the outer and inner plates of the

alveolar process. The cortical plates and the alveolar bone proper, meet at the alveolar crest.

b) Alveolar bone proper: This is the inner wall of the alveolar process which lines the socket. It surrounds the tooth root and provides attachment to the principal fibres of periodontal ligament.

c) Cancellous bone: This is the spongy bone consisting of narrow, irregular bony trabeculae that fills the inner area between the cortical plates and the alveolar bone proper.

4. **Gingiva:** They are the soft tissues which surround the cervical region of teeth. It is that part of the oral mucosa which covers the alveolar bone, defines the contours of the crown and seals the tooth root and periodontal structures from the external environment. It is coral pink in colour and normally pigmented. It consists of free gingiva, attached gingiva and alveolar mucosa. The part of the gingiva below the crest but above the attachment is called the free gingival margin. The potential space between the free gingival margin and the tooth is called the gingival sulcus. Just below the epithelial attachment lie a large number of connective tissue fibres called the gingivo-dental fibres.

2.5 LIGHT

Light is a form of electromagnetic energy that behaves as a particle and a wave. Laser light and ordinary light are significantly diverse. Light produced by lamp is usually a white diffused glow, comprises a narrow band of about 400 nm in the visible wavelength region of the electromagnetic spectrum, which can be seen by the human eye. Table 2.2 shows the wavelength bands of the visible region. Laser light have some additional characteristics: monochromaticity, collimation and coherency.

a) **Monochromaticity:** lasers emit light that is monochromatic or specifically a single wavelength.

b) **Collimation:** refers to laser beam being well focused and does not spread out like ordinary light

Table 2.2 Wavelength range of visible light in ER spectrum.

| Colour | Wavelength region (nm) |
|--------|------------------------|
| Violet | 400-455 |
| Blue | 455-492 |
| Green | 492-577 |
| Yellow | 577-597 |
| Orange | 597-622 |
| Red | 622-780 |

c) Coherency: means that the light waves produced are all similar. They are all in phase with one another and have the same wave shapes.

2.5.1 Basic aspects of light-tissue interaction

The extent of the light interaction with tissue is governed by the specific wavelength of the excitation light used and the optical properties of target tissue. Light encounters with tissue in different ways. It can be reflected, scattered, transmitted or absorbed. The absorbed energy may be also re-emitted as fluorescence. Dental structures have complex composition and these processes occur together in some degree relative to each other. Fig. 2.8 illustrates the different phenomena that occur when light interacts with dental tissues.

a) Reflection: Light photon is reflected from the tissue surface without penetration or interaction with the tissue.

b) Scattering: Photon is scattered from structural components of the tissue.

c) Transmission: Photon is transmitted through the tissue.

d) Absorption: Photon is absorbed by the endogenous substance present in tissue.

e) Fluorescence: It is an inelastic scattering process, also occurs by the absorption of molecules in the tissue.

f) Diffuse reflectance: Photons undergoes multiple scattering and absorption in the tissue.

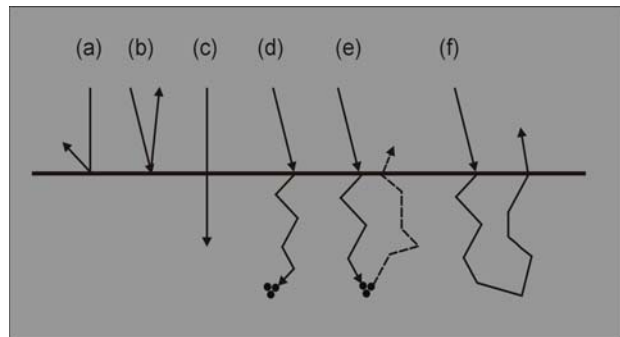


Fig.2.8. Different processes of light-tissue interaction a) Reflection b) Scattering c) Transmission d) Absorption e) Fluorescence f) Diffuse Reflectance. Black dots shown are either tissue chromophore, fluorophore or a scatterer.

In most cases, the degree of interaction is proportional to the absorption of light by tissue. The degree of absorption and the extension of this process are dependent upon the tissue structure, content of water, haemoglobin, enamel, dentin, hydroxyapatite etc. Tissue elements that demonstrate a higher coefficient of absorption

for particular wavelength or spectra of light energy are called chromophores. Absolute values of absorption coefficients for typical tissues lie in the range, 10^2 - 10^4cm^{-1} (Tuchin, 2007). Fig. 2.9 illustrates the optical absorption properties of water, hemoglobin and melanin. Between approximately 600 nm and 1300nm, the absorption due to water is very low. At shorter wavelengths, haemoglobin absorption is large, and at higher wavelengths the strong water absorption drastically reduces light penetration. Light in this wavelength region, often referred to as the tissue optical window, is used for many diagnostic and therapeutic purposes, offering a possibility to reach targets deep into the tissue (Boulnois, 1986).

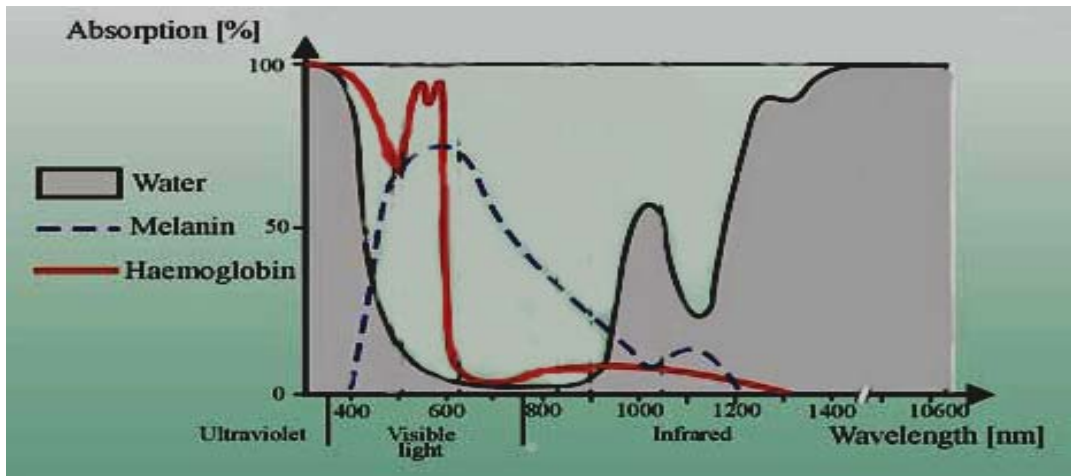


Fig.2.9. Optical absorption properties of water, hemoglobin and melanin.

2.5.2 Optical properties of hard tissues

Optical characteristics of the hard tissues of human teeth are of significant importance in modern dentistry. Optical properties are native properties that characterize biological tissues, which do not depend on the geometry of the structure. Low-intensity laser light can be used for diagnostic applications. The optical properties of dental tissue components resolve the nature and degree of the tissue reaction through the processes of absorption, transmission, reflection and scattering of the light (Dederich, 1991). To make progress in employing optical techniques especially laser methods in dentistry, basic knowledge of the optical characteristics of dental hard tissues is necessary.

2.5.2.1 Spectral properties of enamel and dentin

Enamel is an ordered array of hydroxyapatite crystals surrounded by protein/lipid/

water matrix (Fried, 2003; Zijp and ten Bosch, 1991; Levy and Rizoïu, 1995; Tuchin and Altshuler, 2007). Comparatively well-oriented hexagonal hydroxyapatite crystals of ~30-40 nm in diameter and up to 10 μm in length, are packed into an organic matrix to form enamel rods or prisms with an overall cross section of 4-6 μm (Tuchin and Altshuler, 2007). Fig. 2.10 shows the absorption spectra of enamel. The absorption peaks were seen at 200, 600, 700, 1064, 9320 and 9900 nm (Arcoria and Miserendino, 1995). The specificity of the dentin is known by the dental tubules that communicate with the enamel, pulpal surface and cementum.

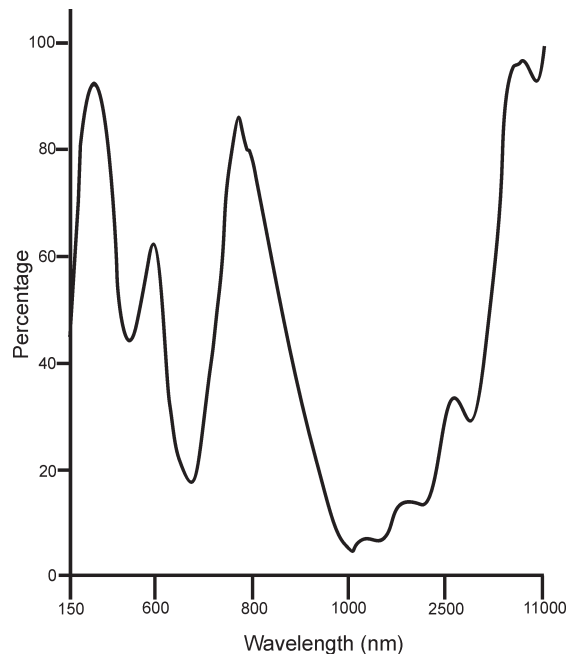


Fig.2.10. Absorption spectra of enamel from 150 to 11000 nm (Modified from Arcoria C and Miserendino L.J. in *Laser in Dentistry*, Eds. L. J. Miserendino and R. M. Pick (Quintessence Publ. Co, Inc, Chicago, et al), 1995; 76.

Enamel and dentin are considered to be optical systems with wave-guiding, absorption and scattering components (Altshuler et al, 1991; Zijp and ten Bosch, 1991). The absorption and transmission of light in teeth is generally dependent on the wavelength of the excitation light (Koort and Frentzen, 1992 a). Ultraviolet laser light is well absorbed by water and hydroxyapatite. However in the mid-infrared region, the absorption of water and hydroxyapatite (HA) varies immensely depending on the wavelength of laser light (Fig. 2.11). Absorption of water and HA is low at wavelength of 2 μm as compared to the high absorption at 3 μm and 10 μm . At 1 μm , both show absorption of about 10,000 times less than that at 3 μm (Hale and Query, 1973; Nagasawa, 1983; LeGeros, 1991).

Figure 2.12 illustrates the transmittance (T), reflectance (R) and absorptance (A) spectra of sound enamel, dentin and hydroxyapatite recorded in the 250-2500 nm wavelength range. The major absorptance peaks of sound enamel are at 283, 1434 and 1944 nm (Levy and Rizoïu, 1995). The dentin has prominent peaks at 283, 1471 and 1942 nm and few minor peaks at 1184, 1737, 2164 and 2264 nm. The

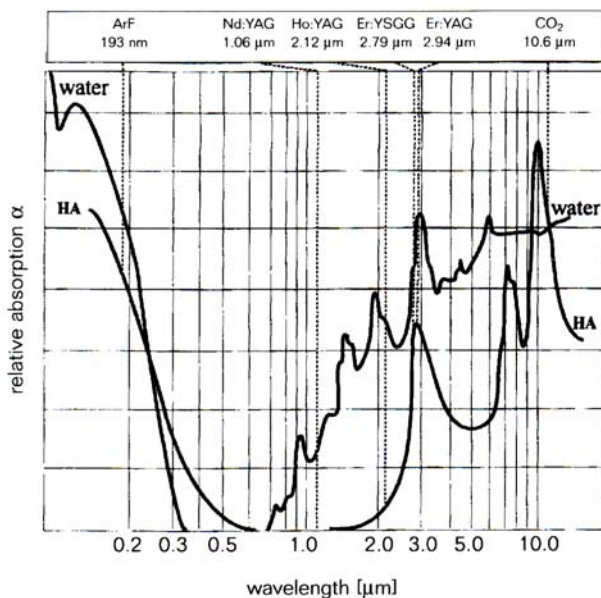


Fig.2.11. Absorption of laser light in water and hydroxyapatite from 200 nm to 10 μm (Adapted from Koort HJ and Frentzen M. in *Laser in Dentistry*, Eds. L. J. Miserendino and R. M. Pick (Quintessence Publ. Co, Inc, Chicago, et al), 1995; 59.

a valley in reflection or transmittance spectrum. The transmittance spectrum shows a valley at 950, 3570 and 9410 nm for enamel and at 950 nm for hydroxyapatite. For dentin, transmission spectra shows valleys at 3000, 5880 and 9090 nm in the far infrared region (Levy and Rizoiu, 1995).

Dental hard tissues are anisotropic (Zijp and ten Bosch, 1993; Fried et al, 1995; Kienle et al, 2003 Altshuler and Erofeev, 1995). Absorption and scattering of light are much stronger in dentin than in enamel. Thus the scattering coefficient is much larger than the absorbing coefficient (Zijp and ten Bosch, 1993; Levy and Rizoiu, 1995). In the visible-near-infrared region, enamel and dentin shows small values of absorption coefficient of $1-4\text{cm}^{-1}$ as compared to high values of scattering coefficient ($15-280\text{cm}^{-1}$). In spite of this lower values, light absorbed by these tissues is relatively high, of 10-20% (Table 2.3). This is due to high efficiency of travelling photons to be absorbed in a scattering medium, caused by the longer photon pathways within the scattering medium (Tuchin and Altshuler, 2007). Light scattering and reflection at the enamel surface is essential for the studies of scattering properties of tooth, which helps to accurately measure the condition of enamel

peaks at 1434 and 1944 nm coincide with the absorption peaks of water (300, 980, 1180, 1450, 1900 and 2940 nm) and hydroxyapatite bands (~ 250 , 1434, 2145 and 2410 nm). Between 2700 and 2900 nm, the absorption of water and hydroxyapatite is very strong (Wigdor et al, 1994). Organic tooth components (protein) are responsible for absorption in ultraviolet region (Tuchin and Altshuler, 2007). The spectra of reflectance and transmittance for enamel, dentin and hydroxyapatite are the reverse of the absorbance spectrum, so each peak in absorption is now

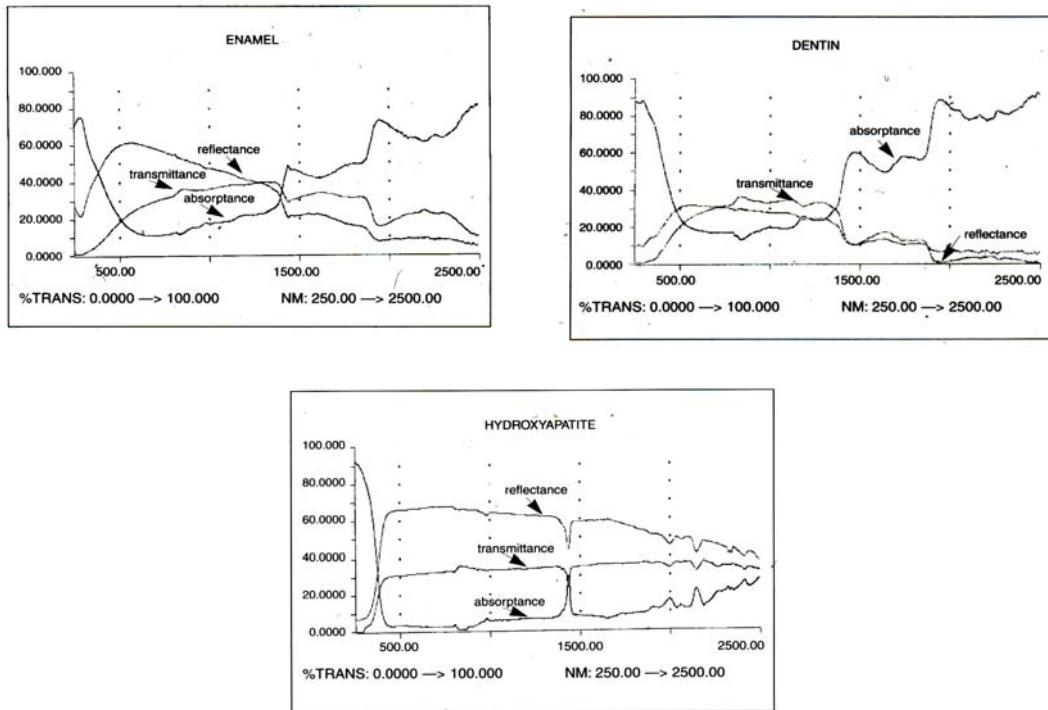


Fig.2.12. Spectra of absorbance, transmittance and reflectance for sound enamel, dentin and hydroxyapatite. (Adapted from Levy G and RizoIU IM. in *Laser in Dentistry*, Eds. L. J. Miserendino and R. M. Pick (Quintessence Publ. Co, Inc, Chicago, et al), 1995; 300-302.

surface (Altshuler and Erofeev, 1995). With laser irradiation, the angular distribution of the backscattered light is defined by the enamel surface curvature, surface macro-roughness (large surface irregularity compare to the wavelength mostly of genetic nature) and surface micro-roughness (comparable with the wavelength irregularities). Due to the first two reasons, the specular component of reflected light may change its direction and angular distribution within only several degrees in dependence of incident light beam location. The third component is diffusive in nature and is mainly associated with the processes of tooth demineralization. With increase in demineralization depth, angular distribution of diffuse light is altered, which in turn reduce its maximum intensity. If successful separation is done using specific wavelength or scattering angle, surface diffuse component can be used as a tool for detecting tooth demineralization and pre-caries (white spots).

Table 2.3 Optical properties of dental hard tissues.

| Tissue | Wavelength (nm) | Absorption coefficient, μ_a (cm^{-1}) | Scattering coefficient, μ_s (cm^{-1}) | Remarks |
|--------|-----------------|--|--|--|
| Dentin | 543 | 4 | 180 | Adapted from Zijp JR and ten Bosch JJ, 1991, 1997; Fried D et al, 1995 |
| | 633 | 4 | 130 | |
| Enamel | 543 | <1 | 45 | |
| | 633 | <1 | 25 | |
| Dentin | 543 | 3-4 | 280 | Adapted from Fried D et al, 1995 |
| | 633 | 3-4 | 280 | |
| | 1053 | 3-4 | 260 | |
| Enamel | 543 | <1 | 105 | |
| | 633 | <1 | 60 | |
| | 1053 | <1 | 15 | |
| Enamel | 200 | ~10 | ~450 | Adapted from Fried D, 2003 |
| | 300 | ~5 | ~270 | |
| | 400 | ~1 | ~150 | |
| | 500 | <1 | ~73 | |
| | 600 | <1 | ~64 | |
| | 700 | <1 | ~50 | |
| | 800 | <1 | ~33 | |
| | 1000 | <1 | ~16 | |

Scattering of dentin depends mainly depends on two processes a) symmetrical processes, caused by randomly oriented mineral crystals ($\mu_s \sim 10^{-3} - 10^{-4} \text{ cm}^{-1}$) and collagen fibrils ($\mu_s \sim 190 \text{ cm}^{-1}$) and b) asymmetrical processes, caused by the oriented dentinal tubules ($\mu_s \sim 1400 \text{ cm}^{-1}$).

2.5.2.2 Waveguide Effects

The waveguide properties of enamel and dentin may have some effects on anisotropy of light propagation within the tooth (Altshuler and Erofeev, 1995; Altshuler, 1995, Altshuler and Grisimov, 1990). The role of waveguides in enamel and dentin is played by enamel prisms and substances between dentinal tubules, respectively (Fig. 2.13). These waveguides are differentiated from conventional optical fibres by being non-uniform and containing scattering particles such as hydroxyapatite microcrystals. Nonetheless, they have waveguide properties and radiation scattered in enamel and dentin can be captured by these natural waveguides and transported to the pulp chamber.

The waveguide light propagation in tooth produces the following optical effects

(Altshuler and Grisimov, 1990; Altshuler and Erofeev, 1995; Altshuler, 1995):

a) Image transmission effect: Each point of the enamel surface is optically connected with a certain point of the pulp chamber surface, hence light propagation on the enamel surface would be transmitted to the pulp chamber surface. Apparently, this image could be fairly distorted, because of scattering and waveguide non-uniformity. For example, 1-mm layer of dentin would limit resolution up to 10lines/mm.

b) Effect of optical transparency anisotropy: Light transmission along and transverse to waveguides is not equal. For a section of dentin cut longitudinally and transversely relative to the dental tubules, these differences could be as large as several dozen times. Therefore, waveguide effect could have significant influence on orientation anisotropy of transmittance.

c) Light field compression effect (optical focon effect):

This is caused by the difference of surface areas of the waveguides at the enamel/dentin junction and at the pulp chamber surface as well as number of waveguides is equal. The light field compression can create an increase in light flux density whenever light is propagating from the enamel/dentin junction to the pulp.

The flux density of light is proportional to the ratio of the area of enamel/dentin junction and the part of the pulp chamber surface that is optically connected with enamel/dentin junction.

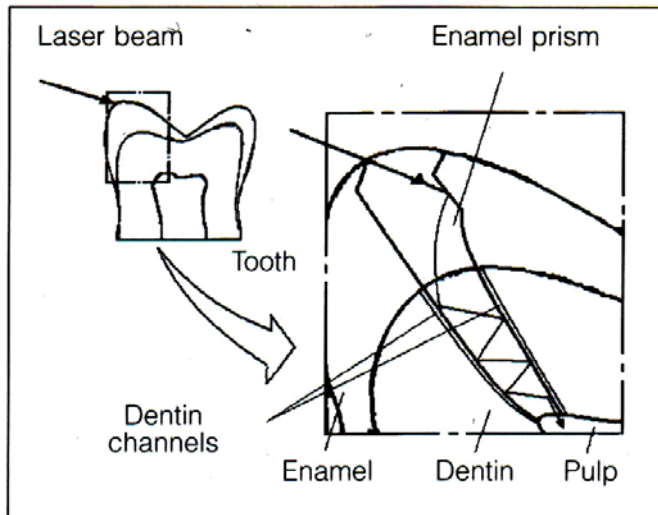


Fig.2.13. Waveguides in human teeth. (Adapted from Altshuler GB and Erofeev AV. in *Laser in Dentistry*, Eds. L. J. Miserendino and R. M. Pick (Quintessence Publ. Co, Inc, Chicago, et al), 1995; 287.

In this way, optical properties of the dental tissue can be achieved by measuring absorption and scattering properties.

2.6 OPTICAL SPECTROSCOPY

Diagnostic techniques based on optical spectroscopy allow non-invasive and real-time characterisation of tissue. Optical spectroscopy depends on the interaction of electromagnetic radiation with dental tissues that occur at the ultraviolet (UV) and visible (VIS) wavelength regions. As compared to current diagnostic approaches, they are fast, quantitative and also provide information about the invasive nature of the disease in highly sensitive manner. In addition, they also elucidate the chemical composition and morphology of the tissue which in turn help in monitoring metabolic parameters of the tissue and also distinguish sound from carious tooth. Further, optical spectroscopic systems are cost-effective and can be easily automated facilitating use by even less skilled personnel. Among all these optical techniques, the present study focuses on fluorescence emission and diffuse reflectance of dental tissues for detecting tooth caries and demineralization. These spectroscopic techniques have the potential to act as an adjunct to dentist so that timely remedial measures can be adopted to stop the tooth decay.

2.6.1 Fluorescence Spectroscopy

The phenomenon of fluorescence was first discovered by Stokes in 1827, when he illuminated fluorite samples with UV light and found these samples emit at longer wavelength. Until the beginning of the 20th century, the potential of fluorescence for medical applications was not considered. In 1911, Stubel found that all animal tissues emitted fluorescent light when irradiated with UV radiation.

2.6.1.1 Basic principles

When a biological molecule is irradiated at an excitation wavelength, which lies within the absorption spectrum of that molecule, it will absorb this energy and be excited from its ground state (S_0) to a higher state (S_1). The molecule can then return back from the excited state to the ground state by generating energy in the form of fluorescence, at emission wavelengths, which are longer than that of the excitation wavelength. This is illustrated schematically in Fig. 2.14. Absorbing molecules, known as chromophores, that release their excess energy by emitting fluorescence light are usually called fluorophores. The fluorescence phenomena exhibit several general characteristics for a particular biologic molecule (Lakowicz, 1983). First, due to losses in energy between absorption and emission, fluorescence occurs at emission wavelengths, which are always red-shifted, relative to the illumination wavelength. Second, the emission wavelengths of fluorescence are independent of the excitation

wavelength. Third, the fluorescence spectrum of a biologic molecule is generally a mirror image of its absorption spectrum.

2.6.1.2 Autofluorescence and Endogenous fluorophores

Tissue autofluorescence originates from native tissues.

Under UV and blue light irradiation, all biological tissues

emit fluorescence from various endogenous fluorophores in tissue with a broad distribution in the visible wavelength region. This fluorescence is referred to as autofluorescence, or endogenous fluorescence. The spectrum is also influenced by the optical properties of tissue. Strong absorbers such as hemoglobin may decrease the overall intensity of the fluorescence spectrum, without changing its shape, by absorbing the excitation light (Chance, 1962; Gillenwater et al., 1998). It can also absorb fluorescence light at certain wavelength which in turn changes the appearance of the recorded fluorescence spectrum by generating dips in the spectrum and the illusive presence of the false peaks. Naturally, the shape of the spectrum also depends on the excitation wavelength, since this will determine what energy transitions in the fluorophores are possible. Most often, excitation in the UV or blue wavelength region is used for laser-induced fluorescence (LIF) studies of tissues. The autofluorescence spectra are very complex, and the contributions from the different fluorophores cannot usually be separated, but can be recognized by their emission peaks.

Biological tissues are made up of a very intricate mixture of molecules. Several of these molecules are fluorescence emitters, when excited with a suitable wavelength. The mixture of all these emission spectra as well as the diffusion and scattering properties of the biological tissues make the overall autofluorescence spectrum broad and quite featureless (Zeweller, 2000).

Table 2.4 lists the major endogenous fluorophores, along with their excitation and emission maxima (Richards-Kortum and Sevick, 1996). These endogenous fluorophores include the aminoacids, structural proteins like collagen and elastin, coenzymes like NADH and flavins, vitamins, lipids and the porphyrins. Their excitation

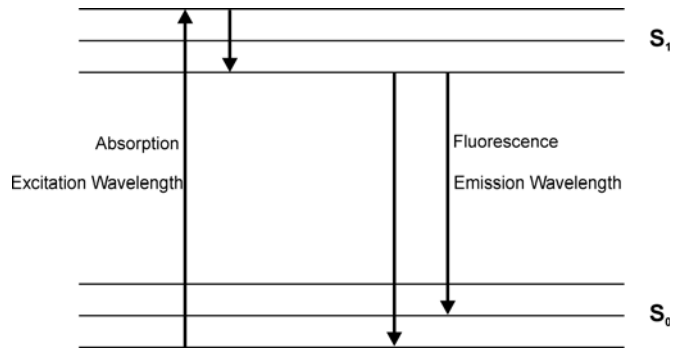


Fig.2.14. Energy level diagram showing the phenomena of absorption and fluorescence.

Table 2.4 Excitation and emission maxima of various endogenous fluorophores.

| Endogenous Fluorophores | Excitation maxima(nm) | Emission maxima (nm) |
|--|----------------------------|--------------------------------------|
| Sound tooth structure | 337, 375 | 430-450, 480-500, 460, 560 |
| Bacteria (mature plaque, dental caries) | 320-380, 407, 360-580, 655 | 590-650, 635, 600-700, 720-800 |
| Porphyrins | 405, 407, 400-450, 630 | 590, 610, 620, 635, 675, 690, 705 |
| Supra and subgingival calculus | 420 | 595, 635, 650, 695 |
| Aminoacids | | |
| Tryptophan | 280, 295 | 350, 340-350, 345 |
| Tyrosine | 275 | 300, 340 |
| Phenylalanine | 260 | 280 |
| Structural proteins | | |
| Collagen | 270, 325, 330, 335 | 380, 390-405, 395, 400, 405, 460-490 |
| Collagen cross-links | 370 | 340, 400, 420, 460 |
| Elastin | 290, 325, 350, 360 | 500, 500-540 |
| Elastin cross-links | 390-420, 400, 420-460 | |
| Coenzymes | | |
| FAD, Flavins | 430, 450 | 515, 535, 550 |
| NADH | 290, 340, 350, 365 | 440, 450, 455, 460 |
| NADPH | 336 | 464 |
| Lipids | | |
| Phospholipids | 436 | 540, 560 |
| Lipofuscin | 340-395 | 430-460, 540 |
| Ceroid | 340-395 | 430-460, 540 |
| Vitamins | | |
| Vitamin A | 327 | 510 |
| Vitamin K | 335 | 480 |
| ... | ... | ... |

maxima lie between 250 and 450 nm, whereas their emission maxima lie in the range 280 and 700 nm. Autofluorescence emission spectra of tissue are basically a convolution of the emission spectra of the endogenous fluorophores of tissue and therefore strongly depend on the wavelength of excitation light (Gupta et al, 2007). Only those endogenous fluorophores are excited and emit fluorescence whose absorption bands have an overlap with the wavelength of excitation light. Since, the excitation and emission light have to propagate through the turbid tissue, the recorded autofluorescence is also influenced by the absorption and scattering at both the excitation and the emission wavelengths (Muller et al, 2001). Fig. 2.15 shows the a) absorption and b) emission spectra of different endogenous fluorophores.

Fluorophores that are speculated to play a major role in caries processes are the structural proteins like collagen, porphyrins and bacteria. Collagen and elastin are fibrous proteins abundant in connective tissues, teeth and bones. Collagen forms the organic part of the dentin and any structural or pathologic association with caries processes, could be reflected in lower autofluorescence intensity (Sarkissian and Le, 2005).

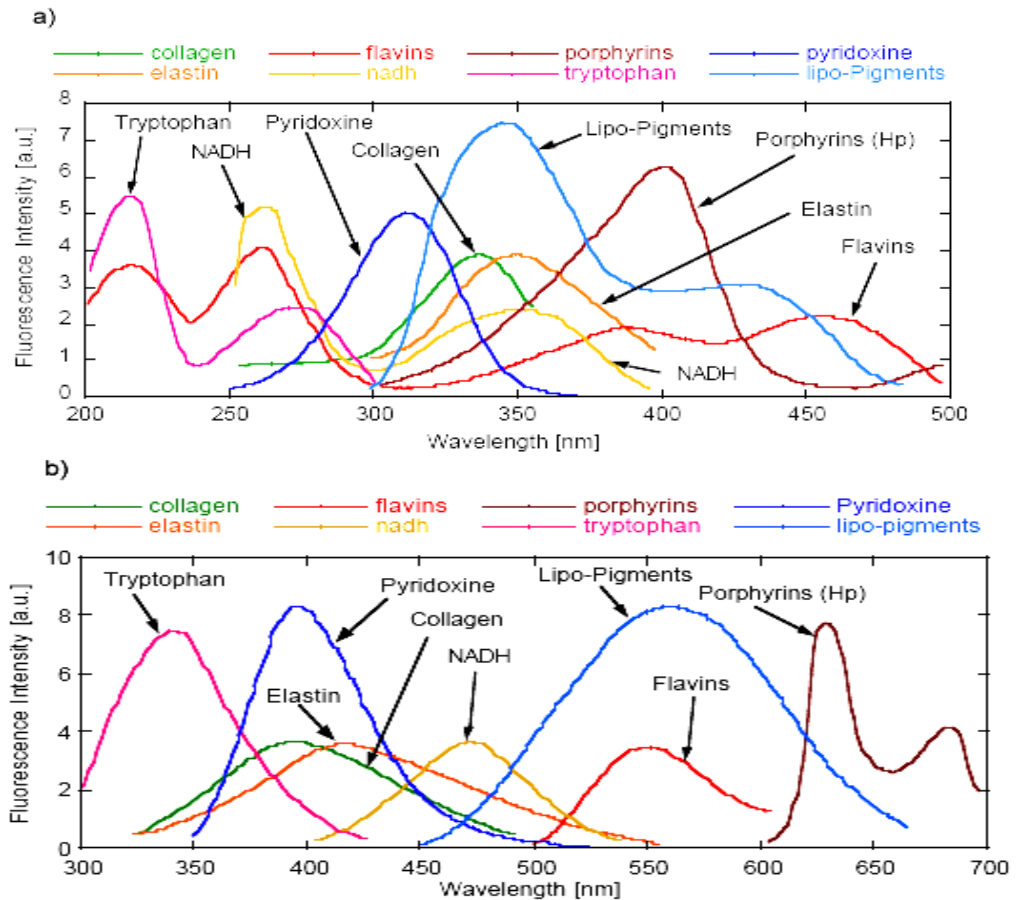


Fig.2.15. a) Absorption spectra and b) emission spectra of different fluorophores in biological tissue. Adapted from Wagner et al, 1998).

Porphyrim derivatives i.e., porphyrins and metalloporphyrins, are responsible for fluorescence emission from carious tooth in the red wavelength region (Konig et al, 1993; Konig and Schneckenburger; 1994, Konig et al, 1998; Lenon et al, 2002; Buchalla et al, 2005). They typically have absorption maxima between 398 and 421 nm and emission maxima between 530 and 633 nm (Konig and Schneckenburger; 1994). The excitation spectra also support the assumption of the presence of porphyrin derivatives due to a maximum around 400 nm that may represent the near-UV Soret band typical for porphyrins. PpIX concentration is found to be higher in gram negative

oral bacteria and its level increases as the dental bio film becomes more mature, which is responsible for the red fluorescence in teeth (Walsh and Shakibaie, 2007). Brick red fluorescence seen under long-wave UV light (366 nm) is due to protoporphyrin production by the pigmented *Bacteroides* species (Brazier, 1986; Konig et al, 1993; Bissonnette et al, 1998), and to coproporphyrin production by *Corynebacterium* species and *Candida albicans* (Konig et al, 1993). When excited with 407 nm UV light, bacterial species such as *Actinomyces odontolytics* (found in dentin carious lesions), *Bacteroides intermedius*, *Prevotella intermedia*, *Corynebacterium* species and *Candida albicans* emit fluorescence at 620-635 nm and 700 nm, whereas Gram positive *Streptococcus mutans*, *Enterococcus faecalis* and various *Lactobacilli* have weaker porphyrin fluorescence in red wavelength region. Thus the maturity of dental plaque, rather than the presence of cariogenic streptococci, is the basis for the red fluorescence when excited with UV-near UV light. In summary, when dental plaque or calculus is present, there is an increase in absorption in the UV spectral region at 350-420 nm, with the appearance of a fluorescence signal in the visible red spectral region at 590-650 nm (Borisova et al, 2006; Kuhnisch et al, 2003).

2.6.1.3 Detection Principle

When a photon from laser source falls on tooth surface, it gets penetrated and absorbed by several endogenous fluorophores in tissue and these absorbed fluorophores re-emit the light in the form of characteristic LIF spectra (Fig. 2.16). During caries processes, variations are seen in the biochemical composition and/or the structure of the tissue, which in turn is reflected in fluorescence spectral shape and

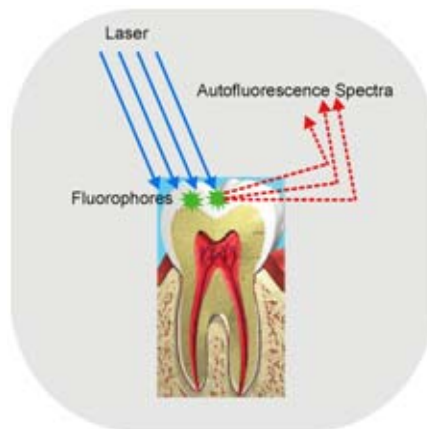


Fig.2.16. Detection principle of LIF

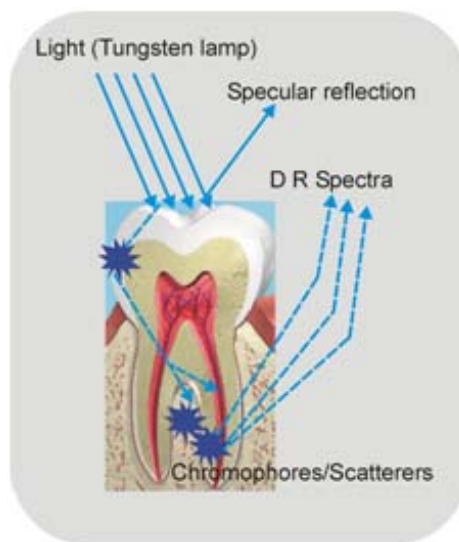


Fig.2.17. Detection principle of DRS

intensity. Generally, alterations in the concentration of these fluorophores take place prior to major structural tissue changes, and this makes LIF very sensitive to early caries detection.

Fluorescence from tissue can be studied in different ways. Excitation spectra are obtained by varying the excitation wavelength while detecting at a fixed wavelength. If the excitation wavelength is constant and the fluorescence is detected at several wavelengths, emission spectra are obtained. In this study, various aspects of the fluorescence spectra such as fluorescence intensity and spectral shape are studied. Changes in fluorescence spectral shape can be understood by different methods; one such possibility is to study variations at different emission wavelengths by changing the excitation wavelength. This method yields fluorescence spectra as a superposition of the fluorescence of all fluorophores present within the tissue volume probed. All these approaches can give information about the endogenous fluorophores, chemical composition and morphology of tissue.

2.6.2 Diffuse Reflectance Spectroscopy (DRS)

In DRS, light remitted from tissue undergoes a combination of elastic scattering and absorption when illuminated in the ultraviolet–visible (UV–VIS) wavelength range, providing information about tissue absorbers and scatterers, which are believed to change during caries formation (Fig. 2.17). In DRS both the diffuse and specular components of reflectance are detected and the spectrum depends on the absorption and scattering properties of the tissue. The absorption coefficient is directly related to the concentration of physiologically relevant absorbers in the tissue, which include oxygenated and deoxygenated haemoglobin. The scattering coefficient reflects the size and density of scattering centers in tissue. Extraction of the physically meaningful information from DR measurements improves our understanding of the physiological and structural features that differentiates sound and caries tooth, as well as improve the diagnostic potential of optical spectroscopic techniques for diagnosis of dental caries. DR technique is cost-effective as compared to laser based techniques, and has the potential to provide real-time, non-destructive, and quantitative means of characterizing tooth caries.

The theory of diffuse reflection has been studied in detail by many authors (Wendlandt and Hencht, 1966; Kortum, 1969). When an inhomogeneous material is illuminated, a portion of the impinging radiation penetrates the sample while the rest is reflected from the surface. The portion that penetrates the sample undergoes scattering at a large number of points in its path. Fraction of radiation that comes

back, out of the sample, is called diffusely reflected component. The returning reflection of directional incoming radiation flux is scattered in many directions due to uneven, broken, bumpy boundary surfaces, where the coarseness is of the same order of magnitude as the wavelength of incident radiation. In contrast, direct or specular reflection occurs when the roughness of the boundary is small in comparison with the wavelength of the reflected radiation.

2.6.3 LIF and DR Spectroscopy in Caries Research: Current Status

Caries diagnosis is a complex process that involves gathering information from the patient's history, and through clinical and radiographic examination. This information is then evaluated to decide whether caries is present and what action, if any, should be taken. In recent years, clinicians and researchers have become anxious about the diagnosis of caries (Kidd and Joyston –Bechal, 1987; Sawle and Andlaw 1988; Weerheijm et al, 1989; Creanor et al, 1990; Verdonschot et al, 1992; Wenzel and Fejerskov, 1992; Weerheijm et al, 1992 a, b; Kidd et al, 1993, Borisova et al, 2004; Rodrigues et al, 2008). Current clinical techniques for caries diagnosis such as visual inspection and radiographs, or bitewing x-rays, although effective in revealing advanced stages of caries (Kidd, 1994; Verdonschot et al, 1999) are unsuccessful in detecting early caries, especially in the complex anatomy of fissure areas (King and Shaw, 1979). Nevertheless, visual inspection with extensive drying of the suspected area allows early and more accurate diagnosis of initial tooth demineralization (Ekstrand, 2004). Tactile examination with dental probe and radiographic evaluation are often ineffective in detecting enamel defects, as they may be too small or inaccessible to the diagnostic tool. Thus there is a need to develop techniques that can act as an adjunct to the dentist so that timely remedial measures can be adopted to stop tooth decay.

In recent years, there has been a high level of research activity in optical spectroscopy directed towards the development of novel, non-invasive technologies for early detection of dental caries. The physical properties of caries lesion are the basis for the detection and quantification of caries by optical methods, among which are LIF and DR spectroscopy. In dentistry, LIF usually refers to measurement of tooth fluorescence, from fluorescent components (known as fluorophores) after irradiating the tooth with specific laser light that is absorbed by the fluorophores. It has been shown that the fluorescence of carious dental tissues is different from that of sound tissues. This disparity could be used to discriminate between sound and carious tooth structure. Studies have shown that caries lesion progresses

slowly, but has the ability to remineralize (Arends and ten Cate, 1981; Zero, 1999). The nature of caries in enamel layer depends on the physical properties of the lesion (Borisova et al, 2006). Topical application of fluoride compounds to the tooth surface is known to enhance remineralization (Jones et al, 2006). It is also very crucial that caries lesions are thoroughly scrutinized during the period of remineralization treatment, because of the possibility of caries to progress rapidly instead of remineralization. Many research groups have used various optical techniques in caries research (Ando et al, 2001; De Josselin de Jong, et al; 1995; Hall et al, 1997). Different excitation wavelengths or light sources were used to characterize dental caries and also to maximise emission from the endogenous fluorophores.

In 1911, Stubel first introduced optical spectroscopy into the field of dental research when he reported the presence of tooth fluorescence under ultraviolet photo-excitation. Later, Eisenberg (1933) reported the presence of tooth fluorescence under blue or violet light excitation. Alfano and Yao (1981) first published the result of a systematic spectroscopic investigation comparing human teeth with and without dental caries. They illuminated the tooth with excitation light at 350, 410 and 530 nm, which emitted fluorescence at wavelengths of 427, 480 and 580 nm, which corresponds to the peaks for hydroxyapatite. In addition, they noted that, within carious regions, for each of these emissions there was a shift towards the red portion of the spectrum. They also pointed out that the relative intensity of light in the red region was greater for carious when compared to sound regions. Using an argon laser excitation at 488 nm, Albin et al (1988) observed a fluorescence peak around 553 nm in sound teeth, which was red-shifted by ~ 40 nm in caries regions. However, Van der Veen and ten Bosch (1995) observed in demineralised root dentin a shoulder like emission with maximum around 520 nm, which was more pronounced in the demineralised dentin, using excitation wavelengths of 460 and 488 nm.

Nitrogen laser-induced autofluorescence spectra that consist of two peaks at 440 and 490 nm were found to be useful for early differentiation between caries and tooth demineralization (Borisova et al, 2004). An *in-vitro* study by Ribeiro et al (2005) evaluated the ability of a laser operating at 405 nm to detect natural caries lesions with different stages of caries activity. They observed that the fluorescence spectra from non-cavitated caries lesions were significantly different from sound tooth structure and that the two spectral bands around 480-500 nm and 620-640 nm are of significance in caries detection. On the other hand, Zezell et al (2007) found four emissions bands at 455, 500, 582 and 622 nm in both sound and caries regions and observed

that the area under the fluorescence bands at 455 and 500 nm differ significantly for caries lesions and sound tissue.

Many others also have investigated the fluorescence of human dentin and enamel (Bjelkhagen et al, 1982; Hafstrom- Bjorkman et al, 1991; Masychev et al, 2000; Matsumoto et al, 1999; Sundstrom et al, 1985). Hibst and Paulus (1998) proposed that the enhanced fluorescence in the presence of caries results from the presence of bacterial metabolites rather than from demineralization. They found an increased fluorescence emission at 640 and 655 nm from carious enamel or dentin as compared to the intact tissues (Hibst and Paulus, 1999). Konig et al (1999) showed that carious lesions exhibited slower fluorescence decay than intact dental hard tissue. The long-lived fluorophore present in carious lesions only emitted in the red spectral region. Fluorescence decay time and spectral characteristics were typical of metal-free porphyrin monomers (Konig et al, 1998), believed to be produced by the bacteria associated with caries.

In the quantitative light induced fluorescence (QLF) method where tooth is illuminated with a blue-green light that produces fluorescence in the yellow region, the demineralized areas appear as dark spots and their intensity is lower than that of sound enamel. Ando et al (2001) reported that the decrease in fluorescence signal intensity during demineralization is due to destruction of the prism structure in enamel layer and disappearance of its waveguide properties. Pretty et al (2003), in an *in-vitro* study on premolar tooth, evaluated the ability of fluorescence to detect demineralization and remineralization adjacent to bonded orthodontic cleats and found that QLF detects early smooth surface caries lesions and can also monitor demineralization adjacent to restorative materials in primary teeth (2002, 2003). Using argon laser (488 nm) excitation, Al Khateeb et al (1997b) observed that it was possible to detect small changes in fluorescence of demineralized enamel during *in situ* remineralization. This method gave good correlation (0.73-0.86) between mineral loss and fluorescence (fluorescence decreases with increasing mineral loss) for artificial and natural caries lesions (Al khateeb et al, 1997b; Emami et al, 1996).

Commercially available DIAGNOdent device (KaVo, Bilerach, Germany) that incorporates a 655 nm diode laser and displays fluorescence of dental tissues as a numerical value ranging from 0 to 99 (higher values for deeper caries), has the ability to detect near-infrared fluorescence from porphyrins produced by oral bacteria (Eibofner et al, 2000; Hibst et al, 2001; Alexander et al, 2003). This device has been extensively used in various studies to detect changes in mineral content, to assess

remineralization changes and in the detection of caries lesions (Hibst and Gall, 1998; Shi et al, 2000, 2001a; Sheehy et al, 2001; Pinelli et al, 2002; Lussi et al, 2001; Lizarelli et al, 2004; Rocha et al, 2003). DIAGNOdent performed effectively as compared to visual-tactile examination and radiography (Attrill and Ashley, 2001). Occlusal surface studies in adults have shown that the device offers considerable advantages over conventional methods for some lesions (Shi et al, 2000; Lussi et al 2001; Sanchez-Figueras, 2003). However, the device was not able to detect *in vitro* remineralization of natural incipient caries of primary teeth (Fausto et al, 2003). Moreover, the DIAGNOdent reported poor sensitivity (approx. 0.4) for detecting enamel lesions (Shi et al, 2000).

Alkurt et al (2008) found that laser fluorescence showed better performance in detecting occlusal caries *in vivo*, than visual examination and bitewing radiography. With an excitation wavelength of 655 nm, the total intensity of the resulting fluorescence light correlates with the existence of carious lesions (Lussi et al., 2004). Shi et al (2001) has reported a sensitivity of 94% and a specificity of 100% for detecting smooth surface caries with the QLF method, but achieved a lower sensitivity (78-82%) for detecting occlusal caries using DIAGNOdent device (Shi et al, 2006). In this study, the *in vitro* diagnostic accuracy of DIAGNOdent measurements in terms of area under the ROC curve was significantly higher (0.96) than that of conventional radiography (0.66). In another study, Lussi et al (2001) reported a sensitivity of 92% for detecting occlusal caries using DIAGNOdent device as compared to visual inspection and bitewing radiography. Whereas, in an earlier study, Ferreira-Zandona et al (1998) observed a sensitivity of 49% and specificity of 67% with ROC value of 0.78 for detecting demineralization in occlusal pits and fissures.

Another quantitative optical technique, DRS is one of the simplest and most cost-effective methods for understanding biological tissue characteristics (Nichols et al., 1997; Zonios et al., 1999; Utzinger et al, 2001). The application of DRS has been quite useful for characterization of small tissue samples and different cell layers with high sensitivity and specificity, but its application in a clinical environment is still very difficult (Bakker et al., 2000). The potential for using diffuse reflectance spectroscopic techniques is greater because elastic interactions are much stronger than inelastic interactions. Several researchers have used diffuse reflectance spectroscopy to study biological tissues and in caries research (Farell et al., 1992; Weersink et al, 1997; Uzunov et al, 2003)

Diffuse reflectance spectroscopy in the UV–VIS wavelength range measures

tissue absorption and scattering, which reflect the intrinsic physiological and structural properties of dental tissue. On illuminating carious tooth with light in 450-900 nm region, a significant reduction in reflectance spectral intensity was observed by Uzunov et al (2003) due to the import of exogenous molecules. They also found that reflectance spectral intensity ratios R_{500}/R_{900} and R_{750}/R_{900} decreases significantly by 158% and 32.4% respectively, between sound and deep cavitation tooth. Borisova et al (2007) observed significant decrease in the reflected light intensity between caries and non-caries lesions in the blue region. They developed an algorithm for differentiation between carious stages with diagnostic accuracy up to 86.1% between precarious stage and sound tooth, and 100% for determination of deep cavitation

2.7 CONCLUSION

LIF and DR spectroscopy are impending tools in dentistry for the early detection of tooth caries and demineralization, which can be used separately or in conjunction. On the basis of the progress made in optical spectroscopy, a compact, non-invasive, near real-time optical point-monitoring system was developed for early detection of dental caries *in vivo*. The next chapter describes the details of the system developed, along with various ethical concerns, study protocol, and different methods of data analysis, processing and interpretation.

Chapter 3

Experimental Methods

3.1 INTRODUCTION

Dental practitioners have been usually plagued with diverse problems pertaining to the diagnosis and treatment of oral diseases. In the past decade, key technologies such as (a) compact lasers, (b) CCD detectors and (c) easy-to-use computing platforms combined with fiber-optic coupled instrumentation has lead to the development of many photonics based diagnostic and therapeutic methods in dentistry. Rapid detection and non-invasive tissue categorization are the most important advantages of photonics based methods.

Optical spectroscopy in dentistry is crucial for early detection of dental caries, to carry out more effective minimally-invasive targeted-therapies and to restore diseased tissues functionally and aesthetically. Optical methods can be based on the properties of light scattering, absorption and fluorescence. In doing so, lasers and classical light sources can be used. All of these methods have one basic principle in common; the optical spectrum of a tissue contains information about the biochemical composition and/or the structure of the tissue, which provide diagnostic information for tissue characterization. Among them, the most promising techniques to detect and classify different stages of caries are those based on the quantitative measurements of tooth autofluorescence and diffuse reflectance. These techniques are non-destructive and allow detection of structural and elemental changes on the surface and inside of tooth.

Many research groups have used optical spectroscopic techniques to describe the spectral properties of tooth structure at different excitation wavelengths (De Josselin de Jong et al, 1995; Hall, 1997; Uzunov et al, 2003; Borisova et al, 2004; Ribeiro et al, 2005). When tooth is irradiated with UV or blue light, several fluorophores in tissue produce a broad fluorescence distribution in the visible wavelength region. This fluorescence is referred to as the autofluorescence, or endogenous fluorescence. Optical properties of caries lesion differ from sound tooth. The fluorescence image of carious area appears darker than the surrounding normal surface, as a result of reduced fluorescence signal from lesion (Ando et al, 2001; Ko et al, 2000; Al Khateeb et al, 1998). Possible explanation for the changes in fluorescence lies with the variation in light scattering, destruction of the prism

structure of enamel and disappearance of its waveguide properties. Strong absorbers, such as haemoglobin, may also influence the overall intensity of the fluorescence spectrum, without changing its shape, by absorbing the excitation light (Chance et al, 1962).

Further, chromophores present in caries have strong absorption in the ultraviolet and blue-green spectral regions. This absorption dominates over signal in the shorter wavelength region and results in diminished diffuse reflectance spectral intensity in the 400-600 nm range (Bonnet et al, 1995; Uzunov et al, 2003). Hence, the use of laser-induced fluorescence and diffuse reflectance spectroscopic techniques still seems to be a promising tool for characterization of dental caries.

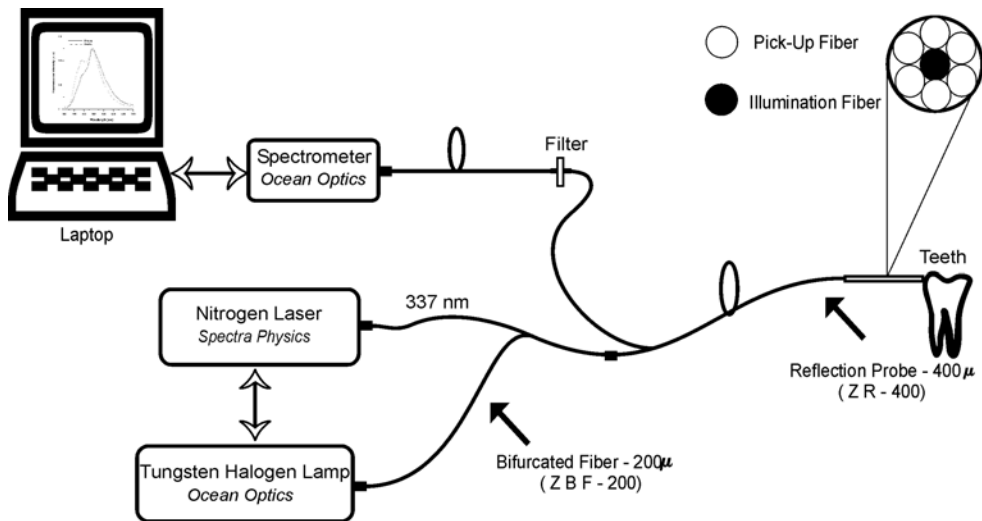


Fig.3.1. Schematic of the LIFRS system developed for caries detection.

3.2 POINT MONITORING SYSTEMS

In recent years, optical spectroscopy has developed into a novel, non-invasive technology for early detection of dental caries. Often, these optical techniques can be either point monitoring or imaging systems. Measurements using point monitoring systems involve the collection of spectroscopic information from a small area of the tooth sample using a fibre-optic probe that has an excitation fibre to deliver the light and a set of collection fibres to collect the tooth fluorescence or reflectance. The

fluorescence light collected is usually very weak compared to the excitation light, hence the detector system must be sensitive and the ambient background light must usually be efficiently suppressed. This can be achieved by using proper detection and filtering systems.

In order to facilitate the sequential measurements of fluorescence and diffuse reflectance from tooth in a clinical setting, we have used a compact, non-invasive LIFRS system that detects the weak fluorescence and diffuse reflectance spectral signatures. Details on data acquisition using LIFRS and the various techniques adopted for data analysis are also given in this chapter.

3.3 DEVELOPMENT OF LIFRS SYSTEM FOR CARIES DETECTION

The LIFRS system for point monitoring of tooth fluorescence and diffuse reflectance is shown in Fig.3.1. The system consists of two light sources that could be switched for alternate recording of fluorescence and diffuse reflectance from the same sample maintained under identical conditions. The diffuse reflectance (DR) spectrum of the sample was obtained using a tungsten halogen lamp (Ocean Optics, USA, Model: LS-1-LL) with a Teflon diffuser at the output port and fluorescence measurements were performed using the 337.1 nm emission from a nitrogen laser (Laser Science, USA, Model: VSL-337, 30kW peak power, 120 μ J pulse energy). Typical emission spectra of a tungsten halogen lamp are shown in Fig. 3.2. The nitrogen laser was operated at a repetition rate of 7Hz and the laser output was focussed on to the central fiber of a 3-meter long bifurcated optical fiber (Ocean Optics, BIF 200 UV-VIS) with the help of a fiber-optic focusing assembly (Laser Science, USA, Model; Hyrax 337702,). This probe has six pick up fibres (400 μ m dia., each) surrounding the central fiber to collect reflectance or fluorescence emanating from the tooth. The probe tip is terminated in a stainless steel ferrule, 15

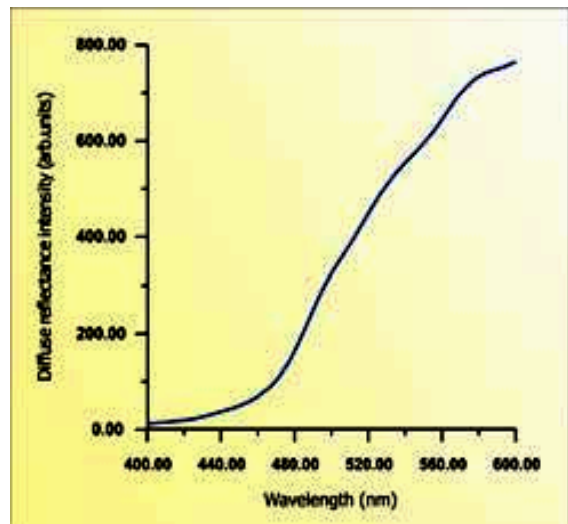


Fig. 3.2 Spectra of tungsten halogen lamp recorded in the 400-600 nm wavelength region, scattered by a ground-glass plate.

cm long and 6 mm diameter (Fig.3.3). The light emanating from the sample is delivered to a miniature fiber optic spectrometer (Ocean Optics, USA, Model: USB 2000FL VIS-NIR), which is connected to the USB port of a laptop computer for spectral data acquisition and storage. The miniature fiber-optic spectro-meter has a 600 lines/mm, 500 nm blazed grating for operation in the 360-1000 nm wavelength range. Fig.3.4 illustrates the optical geometry of collection and illumination fibres, used in this study.

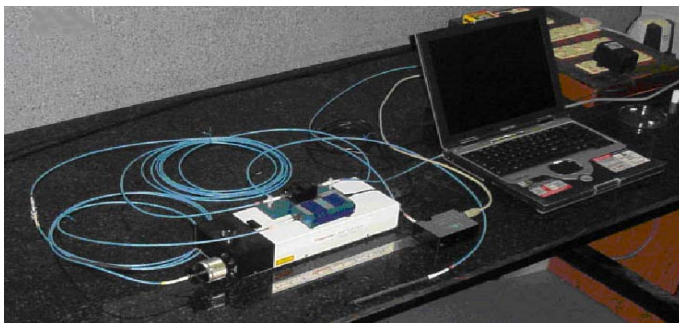


Fig. 3.3 Compact nitrogen laser based LIFRS system developed for caries detection.

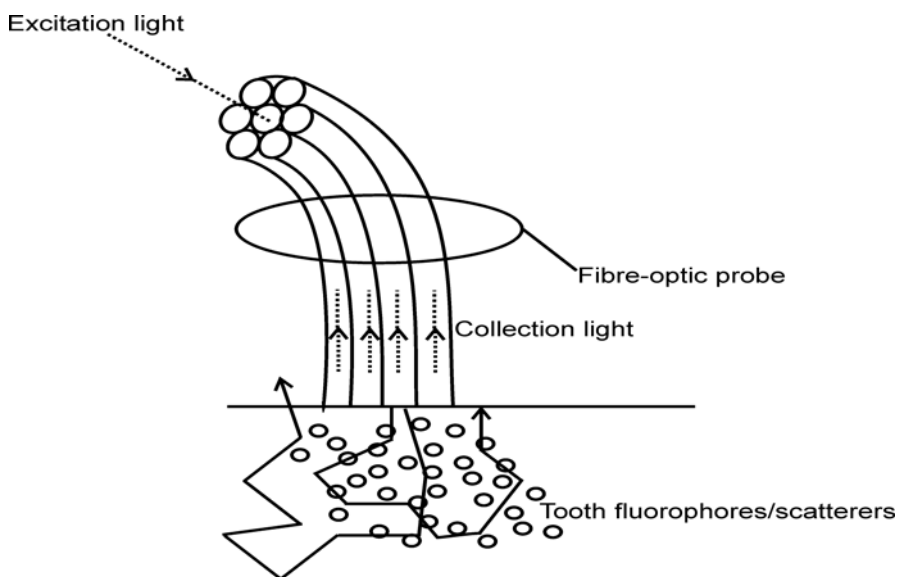


Fig. 3.4 A schematic diagram showing the optical geometry of the fibre-optic probe used in optical contact with the tooth.

During fluorescence studies, a long-wavelength pass filter (Schott, USA, Model: GG385) was mounted inside the inline filter holder (Ocean Optics, USA, Model: FHS-UV) for blocking the scattered laser light from entering the spectrometer. The LIF and

DR spectrum were recorded in the 350–700 nm spectral range at a resolution of 8 nm with the 2048-element linear silicon CCD array of the spectrometer using the OOI Base32 software provided by Ocean Optics Inc., USA. The stainless steel ferrule at the probe tip enables sterilization before and after use in boiling water. A flexible 10 mm long, black PVC sleeve inserted at the probe tip avoids ambient light from entering the detection system and also provides extra hygiene as it is disposable after each measurement (Fig.3.3). The separation between the probe tip and the sample was optimized (by observing the output signal) to a distance of 3.5mm; in which the excitation beam completely overlaps with the collection region. During spectral measurements the output power at the illumination fiber tip is maintained at 1 ± 0.1 mW by monitoring the optical power before and after study on a laser power meter (Nova, Ophir, Israel) that has a suitable photodiode head (Ophir, PD300). The power density at the probe tip is measured in mW/cm^2 , which gives the concentration of photons in a unit area. Total light dose on tooth samples during measurement is measured in J/cm^2 , which is the product of the fluence rate (W/cm^2) and the illumination time (sec). In the present study, light dosage on tooth samples were maintained within $0.002 \text{ J}/\text{cm}^2$, which is lower than the levels that cause any damage to the oral tissues or tooth.

3.3.1 Compact LIFRS system for Clinical Trials

The main drawback of the system when used with 337.1 nm nitrogen laser was the low output power available for the excitation of the fluorescence from tooth which in turn affected the signal to noise ratio of the detection system. Therefore the nitrogen laser was replaced with a 404 nm diode laser (Stocker Yale, Canada, Model: TEC-XXX-404S-50-SF, 50 mW, CW). The modified version of LIFRS system shown in Fig.3.1 is used for clinical trials. Further, in order to provide easy accessibility of the buccal and lingual sides of molar teeth, the fibre-optic probe shown in Fig.3.2 was replaced with a stainless steel hand piece (12.5 cm long) with an angled tip (5cm long and 0.4 cm diameter) shown in Fig. 3.5. This hand piece uses a single fiber for delivering the excitation beam to the tooth and collecting the light emission. Further, the long-wavelength pass filter, Schott: GG385



Fig.3.5. Stainless hand piece used for clinical studies.

was replaced with Schott: UG420, as this system uses a 404 nm diode laser. The whole LIFRS system consisting of a diode laser, tungsten halogen lamp, the inline filter holder and the miniature spectrometer, which was enclosed in a rectangular box of dimensions 12 x 8 x 3 inches made of acrylic sheet. The fiber optic cables and power supply chords were taken out through slots made in the box. These cables could be easily removed and refitted, without the need for realignment, to get the required power levels at the fiber tip. Fig. 3.6 shows the top view of the compact and portable LIFRS system.



Fig. 3.6 Top view of the portable LIFRS developed for clinical studies of dental caries, with diode laser at the bottom, spectrometer to the left, in-line filter holder at top and tungsten halogen lamp aligned at centre of an acrylic box of dimensions 12 x 8 x 3 inches.

3.4 DATA ACQUISITION AND ANALYSIS

3.4.1 Data acquisition using OOI Base32 software

The hand piece is sterilized before use and optical fiber light coupler fixed on the laser head is aligned to provide a Gaussian beam profile at the fiber tip. Prior to measurements, the output power of the laser at the fiber-tip was measured. The hand piece was placed in contact with the tooth to prevent stray light from entering

the spectrometer. The LIF and diffuse reflectance spectra were then recorded alternatively from the tooth samples by point monitoring. Fig.3.7 is a screen shot of the OOIBase32 program showing the *in vivo* LIF spectra from the caries tooth of a patient.

3.4.2 Curve-Fitting of LIF Spectra

In order to determine the peak position of the constituent bands and their relative contribution in the overall spectrum, the LIF spectra were analyzed by a curve-fitting program (Microcal Origin, Ver. 6.0). Gaussian spectral functions were used in curve-fitting as these were found to be most suited in the analysis of LIF spectra [Subhash et al, 1995; Subhash and Mohanan, 1997]. The curve-fitting program uses the Marquardt-Levenberg algorithm and finds the true absolute minimum value of the sum of squared deviations (the value of χ^2) by an iterative process. Best fit of the spectral data, as evidenced from the r^2 (closest to unity) and low χ^2 values were obtained using the minimum number of constituent peaks in the iteration. Curve-fitted parameters such as peak center, peak amplitude, Gaussian curve area and full width at half maximum (FWHM) and their ratios can be used for understanding caries progression and the extent of tooth demineralization.

3.4.3 Statistical Analysis

3.4.3.1 Sensitivity and Specificity

Sensitivity and specificity are two operating characteristics indicative of the diagnostic accuracy of a detection technique (Pretty and Maupome, 2004). A typical diagnostic method will have only two conclusions: either an individual with disease or without. In this thesis, they represent the potential of different spectral criteria in discriminating sound tooth from caries tooth or in classifying different stages of caries. When results of a diagnostic procedure are compared with gold standard, there could be four outcomes.

True Positive (TP), whereby the results of diagnostic method indicate that the individual has the disease, and this assessment is confirmed by the gold standard. True Negative (TN), whereby the procedure results indicate that the person does not have disease, which is in confirmation with the gold standard. False Positive (FP), whereby the procedure results indicate that the person has the disease, but gold standard indicates that the disease is absent. False Negative (FN), whereby the procedure results specify that the person does not have the disease, but the gold

standard indicates that the disease is present. The sum of true positive and false negative decisions (TP+FN) equals the number of individuals with the disease. The sum of false positive and true negative decisions equals the number of individuals without disease.

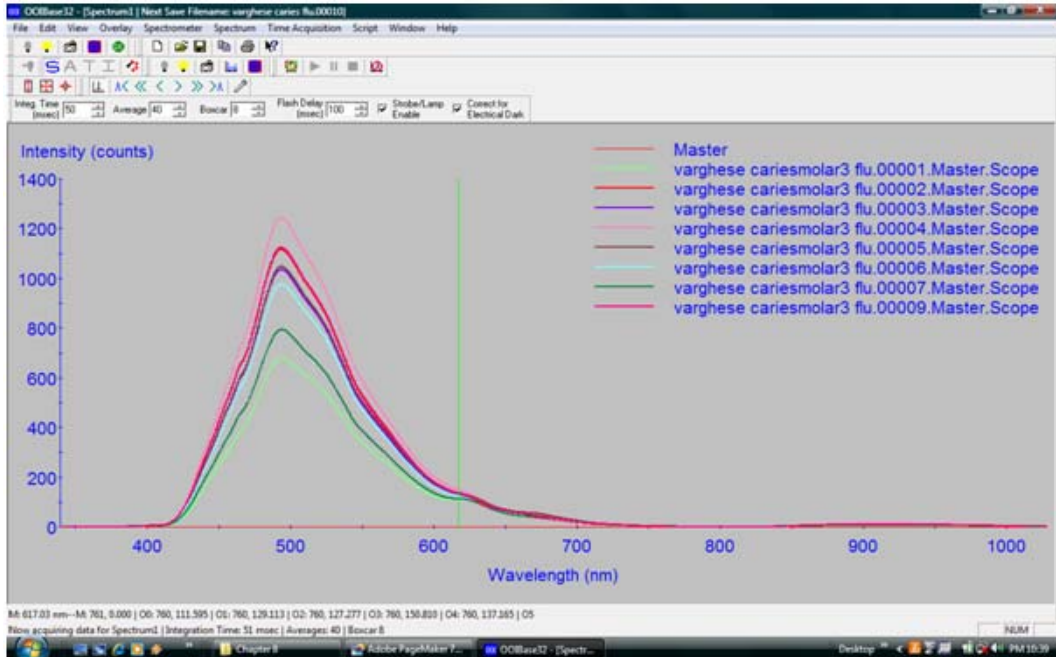


Fig. 3.7 Display of the OOIBase32 program showing the LIF measurement from the caries tooth of a tooth.

Sensitivity is the measure of how accurately a diagnostic procedure is able to correctly identify individuals with the disease and is expressed as $TP / (TP + FN)$. Therefore, a procedure with 100% sensitivity will identify every diseased individual. But, specificity is the measure of how accurately a diagnostic method is able to identify correctly individuals without disease and is expressed as $TN / (FP + TN)$. An ideal diagnostic technique should be highly sensitive and specific, but for many diagnostic procedures these two characteristics are inversely related: an increase in one is often associated with a reduction in the other.

3.4.3.2 Positive and Negative Predictive Values

By quantifying the sensitivity of a diagnostic procedure, it is possible to determine

an operating characteristic of that procedure that establishes if a patient has the disease in question. Quantifying the specificity allows assessment of another operating characteristic of the procedure to determine if the patient does not have the disease. Sensitivity and specificity are relatively independent of the prevalence of a disease (the pre-test probability that an individual patient has the disease), and therefore these parameters are generally stable for the same procedure administered in different study populations. In other words, sensitivity and specificity are inherent properties of the test. They are useful for comparing procedures and for deciding which test to use in a particular clinical setting.

Table 3.1 A 2 x 2 contingency table illustrating the outcomes of a comparison between a diagnostic procedure and gold standard and the use of these values to calculate negative and positive predictive values

| | | Gold standard result | | |
|------------------|----------|----------------------|---------------------|-------------|
| | | Positive | Negative | Total |
| Procedure result | Positive | True positive (TP) | False positive (FP) | TP+FP |
| | Negative | False negative (FN) | True negative (TN) | FN+TN |
| | Total | TP+FN | FP+TN | FN+TN+FP+TP |

Sensitivity: $TP/(TP+FN)$; Specificity: $TN/(FP+TN)$; Positive predictive value (PPV): $TP/(TP+FP)$; Negative predictive value (NPV): $TN/(FN+TN)$

Sensitivity and specificity do not aid in interpreting the result of a particular procedure for an individual patient; they do not help in ruling in or ruling out the disease once the results of the tests are known, and so they have no predictive value. To answer these more practical questions, the predictive values of the diagnostic procedure must be determined. The predictive values are easily derived from the contingency table described in Table 3.1. The positive predictive value (PPV) is the proportion of those whose actual caries increment was high among those who were believed to have a high risk. The negative predictive value (NPV) is the proportion of subjects whose actual caries increment was low among those for whom a low risk was predicted. Whereas, the values for sensitivity and specificity

depend only on the operating characteristics of the procedure itself, the PPV and NPV vary according to the prevalence of the disease. Thus, predictive values cannot be quoted without prior knowledge of disease prevalence in the population from which the estimates are being derived. PPV and NPV are not qualities of the procedure itself; rather, they are functions of both the characteristics of the procedure and the environment in which it is being used. In other words, the accuracy of PPV and NPV values would be lower in general population and when the same screening procedures are applied to high risk populations, they are highly effective in identifying those with the disease.

Sensitivity and NPV go together; given a constant occurrence of the disease, an increase in sensitivity brings about an increased NPV and vice versa. A similar association exists between specificity and PPV. If the sensitivity and specificity remain the same, an increase in the occurrence of the disease results in an increased PPV and a decreased NPV.

3.4.3.3 Receiver Operating Characteristic Analysis

The diagnostic performance of a test to discriminate diseased cases from normal is evaluated using receiver operating characteristic (ROC) curve analysis (Metz, 1978; Zweig and Campbell, 1993). ROC analysis is based on a graphic representation of the reciprocal relation between sensitivity and specificity, calculated for all possible threshold values. When sensitivity and specificity are analyzed jointly, a threshold score or cut-off must be set to divide patients into 2 categories: those presumed to have the disease and those presumed not to have the disease.

A test scored on a continuous scale does not have just one value for the combination of sensitivity and specificity; rather, it has a range of values, with various possible cut-off points. Because reporting only one sensitivity–specificity pair may give an oversimplified picture of the performance of the diagnostic procedure, it is more useful to describe the entire range of values; plotting each pair of scores on an ROC plot is a good way to do this.

The true-positive probability (sensitivity) is plotted as a function of the false-positive probability ($1 - \text{specificity}$), for the entire range of cut-off points. The resulting ROC curve provides a graphic summary of the range of decision thresholds for the test. As the curve approaches the upper left corner of the plot, the true-positive fraction (TPF) approaches 1 (perfect sensitivity) and the false-positive fraction (FPF) approaches

zero (perfect specificity); the closer the curve to the corner, the greater the overall accuracy of the test.

The discriminative ability of a procedure is defined by the distributions of diseased and non-diseased patients. The overlap of these groups determines the shape and position of the ROC curve. A straight line from the lower-left corner to the upper-right corner describes a procedure in which the diseased and non-diseased distributions overlap completely and the TPF and FPF are equal at any threshold. This procedure has no discriminative value and is worthless. A perfect procedure has no overlap between the distributions of diseased and healthy patients and would result in the straight line.

3.4.3.3.1 Area under the Curve

In addition to the relative simplicity of this visual representation of test accuracy, it is possible to perform quantitative analysis yielding summary indices of the discriminatory accuracy of the test. The most common summary index is the area under the curve (AUC), that is, the area under the ROC curve. The AUC is a measure of the accuracy of a diagnostic procedure and is frequently used for comparisons between procedures. The ROC line for a perfect procedure has an AUC of 1.0 or 100%. The closer the AUC value is to 1.0 or 100%, the more accurate the procedure. Fig. 3.8 shows the ROC curve obtained for discriminating sound from dentinal caries using SPSS software (Version 10, SPSS Inc., Chicago, IL, USA) (see Chapter 9).

3.5 IN VITRO STUDIES

Prior to using the LIFRS system in patients, the device was tested in the laboratory by measuring the laser-induced fluorescence and diffuse reflectance spectra from extracted tooth samples using 337 nm nitrogen and 404 nm diode lasers. We used raw LIF spectral intensity, curve fitted LIF amplitude and curve area ratios of the

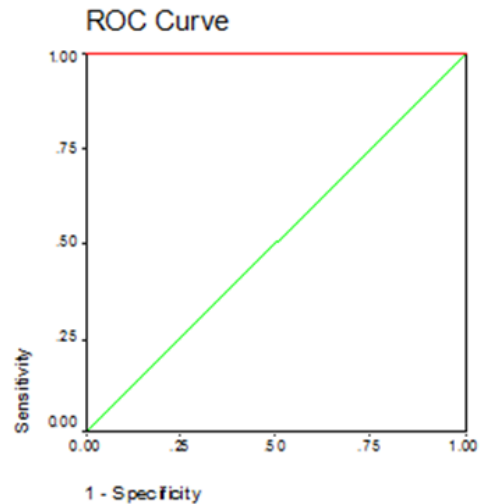


Fig. 3.8 Receiver operating characteristic (ROC) curve obtained for sound from caries tooth. The horizontal red line represents a perfect procedure, with no overlap between the distributions of normal and diseased patients. The diagonal green line represents a procedure for which the diseased and non-diseased distributions overlap completely.

constituent bands to discriminate caries from sound tooth and also to classify different stages of caries. The results were compared with the DR spectral ratios (Subhash et al., 2005). Further, the potential of LIF and DR spectroscopy to detect dental erosion, cyclic de- and re-mineralization were also tested. The fluorescence and diffuse reflectance spectral intensity and ratios were used to detect tooth caries, dental erosion and de- and re-mineralization.

3.6 IN VIVO STUDIES

3.6.1 Ethical Clearance for the Study

A proposal for conducting clinical trials on 100 patients to detect dental caries using LIFRS system was prepared and submitted to Ethics Committee of the Government Dental College, Trivandrum. The proposed work intended to test the applicability of the LIFRS system to detect tooth caries and de-mineralization by measuring autofluorescence and diffuse reflectance from sound and caries tooth, followed by correlation with visual-tactile and radiographic findings. After getting ethical clearance from institutional ethical committee (IEC/C/01-A/2008/DCT), clinical trials were conducted at the Department of Conservative Dentistry and Endodontics at the Government Dental College, Thiruvananthapuram, India. Patients who present themselves at the OP clinic were examined by the clinician and those found suitable based on the visual-tactile findings of the respective tooth were enrolled into the trial.

3.6.2 Inclusion and Exclusion Criteria for the Study

An inclusion and exclusion criterion was followed for selecting patients for the spectral measurements.

1. INCLUSION CRITERIA

- i) Patients belonging to the age groups 20-50 years.
- ii) Patients identified with caries by radiographic and visual impression.
- iii) Patients complaining pain, sensitivities to hot and cold foods.
- iv) Ability to read, understand and sign informed consent.

2. EXCLUSION CRITERIA

- i) Patient refusal.

ii) Patients with fractures, cysts and tumors of oral cavity.

iii) Patients with gingivitis and periodontal diseases.

iv) Patients with diseases that are transmittable.

3.6.3 Conduct of Clinical Trials

The patients enlisted for the study were explained in detail about the pros and cons of the study. Signed and informed consent was taken prior to the study from each patient. A total

of 105 patients, aged between 20 and 50 years with clinically suspected incipient caries or radiographically proven tooth caries were included in the study (Fig. 3.9). Before initiation of measurements, the patients were asked to rinse their mouth with water/saline to reduce the effects of recently consumed food and the measurement



Fig.3.10. Close up view of the tooth samples being examined by point monitoring using the fiber-optic hand piece.



Fig. 3.9 Conduct of clinical trials using the LIFRS system at the Government Dental College, Trivandrum.

site was cleaned with cotton- swab. The studies were carried out *in vivo* tooth, which were selected for the study by an experienced clinician after recording its visual-tactile impression. Fig.3.10 shows a close-up view of oral cavity and molar tooth being examined by point monitoring using the fiber-optic hand piece. After *in-vivo* LIF and DR spectral measurements, radiography of the measured tooth was taken. Depending upon the visual-tactile and radiographic results, the tooth was classified by an experienced clinician, who was blinded to the spectral findings.

3.6.4 Validation Studies

To test the diagnostic accuracy of the developed LIF and DR spectral standards, a blind test was carried out in 40 patients with suspected caries. The LIF spectral ratios from 40 sites in these patients were incorporated into the developed standard and correlated with the clinical and radiographic findings. Based on results obtained, the ROC-AUC, sensitivity, specificity, PPV and NPV of the spectral criteria developed were determined.

3.7 CONCLUSION

An optical spectroscopy system known as “LIFRS” was developed to record LIF and DR spectra of tooth samples by point monitoring. The instrument was then tested on extracted tooth samples in the laboratory. Based on these *in vitro* results, a detailed study protocol was developed for clinical trials. Details of the *in vitro* and *in vivo* studies conducted and the results obtained are exclusively described in the subsequent chapters.

Chapter 4

Tooth Caries Detection by Curve-fitting of Laser-Induced Fluorescence Emission: A Comparative Evaluation with Reflectance Spectroscopy

4.1 INTRODUCTION

Nitrogen laser (337.1 nm) excited fluorescence and white light illuminated DR spectra of extracted tooth samples were measured to detect caries formation. The caries tooth showed lower fluorescence and reflectance intensities in the 350 to 700 nm region as compared to sound tooth. The LIF spectra were analyzed by curve-fitting to determine the peak position of the various bands present and their relative contribution to the overall spectra. The efficacy of using the fluorescence intensity ratios determined from the constituent band peak amplitudes and Gaussian curve areas are compared with those of raw spectral data and reflectance intensity ratios in discriminating caries lesions and the results are presented in this chapter.

4.2 STUDY MATERIAL AND PROTOCOL

Sound and caries tooth belonging to different categories were collected from the dental clinic following extraction from different patients, for various reasons including periodontal problems. The samples were kept in PET bottles, immersed in isotonic saline and transported to the laboratory for later measurements. Usually the samples were collected on the same day of extraction or on the following day and stored at room temperature ($27\pm 3^{\circ}\text{C}$); but measurements were carried out as soon as the samples reached the laboratory. The teeth were categorized as sound, dentin, and pulp level, depending on the depth of cavitation assessed using a periodontal probe. Teeth with clear enamel-intact surfaces were considered as sound, while those with 3–4 mm deep caries were considered as dentin level and those with caries deeper than 4 mm were taken as pulp level. Samples studied covered smooth surface as well as occlusal caries. The results from 90 tooth samples are presented, out of which 10 samples were affected with dentin level caries, 20 had pulp level caries, and the rest sound tooth.

Before measurements, the samples were taken out of the PET bottles and washed in running water. They were then cleared of food particles, lesions or blood clot using an excavator and dried with tissue paper. Visual inspection is then carried out as per protocol for tooth classification. Samples with decalcification, dental plaque, and white/brown spots were excluded. During visual inspection, the samples were categorized based on characteristics such as tooth type (molar, premolars, and incisors), tooth

opacity, discoloration, localized enamel breakdown, and cavitation in opaque or discolored enamel exposing dentin or deep cavitation affecting the pulp level. Clear surfaces without any enamel breakdown or discoloration were considered as sound.

Due to the diverse nature of the carious lesions, 10 sets of laser-induced fluorescence and diffuse reflectance measurements were taken from each selected area (6 mm dia.). The OOI Base32 software was configured to record the spectra, averaged for 40 scans, with boxcar width of 30 nm and an integration time of 100 ms. In order to determine the peak positions of the constituent bands and their relative contributions in the overall spectrum, the LIF spectrum was analyzed by a curve-fitting program using Gaussian spectral functions. Various band intensity ratios are then determined from the constituent band peak amplitudes and Gaussian curve areas and then correlated with those of raw spectral data and diffuse reflectance intensity ratios for discriminating different stages of tooth caries or decay.

4.3 RESULTS

4.3.1 Fluorescence Measurements

Fluorescence spectra of dental tissues differ due to changes in the composition of pathological areas and tissue optical properties. Figure 4.1 shows the averaged fluorescence spectra recorded from 60 normal, 10 dentin, and 20 pulp level caries tooth samples. The overall fluorescence intensity was found lowest for dentin level tooth caries and increased marginally for caries affecting the pulp.

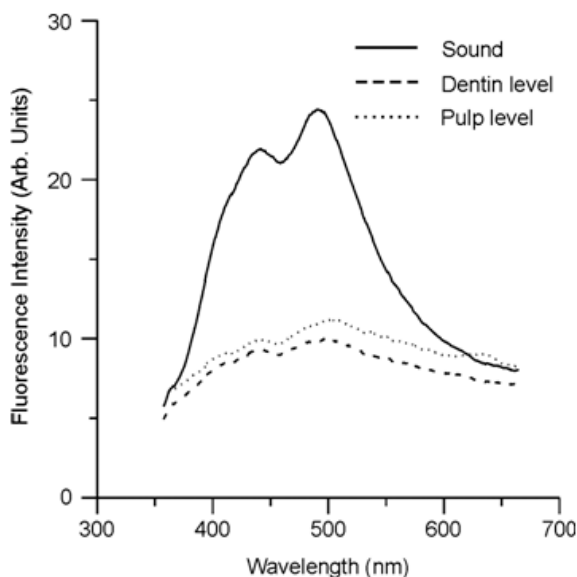


Fig.4.1. *In vitro* laser-induced fluorescence spectra of sound and caries tooth affecting the dentin and pulp with excitation at 337.1 nm. The spectra shown relate to the average of ten measurements on each sample.

The fluorescence spectrum of sound tooth was found to consist of two broad bands showing maximum intensity around 490 and 440 nm, with a satellite peak around 405 nm. The extended tail on the long wavelength side of the 490 nm peak was suggested as due to an emission around 550 nm (Borisova et al, 204). In the case of caries affecting the pulp, an additional peak was observed at around 630 nm, which was absent in sound tooth and dentin level caries. The dentin level caries tooth exhibited the lowest intensity as compared to sound tooth and caries affecting the pulp. There was no significant difference in spectral features for smooth surface or occlusal caries.

Table 4.1 Results of curve-fitting on the averaged LIF spectrum in the 350–690 nm region of sound and caries tooth.

| Tooth | Type | Peak Centre (nm) | FWHM (nm) | Area | Amplitude | χ^2 | r^2 |
|---------------------|----------------|------------------|-----------|--------|-----------|----------|-------|
| Sound | Premolars (9) | 403.80 | 26.99 | 216.91 | 6.41 | 0.013 | 0.999 |
| | | 434.20 | 34.28 | 426.43 | 9.92 | | |
| | 486.88 | 56.22 | 784.32 | 11.12 | | | |
| | 522.45 | 99.83 | 799.26 | 6.38 | | | |
| Dentin level caries | Premolars (4) | 406.72 | 29.78 | 57.40 | 1.54 | 0.004 | 0.995 |
| | | 436.81 | 23.66 | 33.89 | 1.31 | | |
| | 487.25 | 73.89 | 208.47 | 2.25 | | | |
| | 554.52 | 162.90 | 405.95 | 1.99 | | | |
| Pulp level caries | Premolars (10) | 404.41 | 28.01 | 58.63 | 1.67 | 0.003 | 0.998 |
| | | 437.35 | 32.06 | 105.90 | 2.63 | | |
| | 489.76 | 55.90 | 214.17 | 3.05 | | | |
| | 530.23 | 100.56 | 376.48 | 2.98 | | | |
| | 636.78 | 34.00 | 45.09 | 1.05 | | | |

Number of specimens (n) is given in parenthesis; FWHM- full width at half maximum; χ^2 - chi-square; r^2 - correlation coefficient

4.3.2 Curve-fitting analysis

The mean LIF spectra from sound, dentin, and pulp level caries were analyzed by curve-fitting using Gaussian spectral functions. Figure 4.2 (a–c) shows the peak fitted spectrum and the constituent emission bands. It was seen that peak fitting of sound tooth LIF spectra using four Gaussian peaks gives the best fit, with the coefficient of fitting (r^2 value) close to 0.999. In the case of pulp level caries tooth, the fitting had to be performed using five Gaussian peaks to achieve a reasonably good r^2 value of 0.998. Table 4.1 shows the peak positions of the various bands, their Gaussian curve areas, full width at half intensity maximum (FWHM) values and the χ^2 and r^2 values of fitting. The data from pre-molars and molars are grouped together since no significant variation was observed in the LIF spectra between these two types. It is seen that the

522.45 nm peak shifts towards the red region by 32 nm to 554.52 nm in dentin caries and by 8 nm to 530.23 nm in pulp level caries. In addition, a new peak appears at 636.78 nm in pulp level caries. Another notable feature is the broadening of the 522 nm peak by around 63 nm; with concomitant decrease in the Gaussian curve area from 799.26 to 405.95 for dentin level caries. In addition, the 434.2 curve area decreases from 426.43 to 33.89 in dentin level caries and increases to 105.9 in pulp level caries.

4.3.3 Gaussian curve-fitted and raw LIF ratios

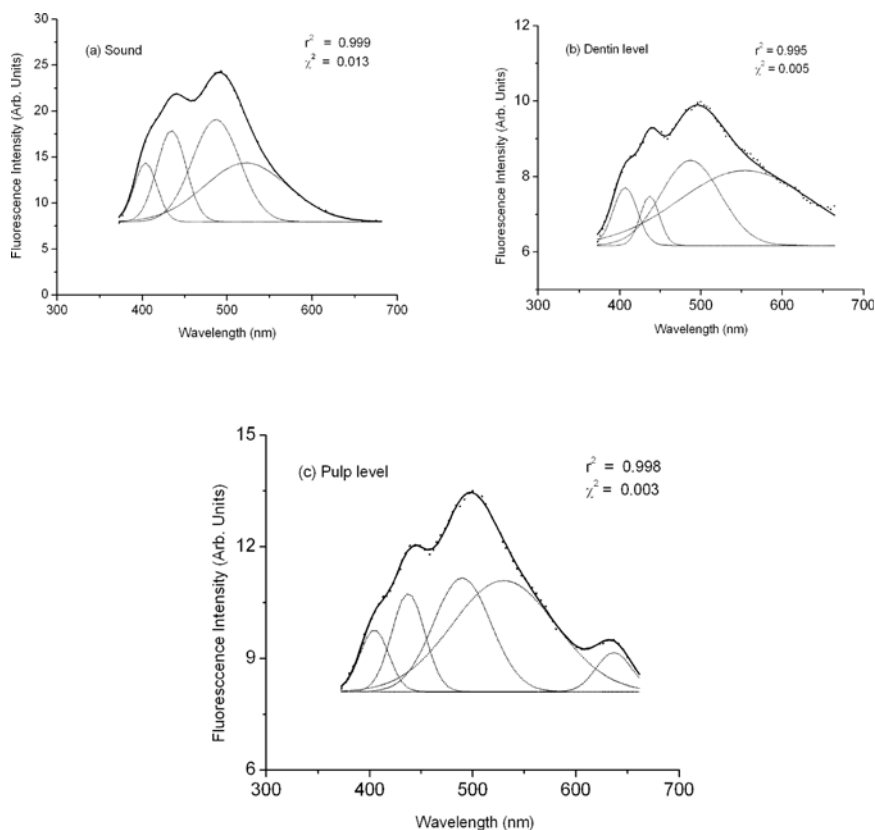


Fig.4.2. The constituent bands of LIF spectra of (a) sound tooth, (b) dentin level caries tooth, and (c) pulp level caries tooth. The dots on the LIF spectrum relate to the data points. The solid line is the curve- fitted line, whereas dotted lines show the constituent bands.

Table 4.2 Fluorescence ratios determined from curve fitted spectral data of mean LIF spectral measurement data.

| Ratios | Curve fitted amplitude | | | Curve fitted area | | | Raw LIF spectrum | | |
|-----------|------------------------|--------|------|-------------------|--------|------|------------------|--------|------|
| | Sound | Dentin | Pulp | Sound | Dentin | Pulp | Sound | Dentin | Pulp |
| F405/F435 | 0.84 | 1.17 | 0.83 | 0.50 | 1.47 | 0.55 | 0.77 | 0.90 | 0.88 |
| F405/F490 | 0.57 | 0.68 | 0.54 | 0.28 | 0.27 | 0.27 | 0.66 | 0.81 | 0.83 |
| F405/F525 | 1.00 | 0.77 | 0.66 | 0.27 | 0.41 | 0.16 | 0.85 | 0.82 | 0.90 |
| F435/F490 | 0.89 | 0.58 | 0.86 | 0.54 | 0.19 | 0.49 | 0.89 | 0.91 | 0.93 |
| F435/F525 | 1.55 | 0.65 | 0.88 | 0.53 | 0.09 | 0.28 | 1.09 | 0.91 | 1.02 |
| F490/F525 | 1.74 | 1.13 | 1.02 | 0.98 | 0.51 | 0.57 | 1.23 | 1.00 | 1.09 |

Table 4.2 shows the different fluorescence ratios (F405/ F435, F405/F490, F405/ F525, F435/F490, F435/F525, and F490/F525) calculated from curve-fitted peak amplitudes, Gaussian curve areas, and raw spectral data. The fluorescence intensity of the LIF spectra at the peak wavelength determined by curve-fitting was used to evaluate the raw fluorescence intensity ratio. As compared to the ratios determined from raw spectral data, the fluorescence ratios calculated from Gaussian area curves and curve-fitted amplitudes for dentin level and pulp level caries show more pronounced variation from those of sound tooth. This is evident in the case of the F435/F490 ratio involving the two main peaks in the raw LIF spectrum, which showed a variation of only 2.2% between sound to dentin and dentin to pulp level caries and 4.5% between sound and pulp level caries. Nevertheless, the F435/F490 ratio determined from the Gaussian curve-fitted areas showed a variation of 157.8% between the dentin and pulp level caries and 64.8% between sound to dentin level caries, whereas this ratio determined from curve-fitted amplitudes gave variations of 48.3% and 34.8%, respectively. It is seen that the curve fitted amplitude and area ratio F405/F435, shows the maximum variance of 194% and 82.8% respectively, during transformation from sound to dentin level caries. Similarly, the curve-fitted area and amplitude F435/F525 ratios show variances of 194.7% and 35.4% during progression from dentin to pulp level caries. This ratio shows good response for transformation from sound to dentin and pulp level caries also. Variations of 82.1% and 58.1% were noted respectively, in

the curve-fitted area and amplitude of F435/F525 ratio during transformation of sound tooth to dentin level caries; and variations of 47.2% and 43.2% were seen respectively, in area and amplitude ratios for sound to pulp level cavitation.

4.3.4 Diffuse Reflectance Measurements

Figure 4.3 shows the *in vitro* diffuse reflectance spectra, averaged from 10 measurements, in the 350 to 700 nm region for 60 sound, 10 dentin, and 20 pulp-level tooth samples. In all these measurements, the reflectance spectral intensity of dentin level caries was found lower than that of sound and pulp level caries. However, beyond 700 nm the spectral intensity of dentin level caries increased and remained higher until 900 nm (spectra not shown). The reflectance intensity ratios (R500/R700, R600/R700, and R650/R700) determined from the recorded mean spectra is presented in Table 4.3. In order to account for sample-to-sample variations, the average reflectance intensity over ± 10 nm interval at the chosen wavelength was used in determining the ratios. The decrease in reflectance intensity ratio from sound to dentin level caries was 17.5% for R500/R700, 25.6% for R600/R700, and 15.3% for R650/R700, whereas these ratios decreased by 50.8%, 28.9%, and 12.9%, respectively on deep cavitation (pulp level caries). Transformation from dentin to pulp level caries was marked only in the R500/R700 ratio (15.3%). Thus, among these ratios, the diffuse reflectance spectral ratio, R500/R700, appears to be most suited to distinguish between different stages of caries tooth formation.

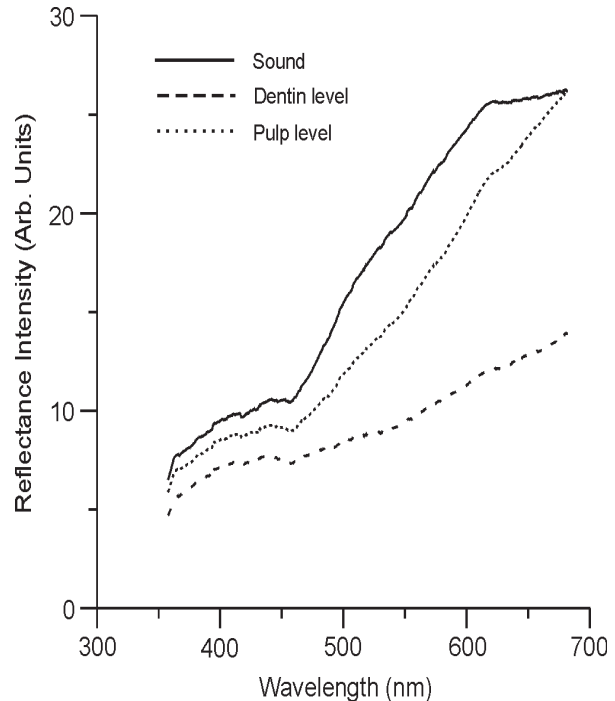


Fig.4.3. Mean *in vitro* diffuse reflectance spectra of sound (60 specimens) and caries tooth, affecting the dentin (10 specimens) and pulp (20 specimens).

Table 4.3 Mean reflectance ratios for sound, dentin, and pulp level of tooth with their standard deviations.

| Tooth Type | n | R500/R700 | R600/R700 | R650/R700 |
|---------------------|----|-------------|-------------|-------------|
| Sound tooth | 60 | 0.63 ± 0.08 | 0.98 ± 0.04 | 1.05 ± 0.03 |
| Dentin level caries | 10 | 0.54 ± 0.05 | 0.78 ± 0.04 | 0.91 ± 0.04 |
| Pulp level caries | 20 | 0.42 ± 0.04 | 0.76 ± 0.03 | 0.93 ± 0.02 |

Ratios given as mean of 10 measurements ± SD; n= number of specimens.

4.3.5 Lesion Profiling

In order to understand the relationship of the cavity profile on the fluorescence or reflectance signals, LIF measurements were carried out across different points around the cavity boundaries and at the center of three pulp-level caries tooth. These were large sized caries, of about 5–7 mm in width and depth, which could easily be accessed with the fiber-optic probe. Figure 4.4 shows the mean LIF spectra, averaged for the three samples, with five measurements each on the cavity edges and central areas. As observed earlier, the 635 nm peak is clearly identifiable in the spectrum and has the same intensity at both the edges and the center, whereas the fluorescence intensity of the 405, 435, and 490 nm peaks increases at the cavity edges. The mean LIF spectra were curve-fitted for obtaining the various spectral signatures. No appreciable shifts were noticed in the constituent peaks in the LIF spectra from the edges and central areas of the cavity. Among the various ratios computed, the F435/F525 ratio showed the maximum variance between the edges and center of the cavity, followed by the F405/F435, F490/F525, and F405/F490 ratios. The F435/F525 Gaussian curve area ratio was found to decrease by 69% from 0.30 at the center to 0.18 at the edges whereas the corresponding amplitude ratios decreased by 38% from 0.99 to 0.72. The percentage increase in the Gaussian curve area ratios, F405/F435 and F405/F490, between the edges and central portions were 44.5% and 34.1%, while there was a decrease of 42% in F490/F525 ratio. The mean diffuse reflectance spectra in the 550–700 nm wavelength range from the cavity edges showed slightly higher intensity as compared to the

center of the cavity. The reflectance intensity ratio (R_{600}/R_{700}) computed from the mean spectra showed an increase of 8.5%, from 0.77 at the cavity center to 0.84 at the edges.

4.4 DISCUSSION

In this study, significant variations between the fluorescence and reflectance spectra of sound, dentin, and pulp level caries was observed. The caries tooth always exhibit lower fluorescence intensity than sound tooth. The sound tooth has the structure and chemical composition of hydroxyapatite. Dental caries is accompanied by the de-calcification of mineral components and dissolution of the organic matrix of hydroxyapatite. Significant variations seen in the fluorescence and reflectance spectrum could be attributed to the changes in the physical structure and chemical composition during the disintegration and decay of tooth enamel leading to caries. The normal enamel of teeth is composed of millions of prisms or rods with waveguide properties that facilitate deep penetration when illuminated with UV-visible light. In case of dental caries, the prism structure is damaged and the waveguide properties are lost so that the irradiated light cannot penetrate deeply. This leads to a reduction in the fluorescence intensity in caries lesion (Fig. 4.1).

With nitrogen laser excitation, Borisova et al. (2004) had also reported a similar decrease in fluorescence intensity for both demineralised and caries tooth. They also observed broad bands centered around 490 nm with a secondary maximum at 440 nm in sound and caries tooth. However, the exact positions of the peaks were hitherto unknown. The curve-fitting of the mean sound tooth LIF spectra were carried out using Gaussian spectral functions and found that the four peaks that constitute the broad LIF emission are centered at 403.80, 434.20, 486.88, and 522.45 nm (Table 4.1). The fitting repeated in dentin and pulp level caries tooth showed

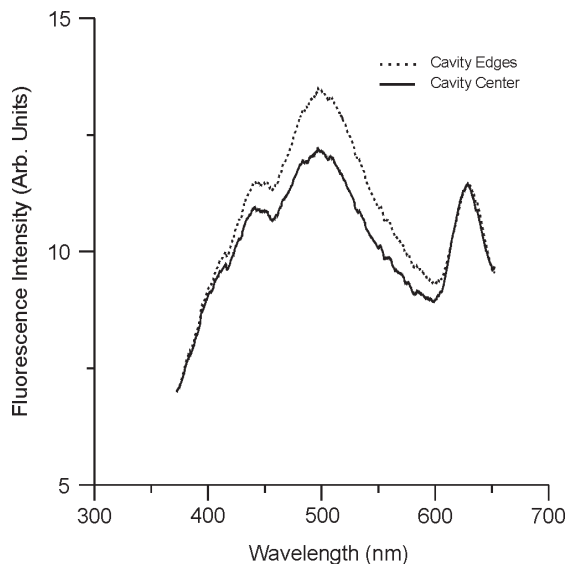


Fig. 4.4. Averaged *in vitro* nitrogen laser-induced fluorescence spectrum at the cavity edges and central areas in pulp level caries tooth.

peak shifts of 32 and 8 nm towards the red region, respectively in dentin and pulp level caries, for the 522 nm peak. In the case of pulp level caries, we observed a new peak at 636.78 nm (Figs. 4.2 c and 4.4) with the same intensity at the cavity center and edges.

Since the correlation coefficients of curve-fitting were very close to unity, for fitting carried out with four peaks, and the residuals of fitting were few and scattered uniformly over the fitted curve, it is to be assumed that the peak wavelength positions of the sound tooth fluorescence identified by the curve-fitting algorithm are fairly accurate. Thus, the shift in peak position of the 522 nm band for dentin level caries and the appearance of the new peak at 636 nm could be useful in identifying the extent or stage of tooth decay. In caries, what we usually see is a dark brown mass consisting of blood cells, food particles, and products of bacteria metabolism. In pulp-level caries, the root system gets affected and there could be blood contamination of the lesions. Protoporphyrin IX (PpIX) formed during the Heme cycle has an emission at 635 nm with UV light excitation. Hence, the appearance of the 636.78 nm peak in pulp level caries (Figs. 4.2c and 4.4) could be due to presence of PpIX in the lesion. During profiling studies inside the cavity of pulp level caries, the 635 nm peak observed in the LIF spectra from the central areas of the lesion overlaps with peak from the cavity edges confirming the uniform presence of PpIX in the entire cavity area (Fig. 4.4).

The demineralised dentin shows emission peaks around 490 and 440 nm during the early stages of demineralization (Borisova et al, 2004). However, during later stages of demineralization, the 440 and 490 nm band broadens due to the appearance of secondary peaks around 405 and 525 nm. These four peaks are prominent in dentin level caries also (Fig. 4.2b). This shows that features related to blood cells are absent in dentin level caries since the root system is not affected and the blood supply to the roots remains intact. There are marked variations not only in the peak emission bands but also in the peak amplitude, FWHM width, and the Gaussian curve area during caries development. The 405 nm band position and FWHM width remain unaffected during caries development. Nevertheless, there is a definite shift in the peak position and variation in the intensity and FWHM width of the 525 nm band, which could be due to the presence of exogenous molecules/fluorophores in the tooth or due to changes in chemical composition during the disintegration process or due to bacterial metabolism products.

Although most of the fluorescence ratios determined from curve-fitted amplitudes

and Gaussian curve areas varied during caries formation, the ratios involving the 435 nm emission peak, such as F405/F435, F435/F525, and F435/F490, appeared more suitable for sighting the evolutionary changes during caries formation (Table 4.2). Transformation from dentin to pulp level caries was seen clearly in the F435/F490 and F435/F525 ratios, while sound to dentin level caries were easily detectable using the F405/ F435 ratios. However, the LIF spectral ratio F435/F525 determined from curve fitted area of the deconvoluted 435 and 525 nm peaks appeared more sensitive to distinguish between different stages of tooth decay from sound to dentin, sound to pulp and dentin to pulp. With respect to detection accuracy, Gaussian curve area ratios fared, in general, better than curve-fitted amplitude ratios. The lesion profiling studies showed that the LIF spectral ratios F405/F435, F435/F525, and F490/F525 are more sensitive as compared to reflectance ratios in the assessment of the shape and extent of pulp level cavities.

The chromophores present in the caries, with strong absorption in the blue-green spectral region, have also resulted in decreased diffuse reflectance spectral intensity in the 400–600 nm range (Fig. 4.3). These spectral changes in caries might be due to the import of exogenous molecules during caries developmental process, as evidenced by the presence of increased absorption in the short wavelength region. The concentration of these exogenous molecules increases due to the presence of food particles, blood cells and bacterial activity. Earlier measurements by Uzunov et al (2003) showed significant decrease in the reflectance spectral ratios by 158% and 32.4% respectively, for R500/ R900 and R750/R900 ratios between sound and deep cavitation tooth. In our measurements, the diffuse reflectance intensity of dentin level caries beyond 700 nm was more than that of the sound tooth, unlike the steady increasing trend shown up to 900 nm for sound tooth, superficial cavity, and deep cavitation (Uzunov et al, 2003). We, therefore, did not compute the ratios beyond 700 nm.

The effectiveness of using laser-induced fluorescence for detection of occlusal caries using the DIAGNOdent device showed that fluorescence technique gives only accuracies similar to that of visual inspection or radiography (Sheehy et al, 2001; Shi et al, 2001; Attril and Ashley, 2001 and Fausto et al, 2003). The main reason for this is the unsuitability of the 655 nm laser emission of this device for excitation of the chemical constituents of teeth and bacterial metabolism products that cause tooth decay. It may further be noted that fluorescence of caries lesions is due to changes in organic content of the lesion rather than mineral loss. However, the use of a UV laser at 337 nm establishes the enhanced capability and accuracy for LIF detection of different stages of caries lesions.

The key advantages of laser-based systems are their high sensitivity and lack of attendant risks of ionizing radiation. This leads to their frequent use in monitoring lesions of dental caries and dental erosion, and such studies could further be extended from visible and UV wavelengths to the near-IR and IR for detailed analysis of the internal composition of tooth. As compared to point monitoring of fluorescence and reflectance signatures, the use of a CCD camera based multi-wavelength imaging device with UV laser excitation would facilitate representation of fluorescence intensity and ratio variations across the lesion and a better understanding of caries constitution and diagnosis. Further *in vivo* studies are required with the LIF system to test its efficacy in a clinical environment. Once the characteristic emission bands, their positions, and relative contributions are identified by curve-fitting, routine monitoring of sound tooth will enable early identification of any physical or chemical changes occurring in the tooth before the development of caries lesions so that preventive measures could be resorted well in advance.

4.5 CONCLUSIONS

The fluorescence ratios showed significant changes depending on the nature and extent of caries and the detection capability was enhanced when contributions from the constituent bands, as determined by curve-fitting of the LIF spectra using Gaussian spectral functions were considered. Based on our findings, it can be presumed that both laser-induced fluorescence, with excitation by a UV laser such as the nitrogen laser, and diffuse reflectance spectroscopy using a white light source have the potential to diagnose different stage of caries. The advantages of using a nitrogen laser at 337.1 nm, as against other visible lasers such as an argon ion laser (488 nm) or the diode laser (655 nm) as in the case of the DIAGNOdent device, for obtaining caries sensitive fluorescence emission signatures have been clearly brought out.

Chapter 5

Investigation of *in vitro* Dental Erosion by Optical Techniques

5.1 INTRODUCTION

Dental erosion is becoming an increasing predicament in dentistry and can be attributed to either exogenous or endogenous factors. Accurate diagnosis of dental erosion in its formational phase is a challenging task. Early detection allows preventive remineralization measures to be taken before physical and chemical changes in tooth enamel and dentin sets in, causing irreversible damage to teeth. Established diagnostic methods cannot detect carious process in its early stage or produce arbitrary data that cannot be correlated to actual mineral loss. Thus, there is a need to develop diagnostic methods than can accurately screen dental erosion at an earlier stage.

Studies has shown that curve-fit analysis of nitrogen excited laser-induced fluorescence (LIF) spectra using Gaussian spectral functions could differentiate different stages of caries formation with improved sensitivities. This chapter explores the importance of tissue fluorescence and diffuse reflectance (DR) in detecting artificial dental erosion. The LIF spectra were analyzed by curve-fitting to determine the peak position of the various bands present and their relative contribution to the overall spectra. The results of curve-fitting were compared with raw spectral data and the DR spectral characteristics to understand the suitability of these techniques in detecting early tooth demineralization and are presented here.

5.2 STUDY MATERIAL AND PROTOCOL

Sound tooth samples were collected from a nearby dental clinic following extraction, for various reasons including periodontal problems and transported to the laboratory in isotonic saline. Four sound teeth were fixed on a glass slide with the buccal side up using an epoxy (Araldite, Huntsman Advanced Materials, India) and sectioned laterally through the center on a precision thin section cutter (Buhler, USA) to obtain two slices of each sample for recording typical enamel and dentin fluorescence and diffuse reflectance spectra. Eight premolars without any clinically visible lesions were selected for dental erosion studies. Before measurements, the samples were washed in running water, cleared of food particles or blood clotting and dried with tissue paper. After making baseline LIF and diffuse reflectance measurements the samples were demineralized with 36% phosphoric acid based etching gel, free of silica (INSTA ETCH,

Raman Research Products, Kolkata, India) for varying treatment periods of 10 s, 30 s, 1 min, 5 min, 6 h and 24 h.

Before commencement of spectral measurement, the samples were brush-washed in running water to remove the applied gel and dried with tissue paper. Ten sets of fluorescence and diffuse reflectance spectra were recorded from sound enamel and dentin areas of each sectioned tooth and from eight premolar tooth samples during various stages of demineralization. The OOI Base32 software was configured to record the spectra, averaged for 40 scans, with boxcar width of 10 nm and an integration time of 350ms.

The mean LIF spectra of clear enamel and dentin recorded from sectioned tooth slices and from the control and demineralized sites during various stages of tooth erosion were curve-fitted using Gaussian spectral functions to precisely locate the peak positions and their variations, if any, over the period of demineralization (Subhash et al, 2005). The deconvoluted peak intensities and Gaussian curve areas were then utilized to determine the fluorescence ratios for investigating the extent of tooth demineralization.

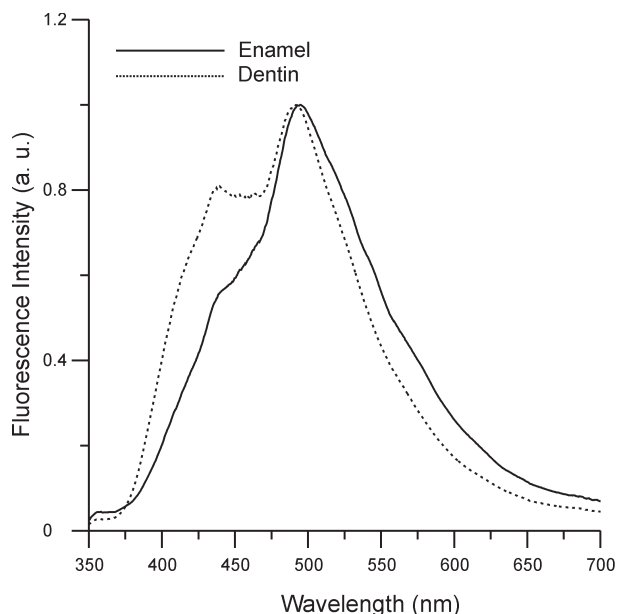


Fig. 5.1 Mean LIF spectra from enamel and dentin tooth slices normalized with respect to the maximum intensity.

5.3 RESULTS

5.3.1 LIF spectral features

5.3.1.1 *Tooth enamel and dentin spectra*

The LIF spectrum of sound tooth enamel recorded from the sectioned tooth samples consist of a broad band around 490 nm with shoulder in 425–475 nm region

that appears to peak around 440 nm in sound dentin areas. The observed changes in fluorescence spectral intensity and shape were studied by normalizing the LIF spectra with respect to the intensity of the 490-nm peak. Figure 5.1 illustrates the normalized fluorescence spectra of sound tooth enamel and dentin. We have noticed a broadening of the 490-nm peak in sound dentin with an apparent shift towards the blue region. Curve-fitting of the mean LIF spectra from sound enamel and dentin using four Gaussian spectral functions gave the best fit of data, with values of correlation coefficient close to 0.999 in most of the fittings. Incorporation of an additional peak did not improve the quality of fit. Figure 5.2a,b shows the peak fitted LIF spectrum with the deconvoluted constituent peaks at 409.11, 438.13, 492.35 and 523.07 nm in sound tooth enamel (a) and at 411.95, 440.11, 487.82 and 523.36 nm in sound dentin (b). Compared to enamel, a red shift of about 2.8 nm was seen in dentin for the 409-nm peak and about 2 nm for the 438-nm peak, whereas a blue shift of 4.5 nm was seen in the 492-nm peak.

5.3.1.2 Tooth demineralization

The spectrum of sound tooth enamel surfaces have a shape similar to that of sound enamel recorded from the sliced samples, but with the advancement of dental erosion, there is a gradual

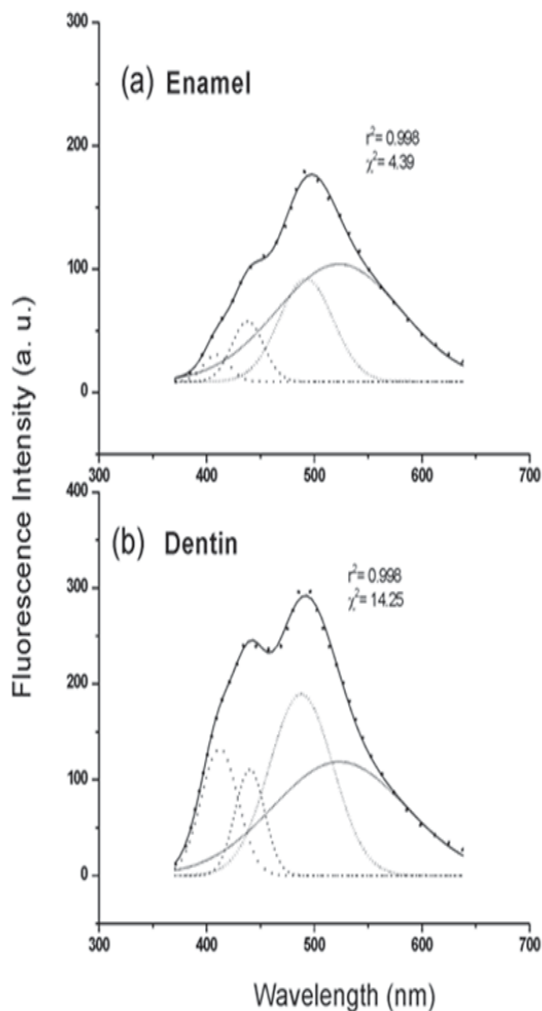


Fig. 5.2 Curve-fitted LIF spectrum showing the constituent bands from **a)** sound enamel and **b)** dentin slices of tooth. The dots on the LIF spectrum relate to the data points. The solid line is the curve-fitted line whereas dotted lines show the constituent bands.

enhancement in the fluorescence spectral intensity as shown in Fig. 5.3a. We have studied the spectral intensity variations by normalizing the LIF spectra with respect to the intensity of the 490-nm band. Figure 5.3b shows the normalized LIF spectra for different stages of tooth demineralization. The notable feature of this spectrum is the increase in relative intensity of the 440-nm peak during demineralization. The LIF spectrum from demineralized tooth surface has the same shape as that of the spectra from sound enamel up to 1 min, but it slowly transforms to that of dentin in 5 min. In about 24 h of dental erosion, the spectrum acquires the shape of dentin spectra demonstrating the complete erosion of the enamel layer. The mean LIF spectra during different stages of demineralization were curve-fitted as before using four Gaussian spectral functions. Table 5.1 shows the peak positions of the various bands, their Gaussian curve areas, full width at half intensity maximum (FWHM) values and the χ^2 and r^2 values of fitting. Since no significant variations were observed in the position of the constituent peaks, they will be henceforth designated as 410, 440, 485 and 525 nm peaks for simplicity.

The fluorescence ratios (F410/F440, F410/F485, F410/F525, F440/F485, F440/F525 and F485/F525) calculated from the curve-fitted peak intensities and Gaussian curve areas of the four peaks are shown in Table 5.2. The fluorescence spectral intensity that corresponds to the peak wavelength determined by the curve-fitting was used to evaluate the raw

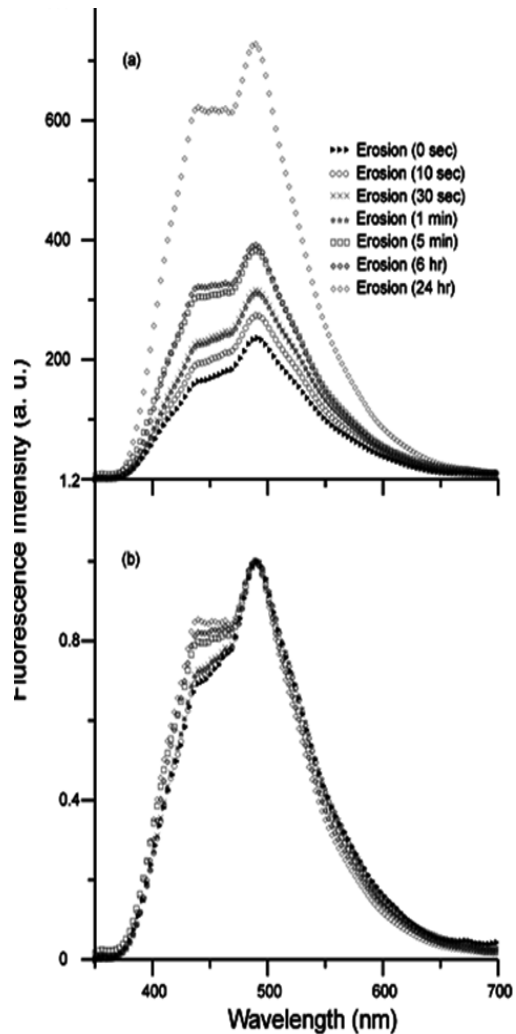


Fig. 5.3a) Mean LIF spectra during various stages of demineralization and **b)** LIF spectra normalized to the intensity at 490 nm band.

fluorescence intensity ratios given in Table 5.2. The ratios calculated from Gaussian spectral curve areas and amplitudes show pronounced variations with respect to the raw spectral LIF ratios. The transformation from the enamel layer to the dentin layer of tooth can be visualized from the sudden increase/decrease in ratios. In all these ratios, marked deviations were seen in 5 min of dental erosion. The overlap of

Table 5.1 Results of curve-fitting on the mean LIF spectrum from the sound and demineralized regions of tooth.

| Tooth | Peak Centre (nm) | FWHM (nm) | Area | Amplitude | χ^2 | r^2 |
|-------|------------------|-----------|--------|-----------|----------|-------|
| Sound | 411.34 | 30.802 | 2394.8 | 62.034 | 8.6 | 0.998 |
| | 439.3 | 28.819 | 3100.5 | 85.843 | | |
| | 487.44 | 55.398 | 9920.3 | 142.88 | | |
| | 522.29 | 114.48 | 14336 | 99.922 | | |
| 10sec | 409.45 | 29.373 | 2630.9 | 71.464 | 11.9 | 0.998 |
| | 437.87 | 30.101 | 4191.6 | 111.11 | | |
| | 486.68 | 57.981 | 13449 | 185.07 | | |
| | 528.78 | 105.62 | 13885 | 104.89 | | |
| 30sec | 410.57 | 29.551 | 3231.6 | 87.252 | 15.62 | 0.998 |
| | 438.54 | 29.606 | 4834.7 | 130.3 | | |
| | 486.42 | 56.987 | 14736 | 206.32 | | |
| | 525.9 | 106.97 | 16777 | 125.13 | | |
| 60sec | 412.14 | 31.291 | 3596.3 | 91.704 | 15.68 | 0.998 |
| | 439.18 | 28.349 | 4074.2 | 114.67 | | |
| | 486.56 | 60.516 | 16474 | 217.2 | | |
| | 532.61 | 107.06 | 15267 | 113.78 | | |
| 5min | 412.6 | 33.71 | 6017.8 | 142.43 | 23.41 | 0.998 |
| | 439.93 | 28.055 | 5070.8 | 144.21 | | |
| | 485.29 | 59.574 | 19523 | 261.47 | | |
| | 526.59 | 112.89 | 19351 | 136.77 | | |
| 6hr | 412.11 | 29.938 | 4854.2 | 129.37 | 23.41 | 0.999 |
| | 438.72 | 28.894 | 6345.2 | 175.22 | | |
| | 484.37 | 59.312 | 20853 | 280.52 | | |
| | 528.62 | 108.11 | 17863 | 131.83 | | |
| 24hr | 409.44 | 29.591 | 9250.6 | 249.43 | 81.72 | 0.999 |
| | 437.76 | 30.807 | 14604 | 378.25 | | |
| | 484.37 | 56.166 | 35242 | 500.64 | | |
| | 522.66 | 106.25 | 33955 | 254.98 | | |

FWHM- full width at half maximum; χ^2 - chi-square; r^2 - correlation coefficient

normalized mean LIF spectra of sound dentin from the sliced tooth and spectra after 5 min of dental erosion (Fig. 5.4) shows that the enamel layer has been completely eroded in 5 min. During this de-mineralization period, the Gaussian curve-fitted amplitude and area F410/F440 ratio given in Table 5.2 varied, respectively, by 37.5 and 54.6%, whereas that derived raw LIF spectra varied by 4.1% only. Maximum variance of 67.7 and 82.4% were observed, respectively, for curve-fitted amplitude and area F410/F525 ratios. In contrast, variations of 33.6 and 46.45%, respectively, were also seen in the curve-fitted amplitude and area F485/F525 ratio.

Figure 5.5 a–c shows various fluorescence ratios derived from curve-fitted Gaussian peak amplitudes (a), Gaussian curve areas (b) and raw LIF spectral intensity (c) of the four emission bands from sound enamel and dentin slices and those from demineralized tooth by taking the mean of the ratios from spectra recorded during 0–1 min of demineralization for enamel and during 5 min–24 h of demineralization for dentin. It can be seen from Table 5.3 that fluorescence ratios obtained for demineralized enamel and dentin have similar trends as that of spectra recorded from enamel and dentin areas of sliced tooth samples. Marked variations are seen in the F410/F440 Gaussian curve area and amplitude ratios and F410/F525 ratios. With

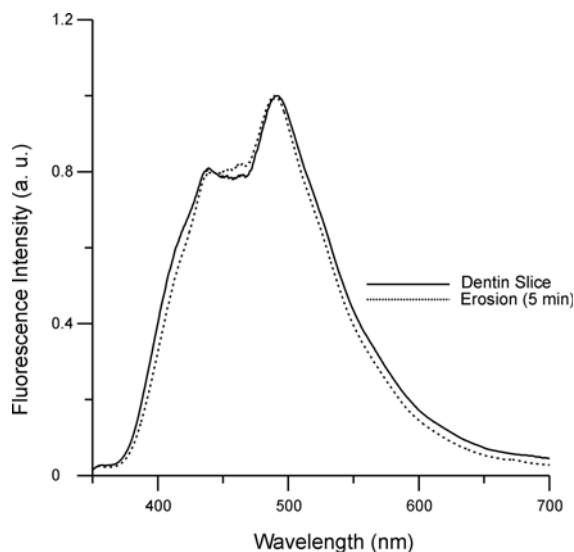


Fig. 5.4 Mean LIF spectra of dentin slice and spectra after 5 min of demineralization normalized to the intensity at 490 nm.

the exception of F440/F485 ratio, there is a pronounced increase in ratio value of dentin as that of enamel in sliced tooth, whereas the ratios show less pronounced variation between demineralized enamel and dentin tooth samples.

5.3.2 Diffuse reflectance characteristics

5.3.2.1 Reflectance spectral features

There are noticeable differences between the diffuse reflectance spectra of sound enamel and dentin recorded from sliced tooth samples. Figure 5.6 shows the averaged spectra from enamel and dentin

slices normalized to the maximum intensity at 625 nm.

5.3.2.2 Tooth demineralization

Ten sets of diffuse reflectance measurements were recorded from each tooth sample during various stages of demineralization and averaged. Although the spectral shape remains the same, the diffuse reflectance intensity follows an increasing trend with demineralization time as shown in Fig. 5.7a. The standard deviation of measurement is shown at two points on the mean spectra during different time periods of erosion. There is a steep increase in intensity up to 1 min of tooth erosion, but the intensity variation is less pronounced afterwards. The averaged spectrum at different stages of demineralization, normalized with respect to the maximum intensity at 625 nm is shown in Fig. 5.7b. The normalized spectra show a reduction in relative intensity with erosion in the spectral window below 625 nm, whereas the trend reverses beyond 625 nm. The reflectance intensity ratios (R_{500}/R_{700} , R_{600}/R_{700} and R_{650}/R_{700}) were calculated from the spectral intensities at 500, 600, 650 and 700 nm, over a spectral interval of ± 5 nm. It is seen that the R_{500}/R_{700} ratio decreases by 26% from 0.53 to 0.39 in 24 h of demineralization, whereas the R_{600}/R_{700} and R_{650}/R_{700} ratios decreased only marginally by 7.6 and 2.6%, respectively. Figure 5.8 shows the mean reflectance intensity ratios R_{500}/R_{700} , R_{600}/R_{700} and R_{650}/R_{700} of sectioned enamel and dentin slices and of the enamel (from recordings taken during 0–1 min) and dentin layers of tooth (from recordings taken during 5 min–24 h) during demineralization. It is

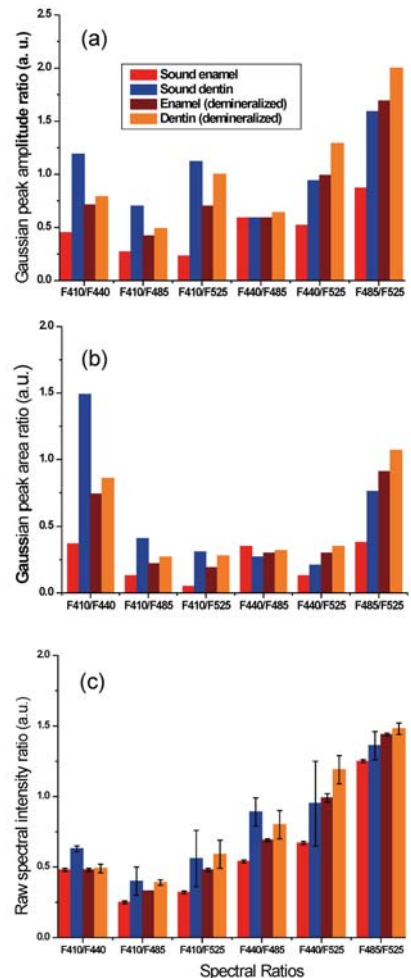


Fig. 5.5 Fluorescence ratios derived from **a)** curve-fitted spectral amplitude, **b)** curve-fitted spectral area and **c)** raw LIF spectral data of sound enamel and dentin slices and those of demineralized samples (mean of ratios at 0, 10 s, 30 s and 1 min representing enamel and mean of ratios at 5 min, 6 h and 24 h representing dentin).

Table 5.2 Fluorescence ratios derived from curve-fitted spectral data and raw LIF spectral data.

| Ratios | Curve-fitted amplitude | | | | | | | | | | | | Curve-fitted area | | | | | | | | | | | | Raw LIF spectrum | | | | | | | | | | | | | | | | | |
|-----------|------------------------|------|------|--------|------|------|--------|------|------|-------|------|------|-------------------|------|------|------|------|------|-------|------|------|-------|-----|----|------------------|-----|----|--------|-----|----|-------|-----|----|-------|--|--|------|--|--|-------|--|--|
| | Sound | | | 10 sec | | | 30 sec | | | 1 min | | | 5 min | | | 6 hr | | | 24 hr | | | Sound | | | 10 sec | | | 30 sec | | | 1 min | | | 5 min | | | 6 hr | | | 24 hr | | |
| | sec | min | hr | sec | min | hr | sec | min | hr | sec | min | hr | sec | min | hr | sec | min | hr | sec | min | hr | sec | min | hr | sec | min | hr | sec | min | hr | sec | min | hr | | | | | | | | | |
| F410/F440 | 0.72 | 0.64 | 0.67 | 0.79 | 0.99 | 0.74 | 0.86 | 0.77 | 0.63 | 0.87 | 0.88 | 1.19 | 0.77 | 0.83 | 0.49 | 0.48 | 0.47 | 0.47 | 0.51 | 0.46 | 0.5 | | | | | | | | | | | | | | | | | | | | | |
| F410/F485 | 0.43 | 0.39 | 0.43 | 0.42 | 0.54 | 0.46 | 0.49 | 0.24 | 0.19 | 0.22 | 0.22 | 0.31 | 0.23 | 0.26 | 0.33 | 0.33 | 0.33 | 0.33 | 0.38 | 0.38 | 0.42 | | | | | | | | | | | | | | | | | | | | | |
| F410/F525 | 0.82 | 0.68 | 0.69 | 0.81 | 1.04 | 0.98 | 0.98 | 0.17 | 0.19 | 0.19 | 0.24 | 0.31 | 0.27 | 0.27 | 0.47 | 0.47 | 0.49 | 0.48 | 0.58 | 0.55 | 0.64 | | | | | | | | | | | | | | | | | | | | | |
| F440/F485 | 0.6 | 0.6 | 0.63 | 0.63 | 0.55 | 0.62 | 0.76 | 0.31 | 0.31 | 0.33 | 0.25 | 0.26 | 0.3 | 0.41 | 0.67 | 0.68 | 0.7 | 0.69 | 0.75 | 0.82 | 0.84 | | | | | | | | | | | | | | | | | | | | | |
| F440/F525 | 0.86 | 1.06 | 1.04 | 1.01 | 1.05 | 1.33 | 1.48 | 0.22 | 0.3 | 0.29 | 0.27 | 0.26 | 0.36 | 0.43 | 0.94 | 0.98 | 1.02 | 1 | 1.11 | 1.19 | 1.28 | | | | | | | | | | | | | | | | | | | | | |
| F485/F525 | 1.43 | 1.76 | 1.65 | 1.91 | 1.91 | 2.13 | 1.96 | 0.69 | 0.97 | 0.88 | 1.08 | 1.01 | 1.17 | 1.04 | 1.43 | 1.44 | 1.46 | 1.44 | 1.47 | 1.45 | 1.53 | | | | | | | | | | | | | | | | | | | | | |

seen from Table 5. 4 that the reflectance ratios after demineralization follow a pattern similar to that of the dissected enamel and dentin ratios, with the R500/R700 ratio showing maximum resemblance.

5.4 DISCUSSION

Dental enamel is crystalline in nature and is composed of various minerals, including the complex calcium phosphate mineral known as hydroxyapatite. Tooth demineralization is a precursor to dental erosion and occurs below a pH of 5.5. The phenomenon of enamel degradation is complex; however, at low pH levels, erosion is most likely to occur (Von Fraunhofer, 2004). A carious lesion is usually rough, pitted and irregular, whereas an erosive lesion is generally smooth and regular. The cavitated lesion is located along the cervical margin

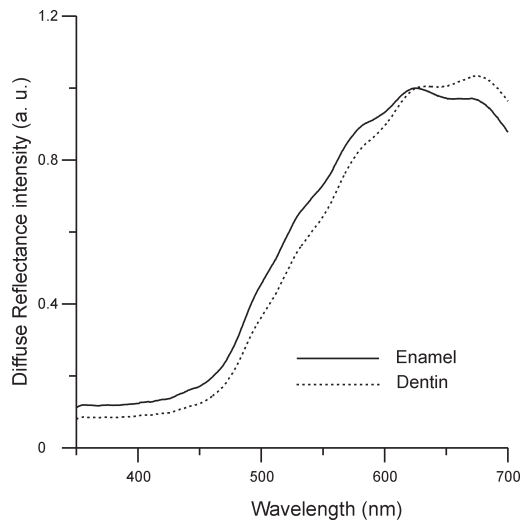


Fig. 5.6 Mean diffuse reflectance spectra of sound tooth enamel and dentin slices normalized with respect to the maximum intensity at 625 nm.

of the restoration and involves both enamel and dentin. The erosive lesions, primarily involving enamel, are found along the perimeter of the restoration. It is likely that an enamel erosive lesion facilitates the creation of a carious lesion especially along the cervical margin.

Table 5.3 Fluorescence ratios derived from curve-fitted spectral amplitude and Gaussian curve area, and the raw LIF spectral data for enamel and dentin in the demineralized state and from the sliced samples.

| Ratios | Curve-fitted amplitude | | | | Curve-fitted area | | | | Raw LIF spectrum | | | |
|-----------|------------------------|--------------|-----------------|-----------------|-------------------|--------------|-----------------|-----------------|------------------|--------------|-----------------|-----------------|
| | Sound Enamel | Sound Dentin | Enamel (demin.) | Dentin (demin.) | Sound Enamel | Sound Dentin | Enamel (demin.) | Dentin (demin.) | Sound Enamel | Sound Dentin | Enamel (demin.) | Dentin (demin.) |
| F410/F440 | 0.45 | 1.19 | 0.71 | 0.79 | 0.37 | 1.49 | 0.74 | 0.88 | 0.48±0.01 | 0.83±0.02 | 0.48±0.01 | 0.49±0.03 |
| F410/F485 | 0.27 | 0.7 | 0.42 | 0.49 | 0.13 | 0.41 | 0.22 | 0.27 | 0.25±0.01 | 0.4±0.1 | 0.33±0 | 0.39±0.02 |
| F410/F525 | 0.23 | 1.12 | 0.7 | 1 | 0.05 | 0.31 | 0.19 | 0.28 | 0.32±0.01 | 0.56±0.2 | 0.48±0.01 | 0.59±0.1 |
| F440/F485 | 0.59 | 0.59 | 0.59 | 0.84 | 0.35 | 0.27 | 0.3 | 0.32 | 0.54±0.01 | 0.89±0.1 | 0.89±0.01 | 0.8±0.1 |
| F440/F525 | 0.52 | 0.94 | 0.99 | 1.29 | 0.13 | 0.21 | 0.3 | 0.35 | 0.67±0.01 | 0.95±0.3 | 0.99±0.03 | 1.19±0.1 |
| F485/F525 | 0.87 | 1.59 | 1.89 | 2 | 0.38 | 0.76 | 0.91 | 1.07 | 1.25±0.01 | 1.36±0.1 | 1.44±0.01 | 1.48±0.04 |

Raw LIF spectral ratios are the mean of 10 measurements ± SD, whereas the curve fitting was done on the averaged spectrum of 10 measurements.

Problems associated with the erosion of enamel and dentin layers can be traced to the increased intake of acidic food and drinks, which gradually dissolve the underlying mineral, both at the surface and at the subsurface resulting in irreversible structural (patho-anatomical) changes in the hard dental tissue. Further, the cariogenic challenges lead to increased surface and subsurface dissolution. Both conditions induce changes in the optical behaviour of the affected enamel. Since the porous enamel scatters more light than sound enamel the net result is that the enamel becomes opaque, at the macroscopic level (ten Bosch, 1996). Optical spectroscopic techniques provide a means to classify and identify these changes so that a proper logical treatment plan can be formulated not only to repair the damage but, more importantly, to eliminate the cause.

In this study, it was noticed (Fig. 5.3a) that enamel destruction due to demineralization leads to an increase in the fluorescence signal intensity in the entire spectral range as observed by Ando et al (2001) and Van der Veen and ten Bosch (1995) during demineralization studies on *in vitro* tooth samples. In contrast, Borisova et al. (2004) had observed a decrease in autofluorescence intensity during demineralization. By normalizing the spectrum with respect to the intensity of the 490-nm band (Fig. 5.3b), it was possible to observe changes in fluorescence spectral

shape and in particular, of the 440-nm band during the demineralization process (Table 5.1). It was seen that the spectral intensity of the 440-nm band actually increases with the extent of demineralization. This increase in intensity at 440 nm could be related to the appearance of the dentin fluorescing compounds associated with the penetration of the demineralizing substances to the dentin layer of the tooth or due to disappearance of prism structure of the hydroxyapatite in enamel with increased demineralization. These changes can be explained more evidently by their chemical composition as sound enamel consists of greater amount of minerals, mainly 96% inorganic material (hydroxyapatite) and a small amount of organic substance and water (4%), whereas sound dentin consists of a larger portion of organic matter (35%) than enamel. Thus, the baseline fluorescence observed could be due to the combined effect of the inorganic matrix with absorbing organic molecules (Hibst and Paulus, 1999; Hunter and Harold, 1987). The emission from organic matter is more intense in the 400–500 nm, and this result in dentin being blue-shifted or relatively more

emissive than enamel at lower wavelengths. Enamel usually exhibits a stronger emission at longer wavelengths due to the emission features of the minerals ensuing in the broadening and red shift of 490-nm spectral band (Fig. 5.1).

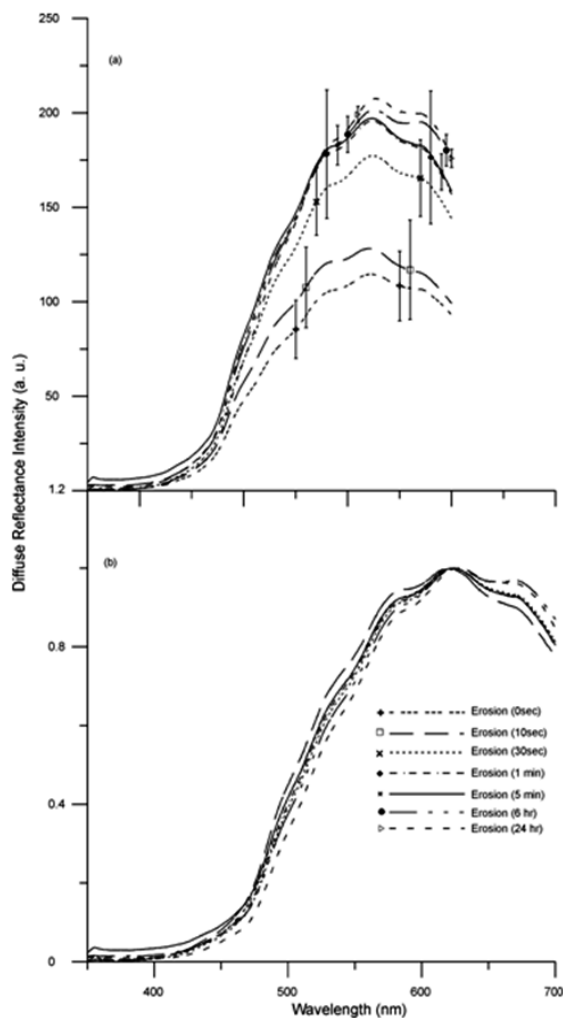


Fig. 5.7 a) Mean diffuse reflectance spectral intensity variation of sound and demineralized tooth during various stages of erosion and **b**) the same diffuse reflectance spectra normalized to the intensity at 625 nm.

Table 5.4 Mean reflectance ratios for enamel and dentin after demineralization and from the enamel and dentin portions of tooth slices.

| Ratios | Sound Enamel | Sound Dentin | Enamel (demin.) | Dentin (demin.) |
|-----------|--------------|--------------|-----------------|-----------------|
| R500/R700 | 0.54±0.03 | 0.37±0.01 | 0.52±0.01 | 0.41±0.01 |
| R600/R700 | 1.06±0.02 | 0.93±0.01 | 1.18±0.01 | 1.09±0.01 |
| R650/R700 | 1.11±0.01 | 1.04±0.01 | 1.18±0.01 | 1.13±0.01 |

Ratios given are mean of 10 measurements ± SD.

Further, by curve-fitting using Gaussian spectral functions, it was possible to resolve the LIF spectra into four constituent peaks centered at 409.1, 438.1, 492.4 and 523.1 nm in sound enamel and at 412.0, 440.1, 487.8 and 523.4 nm in sound dentin. The emission around 410 nm in enamel and dentin could be due to the presence of hydroxypyridinium chromophore, a collagen crosslink (Fujimoto et al, 1977; Walters and Eyre, 1983) and dityrosine (Booij and ten Bosch 1982), as reported earlier. The peak positions given in Table 5.1 could be considered as fairly accurate since the correlation coefficients of fitting were close to unity and χ^2 values were low.

Significant differences in the Gaussian amplitude and area ratios (F410/F440, F410/F525 and F485/F525) were observed during the process of demineralization (Table 5.2). Improved sensitivities were seen in these ratios as compared to those derived from raw LIF spectra. Among the various ratios, the curve-fitted Gaussian curve area ratio, F410/F525 shows maximum sensitivity to distinguish early transformation in the enamel layer. In contrast, curve-fitted Gaussian area ratio F435/F525 was reported to be suitable for discrimination between different stages of tooth decay (Subhash et al, 2005).

The diffuse reflectance intensity in sound tooth is usually lower (Fig. 5.7a) owing to the increased reflection from the enamel surface that limits the amount of radiation inside the tooth to generate back scattering from the underlying enamel and dentine layers. During demineralization, changes in light scattering properties associated with the destruction of the waveguide structure of the enamel enhance the diffuse reflectance spectra. However, the nucleic acids, urocanic acid and proteins that are

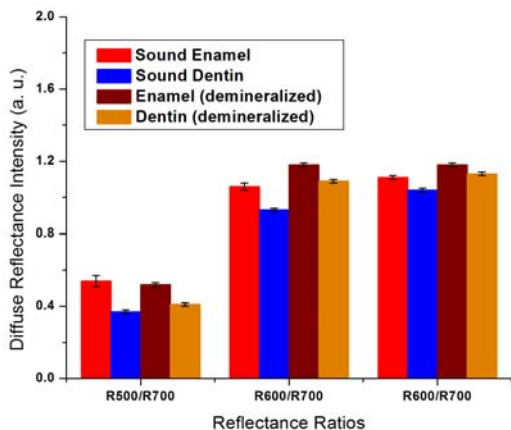


Fig. 5.8 Reflectance ratios of sound enamel and dentin slices, and those of demineralized tooth samples (mean of 10 measurements each at 0, 10 s, 30 s and 1 min of demineralization depicted as enamel and mean of 10 measurements at 5 min, 6 h and 24 h of demineralization depicted as dentin).

junction (DEJ) and that there is a marked increase in hardness at the enamel surface. The deeper layers of the enamel are softer and have a lower specific gravity than the enamel surface and concluded that the increase in hardness is associated with increase in specific gravity. This could be responsible for the gradual variation in the fluorescence and diffuse reflectance spectral intensity during demineralization (Figs. 5.3 and 5.7).

Of all the structural components of the tooth, enamel is the most resistant to acid dissolution, but with continued exposure to acid, it weakens, and demineralization progresses through the enamel surface in a linear fashion, following the direction of the enamel rods at a constant rate (Anderson and Elliott, 2000). Enamel rods, which vary in diameter from 8 μm near the external surface and 4 μm near the dentin border, are oriented from the DEJ towards the external surface of the tooth in a perpendicular direction. There are more enamel rods toward the DEJ and less near the external surface of the tooth. At the cervical margin, enamel is thinner, and the enamel rods are oriented apically (Roberson et al, 2002). Viewed cross sectional, enamel rod is best compared to a keyhole with the top, or head, oriented towards the crown of the tooth with the bottom, or tail, oriented towards the root of the tooth. During dental

present in the tooth have strong absorption in ultraviolet and blue-green spectral region that dominates over signal in the shorter wavelength region. This result in a diminished diffuse reflectance spectral intensity in the 400- to 600-nm range in the spectra normalized at 610 nm (Fig. 5.7b). Among the reflectance ratios studied, the R500/R700 ratio gives the best sensitivity for identifying erosive changes to the tooth enamel. This ratio was also found suited in an earlier study for diagnosing different stages of tooth caries (Subhash et al, 2005).

Karlstrom (1931) reported that hardness of tooth enamel increases outward from the dento-enamel

junction (DEJ) and that there is a marked increase in hardness at the enamel surface. The deeper layers of the enamel are softer and have a lower specific gravity than the enamel surface and concluded that the increase in hardness is associated with increase in specific gravity. This could be responsible for the gradual variation in the fluorescence and diffuse reflectance spectral intensity during demineralization (Figs. 5.3 and 5.7).

erosion, etchants remove the outer 10 micrometers on the enamel surface and makes a porous layer 5–50 μm deep (Summit et al, 2001). This roughens the enamel microscopically and results in a greater surface area on which to bond. The effects of acid etching on enamel can vary. Important variables are the amount of time the etchant is applied, the type of etchant used, and the crystal orientation in enamel (ten Cate, 1998).

5.5 CONCLUSIONS

Loss of too many minerals during demineralization leads to fast development of caries. This underscores the importance of early detection of tooth demineralization. Caries affecting pulp and dentin can be easily detected by visual inspection, but it is a tedious task to track mineral loss during early transformations in the enamel structure. Nevertheless, formation of tooth cavity is an advanced symptom of a bacterial disease or chemical dissolution that has been in progress for some time. On the basis of the results obtained in the present study, the UV laser-based ratio technique appears to have the potential for *in vivo* monitoring of demineralization changes in tooth. Among the fluorescence ratios studied, the F410/F525 derived from curve-fitted Gaussian amplitude and area gives better sensitivity as compared to that derived directly from the recorded LIF spectrum. Although the R500/ R700 reflectance ratio also has the potential to detect demineralization changes, the increase in sensitivity of the F410/ F525 ratio achieved through curve-fitting using Gaussian spectral functions makes it more suited for monitoring early transformations to the enamel layer. The information contained in the LIF spectral shape and constituent peaks contribution associated with changes in the intrinsic fluorophores content allow accurate differentiation between carious formation and early demineralization in tooth. Further *in vivo* studies are required using the LIFRS system to test its efficacy in a clinical environment for revealing early mineral loss and tooth demineralization.

Chapter 6

Spectroscopic Investigation of De- and Re-mineralization of Tooth Enamel *in vitro*

6.1 INTRODUCTION

Cyclic demineralization and remineralization of the tooth replicate the natural process of demineralization and remineralization that takes place in the oral cavity environment. Characterization of the behaviour of tooth enamel lesions in a simulated natural environment by optical methods leads to improvement in sensitivities for detection of early demineralization and helps to introduce appropriate treatment modalities that avoid the risk of aesthetic damage or restorative intervention. Towards this, nitrogen laser-induced fluorescence and tungsten halogen lamp-induced DR spectra were recorded on a miniature fiber-optic spectrometer from tooth samples subjected to cyclic de- and re-mineralization (CDR) for 10 days, followed by continuous remineralization (CR) for 14 days. The LIF and DR spectral intensities were found to decrease with CDR, but get reversed during CR. This chapter presents the applicability of LIFRS to detect de- and re-mineralization changes in tooth *in vitro* and correlates the results of curve-fitting with those obtained from raw spectral data and DR measurements.

6.2 STUDY MATERIAL AND PROTOCOL

Twenty five sound teeth were collected from a nearby dental clinic following extraction, for various reasons including periodontal problems and transported to the laboratory in isotonic saline. Prior to measurements, the samples were washed in deionized water, cleared of food particles or blood clotting and dried with tissue paper. A square window of dimensions 3.5 mm × 3.5 mm was made on buccal side of each tooth by painting the remaining portions with acid resistant nail polish. After recording the baseline spectra, tooth samples were exposed to demineralization and remineralization by a cyclic process to stimulate a near natural *in vivo* environment (Jones et al, 2006). The daily schedule for cyclic treatment consisted of 6 hr demineralization and 17 hr remineralization. During demineralization, each tooth sample was immersed in 40 mL aliquot buffer solution containing 2.0 mmol/L calcium, 2.0mmol/L phosphate and 0.075mol/L acetate, maintained at pH 4.3 and 37°C temperature. Afterwards, each sample was remineralized in a 20mL solution of 1.5mmol/L calcium, 0.9 mmol/L phosphate and 150mmol/L potassium chloride maintained at pH 7.0 and 37°C temperature. Tooth samples were subjected to 10

days of cyclic demineralization and remineralization (CDR) regime, which represents an early caries lesion. The tooth samples were then subjected to continuous remineralization (CR) for 14 days in the above mineralizing solution, with the addition of 2-ppm F⁻ in the form of NaF to enhance the remineralization effect.

The LIF and diffuse reflectance spectra were then recorded in the 350-700 nm spectral range using the OOI Base32 software (Ocean Optics Inc., USA) after each phase of de-mineralization/remineralization treatment of tooth lesions. The OOI Base32 software was configured to record the spectra, averaged for 40 scans, with a boxcar width of 10 nm and an integration time of 350 ms. Ten sets of autofluorescence and diffuse reflectance spectra were recorded sequentially from the exposed region of tooth samples after each treatment of CDR and CR. The mean spectra from each treatment is then determined and used in data analysis. The mean LIF spectra from the sound, demineralized and remineralized regions were curve-fitted using Gaussian spectral functions. The deconvoluted peak intensities and Gaussian curve areas were then utilized to identify de- and remineralization changes in tooth enamel.

6.2.1 Visual assessment of lesions

An experienced clinician, who was blinded to the spectral findings examined each tooth after completion of fluorescence and diffuse reflectance measurements. Any signs of demineralization, normally a white spot or surface roughness along with the

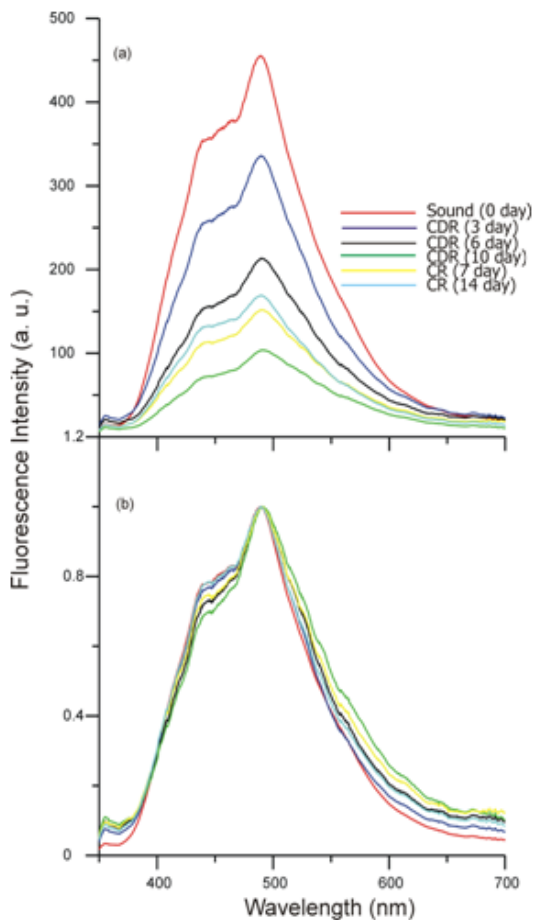


Fig.6.1. a) Mean LIF spectra during CDR and CR, and **b)** LIF spectra normalized to the intensity at 490 nm.

time at which it occurred, were recorded. An analysis of variance (ANOVA) was performed to detect whether the average LIF and DR spectral intensities differed between the sound, demineralized and remineralized enamel groups.

6.3 RESULTS

6.3.1 LIF spectral features

The fluorescence spectrum of sound tooth consists of a broad peak at 490 nm with a less intense shoulder around 440 nm. Although the spectral shape remains the same during de-mineralization and re-mineralization, the fluorescence intensity follows a decreasing trend in 10 days of CDR and an increasing trend in 14 days of CR, as shown in Fig. 6.1a. In order to ascertain changes in the emission peak intensity, the LIF spectra were normalized with respect to the intensity of the 490 nm peak as shown in Fig. 6.1b. Fig.6.2 shows the extent of change in the 440 nm peak intensity after CDR and CR. A gradual decrease in intensity was observed for the 440 nm band during CDR, which was followed by an intensity enhancement in CR. Further, beyond 500nm, we noticed a corresponding increment in intensity followed by a decline in the long wavelength tail of the 490 nm peak.

The mean LIF spectra during various stages of CDR and CR were curve-fitted using Gaussian spectral functions. It can be seen that peak fitting of LIF spectra using four Gaussian spectral peaks gives the best fit, with an r^2 value of 0.998. Table 6.1 shows the peak position of the various bands, their Gaussian curve areas, full width at half intensity maximum (FWHM) and the χ^2 and r^2 values of fitting during different stages of CDR and CR. In sound tooth, the four bands are located at 411.32, 440.08, 484.37 and 521.98 nm. These

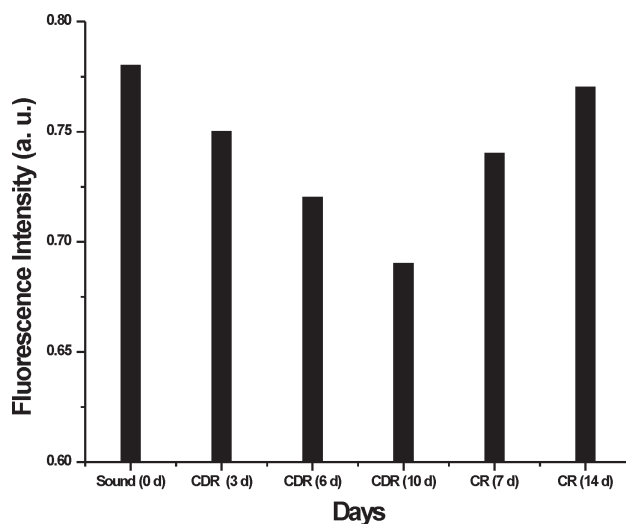


Fig.6.2. Mean fluorescence spectral intensity variation at 440 nm during CDR and CR.

bands will henceforth be designated as 410, 440, 485 and 525 nm peaks, for simplicity. It is seen that the 525 nm peak shifts towards the red region by 35.3 nm during CDR and these shifts gets completely nullified in 14 days of CR (Table 6.1). In addition, it was observed that the FWHM width of the 525 nm peak reduced by 27.7 nm in 10 days of CDR, which gets reversed within 14 days of CR whereas an opposite trend was observed in the case of the 485 nm peak, as shown in Fig.6.3. Furthermore, a decreasing trend followed by an enhancement is observed in the curve-fitted peak amplitude and Gaussian curve area of all the four peaks at 410, 440, 485 and 525 nm during CDR and CR. However, these variations were pronounced for the 410 and 525 nm peaks, as shown in Fig. 6.4(a, b).

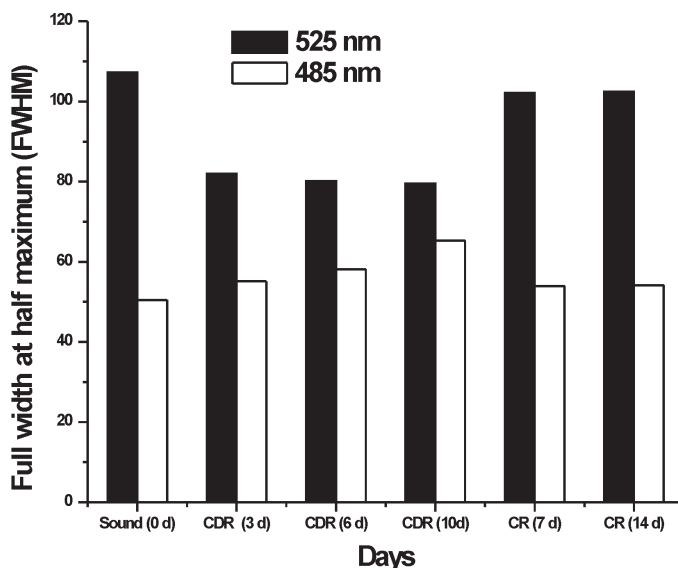


Fig.6.3. Width (FWHM) of 525 and 485 nm peaks obtained by curve fitting.

6.3.2 Diffuse reflectance spectral features

Fig. 6.5 a, b shows the mean diffuse reflectance spectra during various stages of CDR and CR, and the same normalized to the intensity at 675 nm. It can be seen that CDR produces a gradual decline in spectral intensity, whereas CR produces an increase in intensity (Fig. 6.5a). However, in the normalized DR spectra there are no noticeable changes in the spectral shape, except for a slight decrease in spectral intensity in the 450 to 600 nm region.

6.3.3 Spectral intensity and curve area plots

The temporal profile of raw LIF intensity at 440 and 490 nm and the DR spectral intensity at 500 nm is plotted in Fig. 6.6a along with changes in the Gaussian curve area of the deconvoluted peaks at 410 and 525 nm in Fig. 6.6b during CDR, whereas

the corresponding changes during CR is shown in Fig. 6.7(a, b). The overall fluorescence and diffuse reflectance spectral intensities and Gaussian curve areas of the constituent bands were found to decrease gradually with CDR (Fig. 6.6) owing to mineral losses in tooth, whereas the intensity increases with CR owing to mineral restoration (Fig. 6.7). As compared to the variations seen in raw spectral intensity at 440, 490 and 500 nm, the Gaussian curve area of 410 and 525 nm peaks show a pronounced variation. This can also be seen from the slope of the corresponding lines in Fig. 6.6 and 6.7.

Table 6.1. Results of curve-fitting on the mean LIF spectrum from sound and exposed areas of tooth during CDR and CR.

| Tooth | Peak Centre (nm) | FWHM (nm) | Area | Amplitude | χ^2 | r^2 |
|-------------|------------------|-----------|--------|-----------|----------|-------|
| Sound | 411.32 | 33.722 | 6064.6 | 143.49 | 32.79 | 0.998 |
| | 440.08 | 30.699 | 7637.9 | 198.52 | | |
| | 484.37 | 50.489 | 17575 | 277.74 | | |
| | 521.98 | 107.23 | 27189 | 202.31 | | |
| CDR(3 day) | 406.83 | 23.869 | 1891 | 63.21 | 12.68 | 0.999 |
| | 436.13 | 33.589 | 6685.5 | 158.81 | | |
| | 485.23 | 55.147 | 16718 | 241.88 | | |
| | 534.02 | 81.969 | 10450 | 101.72 | | |
| CDR(6 day) | 406.79 | 22.62 | 967 | 34.109 | 5.56 | 0.998 |
| | 435.74 | 32.658 | 3563.5 | 87.062 | | |
| | 486.74 | 58.101 | 11474 | 157.57 | | |
| | 541.7 | 80.143 | 6177.6 | 61.503 | | |
| CDR(10 day) | 408.41 | 23.765 | 544.96 | 18.297 | 1.57 | 0.998 |
| | 436.12 | 28.753 | 1218.6 | 33.816 | | |
| | 488.95 | 65.254 | 6675.4 | 81.623 | | |
| | 557.37 | 79.485 | 2902.1 | 29.132 | | |
| CR(7day) | 408.1 | 23.232 | 840 | 28.849 | 2.34 | 0.999 |
| | 436.66 | 30.588 | 2302.8 | 60.069 | | |
| | 485.54 | 53.986 | 5681.3 | 83.967 | | |
| | 523.99 | 102.13 | 7594.8 | 59.331 | | |
| CR(14 day) | 408.76 | 26.759 | 1302.3 | 38.832 | 3.29 | 0.999 |
| | 437.6 | 30.59 | 2775 | 72.382 | | |
| | 484.25 | 54.182 | 6866.1 | 101.11 | | |
| | 523.39 | 102.46 | 8161.8 | 63.56 | | |

Abbreviations: FWHM- full width at half maximum; χ^2 - chi-square; r^2 - correlation coefficient; CDR- cyclic demineralization and remineralization; CR- continuous remineralization

Visual inspection of the teeth failed to detect any signs of demineralization until 6 days. At the 10th day, visual evidence of demineralization was noted in all experimental samples. Spectral data were analyzed by ANOVA and statistically significant differences in mean spectral intensities ($p < 0.05$) were noticed between sound, demineralized and remineralized enamel in LIF and DR spectral measurements,

demonstrating a significant decrease in spectral intensity during demineralization and an increase during remineralization.

6.4 DISCUSSION

Tooth enamel is a very highly mineralized tissue consisting of approximately 96% of dry weight as inorganic material while the rest is water and organic material (Hunt, 1959; Dawes, 2003). Demineralization and remineralization have a vital impact on the strength and hardness of dental enamel. Usually, a tooth is in a constant state of cyclic or back-and-forth demineralization and remineralization due to interactions with fermentable carbohydrates and surrounding saliva. Initial enamel caries develop when

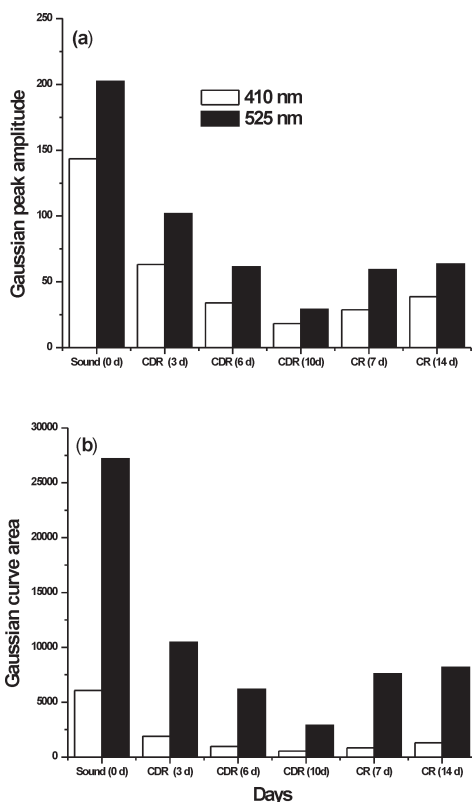


Fig.6.4(a, b). Curve-fitted peak amplitude and Gaussian curve area of 410 and 525 nm peaks.

the pH level at the tooth surface is lower than which could be counterbalanced by remineralization. It has been found that at lower pH, millions of calcium and other mineral ions are released from the hydroxyapatite latticework, which eventually leads to loss in structural integrity of tooth enamel. Caries advance may be arrested at this stage. In the present CDR study, the pH was maintained at a lower value of 4.3 by periodic monitoring using a pH meter. Monitoring demineralization and remineralization of dental hard tissues is essential for the prevention and minimally invasive treatment of dental caries. Optical spectroscopic techniques provide an approach to identify these incipient changes in enamel so that a proper restorative procedure can be formulated to prevent caries progression.

We have used the *in vitro* cyclic demineralization and remineralization which is the best possible way to simulate an *in vivo* environment for studying the dynamics of tooth caries development (ten Cate,

1990; White and Featherstone, 1987; Featherstone et al, 1986). This is because in the oral cavity, the demineralization process involves cycles of acid attack following dietary carbohydrate intake, which results in an increase in acid production by the oral micro flora, leading to the dissolution of minerals. As time goes on, there is a reversal of the acidic environment to the neutral status, due to various physiological and chemical factors. This return of acidic pH to neutral status results in deposition of lost minerals, thus retaining the tooth integrity (Loesche WJ, 1986).

In our CDR study, it was observed (Fig. 6.1a) that impairment of enamel due to demineralization leads to a decrease in the fluorescence signal intensity whereas remineralization produces an increase in intensity during CR treatment. By normalizing the spectrum with respect to the intensity of the 490 nm band (Fig. 6.1b); we were able to observe changes in fluorescence spectral intensity of the 440 nm band that appears as a shoulder to the 490 nm peak. Borisova et al (2004) also observed a significant reduction in the intensity of fluorescence signal of demineralized and carious tooth.

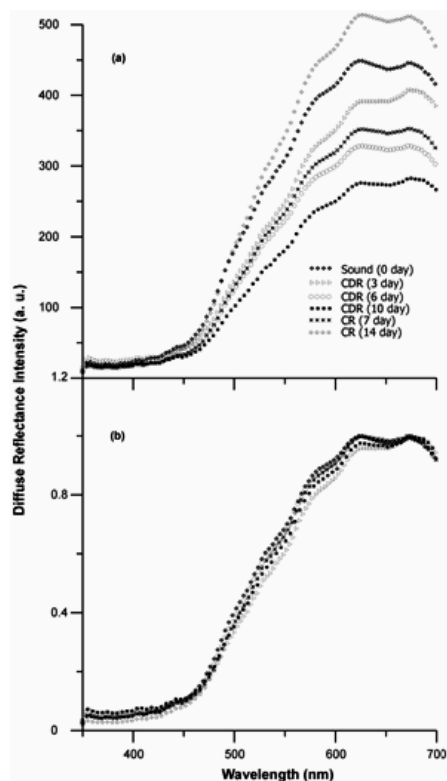


Fig.6.5 a) Mean DR spectral intensity during CDR and CR and **b)** DR spectra normalized to the intensity at 675 nm.

Normally, tooth enamel is composed of millions of prisms or rods with waveguide properties that facilitate deep penetration when illuminated with UV-visible light. During tooth demineralization, the prism structure is damaged and the waveguide properties are lost so that the irradiated light does not penetrate deeply (Ando et al, 2001). This leads to a reduction in the fluorescence intensity (Fig. 6.1 and Fig. 6.2). It was also reported that changes in fluorescence might be due to the changes in the calcium and phosphate mineral content of tooth enamel, which makes them soft (Al-khateeb et al, 1997a). Demineralization of tooth enamel is not a simple chemical interaction between enamel crystals and surrounding fluid, because enamel is a microporous solid and these inter-crystalline spaces are filled with tissue fluid from the pulpo-

dentinal organ. The fine mesh work of protein that covers enamel crystals also influences the chemical behaviour of the enamel.

The LIF spectra of sound tooth was resolved into four constituent peaks centered at 411.32, 440.08, 484.37 and 521.98 nm by curve-fitting using Gaussian spectral functions, which falls close to the values reported in an earlier study for detection of *in vitro* dental erosion (Shiny et al, 2008). The emission peak around 410 nm could be attributed to the presence of hydroxypyridinium chromophore, a collagen crosslink and dityrosine, as reported earlier (Fujimoto et al, 1977; Walters and Eyre, 1983; Booij and ten Bosch, 1982). There are noticeable variations not only in the peak emission but also in the peak amplitude, FWHM width, and the Gaussian curve area during CDR and CR. The variations in

the curve-fitted peak amplitude and Gaussian curve area of the 410 and 525 nm peaks (Table 6.1, Fig. 6.4) and the shift in peak position and variation in the FWHM width of the 525 nm peak during CDR and CR (Fig. 6.3) has the potential to be utilized to understand the de- and re-mineralization status of tooth in an *in vivo* environment. This variation observed in peak position and FWHM width of the 525 nm could be due to the changes in chemical composition during the disintegration process as observed during caries development (Subhash et al, 2005). The red-shift of the 525 nm peak during CDR is similar to the shift seen in dentin and pulp level caries. Therefore, these changes in spectral characteristics could be useful in the identifying the extent of demineralization and stage of tooth caries (Subhash et al, 2005).

Further, the concurrent increase and decrease in spectral intensity noticed beyond 500 nm during CDR and CR could be due to an energy transfer between the levels

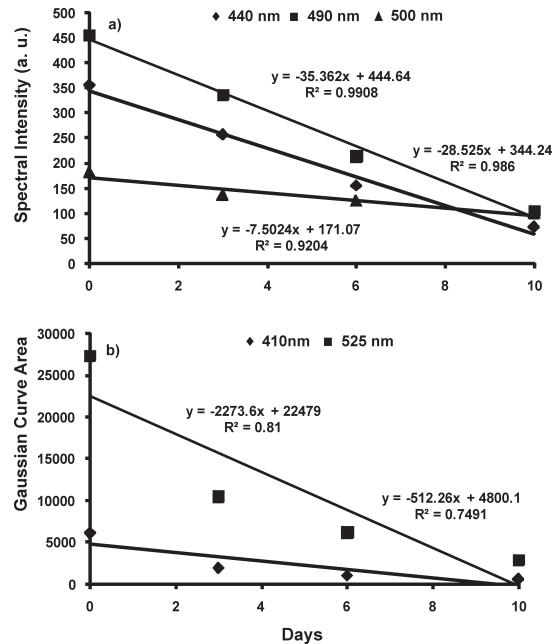


Fig.6.6. a) Temporal variation in mean LIF spectral intensity at 440, 490 nm and DR intensity at 500 nm during CDR and **b)** Temporal variations calculated from Gaussian curve area for 410 and 525 nm peaks during CDR.

involved in the 440-nm emission and the long wavelength tail of the 490 nm band. The red shift of the 525 nm peak seen in the curve-fitted spectra during CDR and its complete retrace to initial values (Table 6.1) during CR supports this hypothesis.

The diffuse reflectance intensity in sound tooth is higher owing to increased reflection from the enamel surface. This leads to a lower amount of radiation entering beyond the enamel to generate sufficient back scattering from the underlying enamel and dentine layers. Further, during demineralization, changes in light scattering properties associated with the destruction of the waveguide structure of the enamel diminish the diffuse reflectance spectra (Ando et al, 2001).

However, the nucleic acids, urocanic acid and proteins that are present in tooth have strong absorption in the ultraviolet and blue-green spectral regions and this dominates over signal in the shorter wavelength region and results in diminished diffuse reflectance spectral intensity in the 400-600 nm range (Fig. 6.5). It is also seen that an increase in mineral volume from fluoride-enhanced remineralization significantly decreases optical reflectivity of artificial lesions within an enlarged surface zone, whereas reflectivity does not necessarily decrease in the body of underlying lesion after remineralization (Jones and Fried, 2006).

As carious lesion undergoes remineralization, the deep porosities accumulate more mineral than lesion surface zone. It is also reported that successful remineralization of the surface zone limits the continued diffusion of ions into the deeper regions of the lesion, which was observed during *in vivo* remineralization studies of early caries (Arends and Gelhard, 1983). As lesion progresses, the mineral

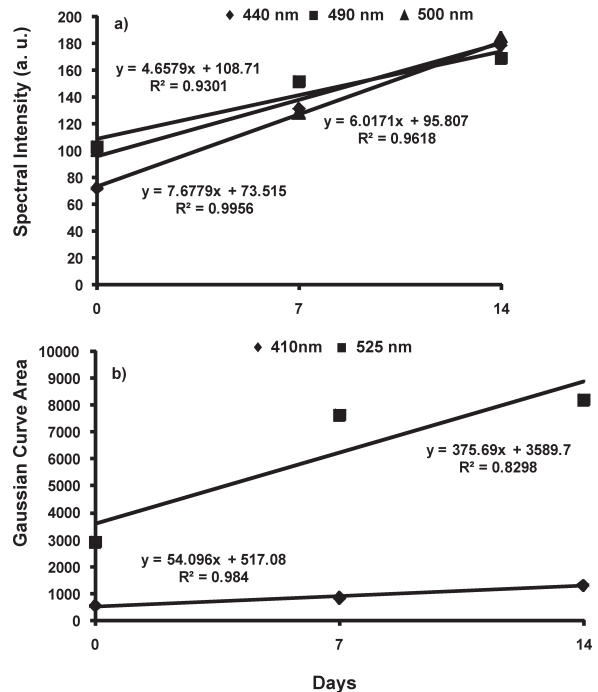


Fig.6.7. a) Temporal variation in mean LIF spectral intensity at 440, 490 nm and DR intensity at 500 nm during CR and **b)** Temporal variations calculated from Gaussian curve area for 410 and 525 nm peaks during CR.

content at specific depth does not vary significantly after a certain volume; instead, diffusion of ions through this area doesn't affect the mineral volume (Arends et al, 1997), whereas in remineralization, mineral volume is increased mainly by growth of the remaining crystals, restoration of partially demineralized crystals and the deposition of newly formed crystals (Yanagisawa and Miake, 2003), which might be the reason for the gradual variations in fluorescence and DR spectral features during remineralization (Fig. 6.1 and Fig. 6.5). Also, remineralization process is slower as compared to demineralization, when mineral uptake occurs in very small quantities.

6.5 CONCLUSIONS

The study shows that both LIF with excitation by a UV laser (337 nm) and DR spectroscopy with white light illumination have the potential to identify de- and remineralization changes in tooth from spectral intensity variations. Among the various parameters studied, variation in the FWHM width and peak position of the 525 nm peak deconvoluted by curve-fitting, and the changes in the Gaussian amplitude and curve area of the 410 and 525 nm peaks appear to be effective in identifying incipient changes in tooth. Although the diffuse reflectance intensity variation during CDR and CR are marked, the information contained in the LIF spectral intensity and constituent peak contributions achieved through curve fitting are more suited for monitoring of early transformations in tooth enamel. Nevertheless, these modalities need to be further explored in a clinical environment to test its efficacy for monitoring changes in mineral content.

Chapter 7

Characterization of Dental Caries by LIF
Spectroscopy with 404 nm Excitation

7.1 INTRODUCTION

Despite our improved understanding of the caries process and the availability of effective intervention, caries lesions still progress to the stage where tooth structure is compromised and invasive intervention and restoration are required. Studies have shown that non-cavitated caries lesions are significantly more prevalent than cavitated caries lesions. This chapter reports the performance of the laser-induced fluorescence (LIF) spectroscopy in detecting dental caries and to classify between different stages of caries with excitation at 404 nm from a diode laser. Towards this, *in vitro* LIF spectra were recorded from 16 sound, 10 non-cavitated and 10 cavitated molar teeth. Autofluorescence spectral intensity of caries lesions were found lower than that of sound tooth and decreased with the extent of caries. The LIF spectra of caries tooth showed two peaks at 635 and 680 nm in addition to the broad band seen at 500 nm in sound tooth. The efficiency of using the fluorescence spectral intensity ratios in identifying caries lesions was studied and the results are presented.

7.2 STUDY MATERIAL AND PROTOCOL

Sound and caries tooth samples belonging to different categories were collected from a nearby dental clinic following extraction, for various reasons including periodontal problems and were transported to the laboratory in isotonic saline. Usually the samples were stored at room temperature (27 ± 3 °C) and measurements were carried out as soon as the samples reached the laboratory. The tooth samples were classified clinically, by an experienced dental practitioner, depending on the visual-tactile or radiographic examination before extraction from the patient. Clear enamel-intact tooth surfaces were considered as sound, while enamel caries with intact surface, with loss of luster, surface roughness, white spot and brown lesions were considered as non-cavitated lesions and those with visible cavitation, deeper than 3-4 mm were taken as cavitated lesion. The study samples included 16 sound, 10 non-cavitated and 10 cavitated molar teeth. Samples studied covered occlusal surface caries.

7.2.1 Experimental Methods

Before measurements, the samples were taken out of the PET bottles and washed

in running water. They were then cleared of food particles or blood clot using a tooth brush and water and then dried with tissue paper. Visual inspection was again carried out as per the protocol for tooth classification. During visual-tactile inspection, the samples were categorized based on characteristics such as tooth type, tooth discoloration, localized enamel breakdown, and cavitation in enamel exposing dentin or affecting the pulp.

Due to the diverse nature of the caries lesions, 12 sets of LIF measurements were taken from each selected area (6 mm dia.) and averaged for data analysis. The OOI Base32 software was configured to record the spectra, averaged for 40 scans, with boxcar width of 8 nm and an integration time of 50ms. Fluorescence intensity ratios are then determined from the emission peak intensity of the mean spectra for discriminating different stages of dental caries. To account for the broad nature of the peaks and sample-to-sample variation in peak position due to changes in chemical composition or fluorophore content of tooth, the mean LIF spectral intensity over an interval of ± 10 nm at the emission peak was used to determine the LIF spectral ratios. ANOVA was performed to detect whether the average LIF spectral intensity differed between the groups belonging to sound, non-cavitated and cavitated caries lesions.

The ROC curve areas were then determined to classify different stages of caries. In ROC analysis, which is an excellent statistical approach for new techniques with numerical values, the sensitivities for detecting dental caries are plotted against values of 1 minus the specificity. The more precisely a technique separates the data classes, the closer would be the corresponding ROC-AUC to unity. In the present study, tooth without lesion were considered as sound, while tooth with loss of lustre, surface roughness and visible cavitation were considered as caries lesion. This allows one to make a fair judgment on the efficacy of methods without being constricted to a single value of sensitivity and specificity, which largely depends on the cut-off value chosen (Metz, 1978).

7.3 RESULTS

7.3.1 LIF spectral features

Fluorescence spectra of dental hard tissues vary due to alteration in the chemical composition of pathological areas and tissue optical properties. Figure 7.1 shows the averaged fluorescence spectra recorded from 16 sound, 10 non-cavitated and 10 cavitated tooth samples, normalized to the maximum intensity around 500 nm. The

overall fluorescence intensity of caries lesions were found lower than that of sound tooth and decreased with the extent of caries. However, the fluorescence spectral intensity in the red wavelength region was greater for carious when compared to sound regions. The LIF spectrum of sound tooth shows a broad emission around 500 nm with a long tail extending towards the red region. In non-cavitated and cavitated caries lesions, two additional peaks were seen at 635 and 680 nm. In cavitated caries lesion, the 500 nm band appears broadened and red-shifted by about 10-15 nm.

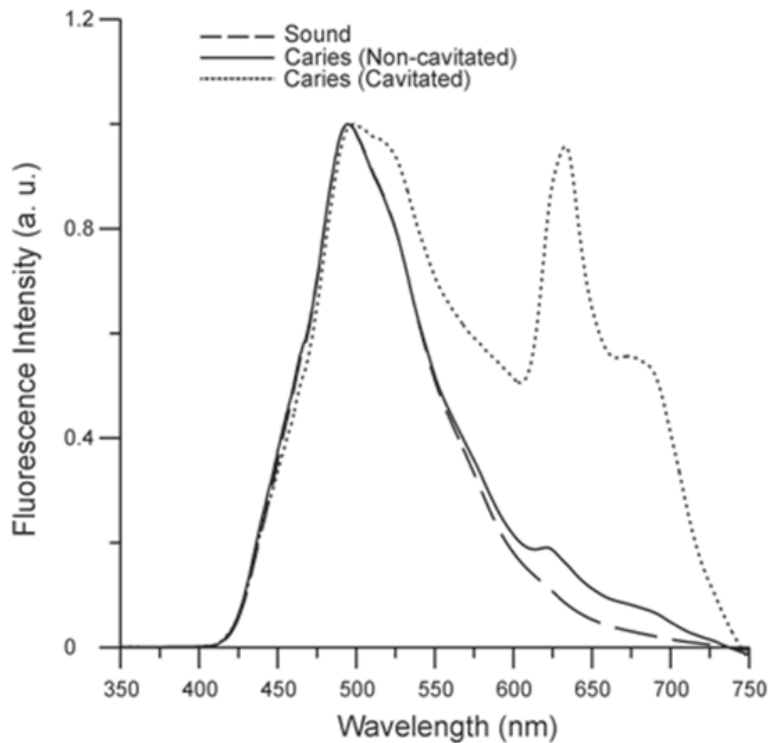


Fig.7.1. Mean LIF spectra from sound and caries lesions belonging to different stages, normalized to fluorescence peak intensity. Sound spectra represent the mean of 12 measurements each in 16 samples, whereas the spectrum from non-cavitated and cavitated caries lesions is the mean of 12 measurements in 10 samples.

7.3.2 LIF intensity ratios

Mean LIF spectral intensity ratios (F_{500}/F_{635} and F_{500}/F_{680}) determined from

sound and caries tooth samples of diverse categories are shown in Table 7.1. It is observed that both fluorescence intensity ratios calculated from caries tooth are always lower than those of sound tooth. The F500/F680 ratio shows maximum variance of 30% between sound and non-cavitated caries lesions and 93% between sound and cavitated caries lesions, whereas between non-cavitated and cavitated caries lesions, both fluorescence ratios show a variation of 89%.

One way ANOVA test was also used to determine the variations in average spectral intensity among each groups. Statistically significant differences in mean spectral intensities were noticed at 99% confidence interval ($p < 0.001$) between sound, non-cavitated and cavitated caries lesions.

Table 7.1 Mean laser-induced fluorescence spectral ratios from sound and carious tooth belonging to different categories.

| Tooth types | Specimen No. | F500/F635 (%) | F500/F680 (%) |
|----------------------|--------------|-----------------|-----------------|
| Sound tooth | 192 | 12.6 ± 1.8 | 34.4 ± 4.4 |
| Non-cavitated caries | 120 | 10.3 ± 2.8 (19) | 24.0 ± 5.7 (30) |
| Cavitated caries | 120 | 1.1 ± 0.6 (91) | 2.4 ± 0.9 (93) |

The percentage given in parentheses denotes the variation with respect to the sound tooth

7.3.3 Diagnostic performance of LIF spectroscopy

ROC curve analysis was used to check the diagnostic accuracy of discriminating diseased from normal cases. In general, an area under the ROC curve close to 0.5 signifies the failure of the method used, whereas an area > 0.9 indicates good discrimination, demonstrating excellent separation between the two classes. In the present study, high values were observed for the area under ROC curves with the LIF spectroscopic method to detect dental caries and to classify different stages of caries. The results for distinguishing sound tooth from cavitated and non-cavitated lesions, and between cavitated and non-cavitated lesions are shown in Table 7. 2. Characterization was most successful for discriminating caries lesions from sound tooth (ROC-AUC: 0.94 ± 0.01 for F500/F635 and F500/F680). The maximum ROC-AUC value of 1.00 was observed for both ratios between sound and cavitated caries lesions. The ROC-AUCs obtained for discriminating sound from non-cavitated caries lesions were 0.84 and 0.89 for F500/F635 and F500/F680 ratios, respectively. Further, an ROC-AUC of 0.84 was obtained for distinguishing non-cavitated and cavitated caries lesions. Among these two ratios,

the F500/F680 was more suited to discriminate all caries lesions from sound tooth (ROC-AUC: 0.94). These studies suggest that information on the stage of caries could be extracted from autofluorescence characteristics of cavitated and non-cavitated lesions.

Table 7.2 Area under the ROC curve for discriminating different types of caries lesions using fluorescence intensity ratios.

| Tissue Type | F500/F635 | F500/F680 |
|--|-----------|-----------|
| Sound versus caries | 0.93 | 0.95 |
| Sound versus non-cavitated lesions | 0.84 | 0.89 |
| Sound versus cavitated lesions | 1.00 | 1.00 |
| Non-cavitated versus cavitated lesions | 0.84 | 0.84 |

Caries: combined values of non-cavitated and cavitated caries lesions

7.4 DISCUSSION

Dental caries is a chronic, endemic disease. The chronic nature of the disease is manifested in slow lesion progression, and this offers a window of opportunity for intervention, to reverse mineral loss or at least arrest lesion progression, before the development of irreversible damage to the dental hard tissues. Most of the optical techniques are based on the differences in fluorescence between sound tooth enamel and caries lesion.

In this study, significant variation was observed between the fluorescence spectra of sound tooth and that of different caries tooth (Fig. 7.1). The caries tooth always exhibit lower fluorescence intensity than sound tooth. This could be attributed to the changes in the fluorophore content and to the absorption and scattering properties of the caries layer. Normally, tooth enamel is composed of millions of prisms or rods with waveguide properties that facilitate deep penetration when illuminated with light. In case of dental caries, the prism structure is damaged and the waveguide properties are lost so that the irradiated light cannot penetrate deeply. This leads to a reduction in the fluorescence intensity of caries lesion (Ando et al, 2001). Changes seen in the fluorescence spectrum could also be attributed to the changes in the physical structure and chemical composition during the disintegration of tooth enamel leading to caries formation or due to the import of exogenous molecules during the caries process. This clearly supports the progressive rise of fluorescence spectral intensity in the red wavelength region during caries progression, with concomitant decrease in the

autofluorescence emission around 500 nm.

Another possible explanation for the changes in fluorescence lies with the variation in light scattering. When tooth is illuminated by blue light, it gets absorbed by the chromophores in the tooth. In dental caries, the light propagation directions are different as compared to sound tooth so that more fluorescent photons are emitted in sound tooth than in caries lesion (Ando et al, 2001). König et al (1999) also observed that carious lesions exhibited slower fluorescence decay than intact sound tissue. The long-lived fluorophore present in carious lesions only emitted in the red spectral region.

With 404 nm laser excitation, a broad autofluorescence emission was observed around 500 nm in sound tooth from natural enamel (König et al, 1998). Also emissions at 635 and 680 nm from endogenous porphyrins, particularly protoporphyrin IX (PpIX), meso-porphyrin and coproporphyrin in bacteria were observed (Hibst et al, 2001). PpIX concentration is reported to be higher in Gram-negative oral bacteria and its level increases as the dental biofilm becomes more mature, which is responsible for the red fluorescence in teeth (Walsh and Shakibaie, 2007).

When excited with 366 nm UV light, caries tooth was shown to exhibit a brick red fluorescence, which is due to protoporphyrin production by the pigmented *Bacteroides* species (Brazier, 1986; König et al, 1993; Bissonnette et al, 1998), and coproporphyrin production by *Corynebacterium* species and *Candida albicans* (König et al, 1993). With 407 nm UV light, bacterial species such as *Actinomyces odontolytics* (found in dentin carious lesions), *Bacteroides intermedius*, *Prevotella intermedia*, *Corynebacterium species* and *Candida albicans* emit fluorescence at 620-635 nm and 700nm, whereas Gram-positive *Streptococcus mutans*, *Enterococcus faecalis* and various *Lactobacilli* showed weaker emissions in the red wavelength region. Thus the maturity of dental plaque, rather than the presence of cariogenic streptococci, forms the basis for red fluorescence when excited with near-UV or UV light. In summary, when dental plaque or calculus is present, there is an increase in absorption in the UV spectral region of 350-420 nm, with fluorescence emission in the red spectral region of 590-650 nm (Borisova et al, 2006; Kuhnisch et al, 2003).

Significant differences in the fluorescence intensity ratios (F500/F635 and F500/F680) were observed during caries process. As compared to the mean fluorescence spectral intensity ratios of sound tooth given in Table 7.1, the caries tooth belonging to different stages has lower ratios. The F500/F680 ratio shows maximum sensitivity to distinguish early caries formation. Both the fluorescence intensity ratios used to

classify the sound tooth from caries show very low independent Student t-test values, $p < 0.001$.

Shi et al (2001) has reported a sensitivity of 94% and a specificity of 100% for detecting smooth surface caries with the QLF method, but could achieve only a lower sensitivity (78-82%) for detecting occlusal caries using DIAGNOdent device (Shi et al, 2000). In this study, the *in vitro* diagnostic accuracy of DIAGNOdent measurements in terms of area under the ROC curve was significantly higher (0.96) than that of conventional radiography (0.66) (Shi et al, 2000). However, Lussi et al (2001) reported a sensitivity of 92% for detecting occlusal caries using DIAGNOdent device as compared to visual inspection and bite-wing radiography. In another study, Ferreira-Zandona et al (1998) observed a sensitivity of 49% and specificity of 67%, with ROC value of 0.78, for detecting demineralization in occlusal pits and fissures. Further, Angnes et al (2005) observed that visual inspection was the most valid method for caries diagnosis followed by laser-induced fluorescence, in terms of ROC-AUC, sensitivity and specificity. Using a 405 nm diode laser, Ribeiro et al (2005) reported significant differences in the spectral ratios of integrated fluorescence in the wavelength region between 480-500 nm and 620-640 nm for sound tooth and all smooth surface non-cavitated caries with $p < 0.001$. However with the same laser, Zezell et al (2007) observed fluorescence from natural and cut surfaces of caries lesions to be nearly the same for shiny and dull lesion, but different for brown lesion ($p < 0.05$).

Attrill and Ashley (2001) found that laser fluorescence was more accurate for detecting occlusal caries as compared to visual examination and intraoral radiography. In another study by Olmez et al (2006) observed that for occlusal caries detection, LIF shows higher sensitivity and specificity as compared to visual inspection and bitewing radiography. However, Burin et al (2005) assessed the efficiency of LIF, visual examination and bitewing radiography and found that visual inspection was as valid as LIF, which should be considered a better adjunct than bitewing radiography for caries diagnosis.

This study shows comparatively better sensitivity in discriminating caries lesions from sound tooth using LIF spectral signatures (mean ROC-AUC = 0.94 ± 0.01). However, for detecting non-cavitated caries lesion (early enamel caries) the ROC-AUC was slightly lower at 0.87 (Table 7. 2).

Diagnostic algorithms based on the endogenous porphyrins produced by oral bacteria have been successfully brought out in this study. We have demonstrated

that by using the LIF spectral ratios, it is possible to characterize both lesion types and more significantly, discriminate caries from sound tooth. Moreover, it confirms the previous result that sound and caries tooth can be discriminated through the use of LIF spectroscopy (Borisova et al, 2004; Ando et al, 2001; Subhash et al, 2005 and Ribeiro et al, 2005).

7.5 CONCLUSIONS

Early diagnosis of caries lesion provides for more efficient remedy for caries progression, avoiding operative treatment. It appears that the information presented by non-invasive LIF spectroscopy has the capability to successfully detect dental caries and to classify different stages of caries. Among the LIF ratios studied, F500/F680 ratio is found to be more suited to comprehend caries progression and also to discriminate sound tooth from caries. It is observed that the fluorescence spectral signatures vary with respect to the changes in endogenous fluorophores during tooth caries development and therefore allow accurate diagnosis of the stage of dental caries from LIF spectral intensity ratios. Further *in vivo* studies are necessary with LIF to test the efficacy of these ratios to diagnose caries in a clinical setting.

Chapter 8

Clinical Trial for Early Detection of Tooth Caries
using Fluorescence Ratio Reference Standard

8.1 INTRODUCTION

Laser-induced fluorescence (LIF) has been increasingly used in recent years as a powerful tool for caries detection. The fluorescence detection technique may be an alternative to the dental probe or radiographic examination. This chapter presents the clinical applicability of a diagnostic algorithms or fluorescence reference standards (FRS) based on LIF spectral ratios to discriminate different stages of caries and to detect early tooth caries. Towards this, LIF emission spectra were recorded in the 400-800 nm spectral range on a miniature fiber-optic spectrometer in 105 patients, with excitation at 404 nm from a diode laser. The spectral results were correlated with visual-tactile and radiographic examinations. The LIF spectra of sound tooth shows a broad emission at 500 nm that is characteristic of natural enamel whereas in carious tooth, additional peaks were seen at 635 and 680 nm, due to emission from porphyrins present in oral bacteria. In order to discriminate different stages of tooth caries, FRS ratio scatter plots of the fluorescence intensity ratios F_{500}/F_{635} and F_{500}/F_{680} were developed to differentiate sound from enamel caries, sound from dentinal caries and enamel caries from dentinal caries using spectral data obtained from 65 carious sites and 25 sites of sound tooth in 65 patients. The sensitivity, specificity, PPV and NPV of the FRS to detect tooth caries are calculated and presented. A blind-test was carried out in 40 patients at 15 sound and 40 carious sites to check the accuracy of the developed standard for early detection of tooth caries.

8.2 STUDY MATERIAL, PROTOCOL AND ETHICAL ISSUES

The study was conducted at the Department of Conservative Dentistry and Endodontics of the Government Dental College, Thiruvananthapuram, India. Ethical approval for the study was provided by the Institutional Ethical Committee of the Government Dental College, Thiruvananthapuram (IEC/C/01-A/2008/DCT). All volunteers were provided with patient information sheet and consent forms. After explaining details of the study, consent form was endorsed by each patient prior to the initiation of study.

A total of 105 patients, aged between 20 and 50 years, with clinically suspicious incipient caries or radiographically proven tooth caries participated in the study. An experienced clinician identified the tooth for spectral measurement in each patient and recorded its visual-tactile findings. If clinical observation was positive, bitewing radiographs were taken. Thereafter, LIF measurements were carried out.

After positioning the patients in the dental chair, visual-tactile examination was performed, with the aid of a light reflector, air/water spray and dental mirror. The teeth observed as sound during clinical examination were included as control in the study. Samples studied covered smooth surface as well as occlusal caries. The study population comprised of 40 sound (clear enamel-intact tooth surfaces), 50 enamel (white spot, loss of luster and rough) and 55 dentinal caries lesions (localized enamel breakdown or cavitation in opaque or discolored enamel exposing the dentin). Samples with any kind of staining, hypoplasia and fluorosis were excluded.

Before initiation of measurements, the patients were asked to wash their mouth with saline to reduce the effects of recently consumed food. The oral cavity was then cleaned and the measurement site dried with cotton-swab. The OOI Base32 software was configured to record the spectra, averaged for 40 scans, with boxcar width of 8 nm and an integration time of 50 ms. Due to the diverse nature of the caries lesions, 15 sets of LIF measurements were taken from each of the caries lesions and sound tooth of the same patient for comparison, and the mean spectra of each site is determined for

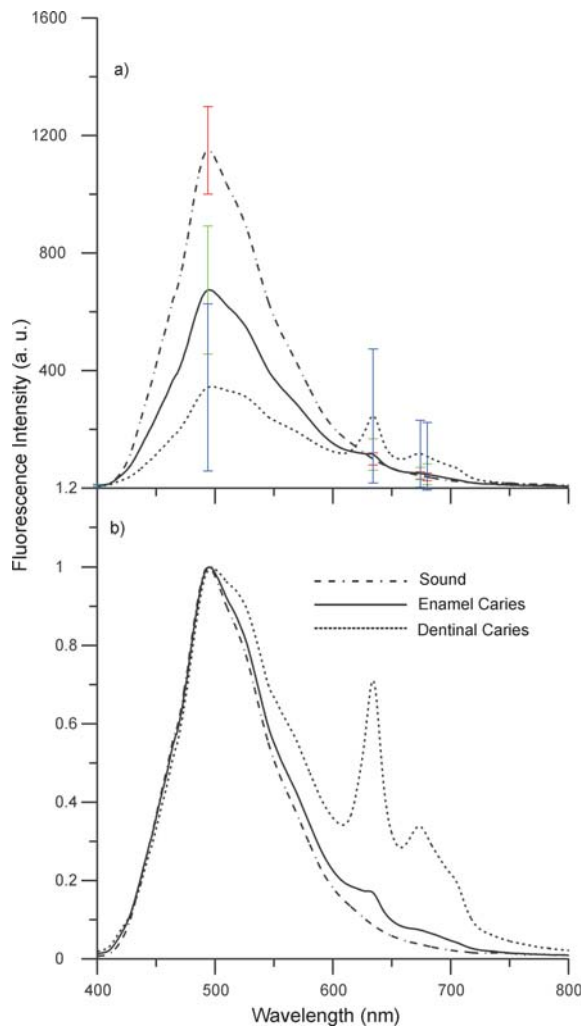


Fig. 8.1a). Mean *in vivo* LIF spectra from sound and caries lesions belonging to different stages and **b)** LIF spectra normalized to maximum fluorescence emission intensity. Sound tooth spectra represent the mean of 15 measurements each in 25 samples, whereas enamel caries spectra is of 15 × 30 measurements and the dentinal caries spectra is of 15 × 35 measurements.

the same patient for comparison, and the mean spectra of each site is determined for

further analysis. Depending upon the visual-tactile and radiographic results, each tooth was classified as sound, enamel or dentinal caries by the clinician, who was blinded to the spectral findings. ANOVA was performed to detect whether the average LIF spectral intensity differed between each of these groups.

Fluorescence intensity ratios are then calculated from the recorded mean spectra and correlated with visual-tactile and radiographic findings. To account for the broad nature of the peaks and sample-to-sample variation in peak position due to changes in chemical composition and fluorophore content of the tooth, the mean LIF spectral intensity over an interval of ± 10 nm at the emission peak was used to determine the LIF spectral ratios. In-order to discriminate sound from enamel caries, sound from dentinal caries and enamel from dentinal caries, fluorescence reference standard (FRS) scatter plots of the respective intensity ratios (F500/F635 and F500/F680) were developed using the spectral data obtained from 65 carious sites (30 enamel caries and 35 dentinal caries) and 25 sites of sound tooth in 65 patients. A blind-test was carried out in 40 patients and the data obtained from 40 carious sites and 15 sound sites were used to check the accuracy of the developed standard. An independent Student *t*-test was performed on the FRS ratios to discriminate different stages of caries, and to determine the statistical significance of the developed method for early detection of dental caries.

8.3 RESULTS

8.3.1 LIF spectral features

Fig. 8.1a) shows the mean *in vivo* LIF spectra recorded from 25 sites of sound tooth, 30 sites of enamel caries and 35 dentinal caries lesions and Fig. 8.1b), the same LIF spectra normalized to the peak emission intensity. The standard deviation is shown for the prominent peaks in the mean LIF spectra of sound and caries tooth belonging to various stages of decay. The overall fluorescence intensity of caries lesions were found lower than that of sound tooth. Nevertheless, the fluorescence spectral intensity in the red wavelength region was greater for caries lesions as compared to sound tooth. The LIF spectrum of sound tooth shows a broad emission around 500 nm with a long tail extending towards the red wavelength, whereas, two additional peaks are seen at 635 and 680 nm in caries tooth. In advanced caries lesion, 500 nm band appears broadened and red-shifted by about 30 nm. The peaks at 635 and 680 nm are very prominent in advanced caries lesions. However, the 680 nm peak appears broadened in incipient caries. The spectra shows a sharp rising

edge in the short wavelength side (400-450 nm), which is due to absorbance of the 420 nm long-wavelength pass filter (Schott UG420) used for blocking the back-scattered laser light from entering the spectrometer.

One way ANOVA test was used to determine the average spectral intensity variation among the 3 groups. Statistically significant differences in mean spectral intensities ($p < 0.001$) were noticed between sound tooth, enamel caries and dentinal caries lesions.

Table 8.1 Mean LIF spectral ratios determined from in vivo LIF spectral data from sound and caries tooth.

| Tooth Types | Population (n) | F500/F635 | F500/F680 |
|-----------------|----------------|---------------|----------------|
| Sound | 40 | 10.94±1.7 | 27.89±6.8 |
| Enamel Caries | 50 | 6.48±1.7 (41) | 14.59±6.3 (48) |
| Dentinal Caries | 55 | 2.59±1.4 (76) | 5.16±3.4 (82) |

The percentage given in parentheses shows the variation with respect to the sound tooth

8.3.2 LIF intensity ratios

Mean LIF spectral intensity ratios (F500/F635 and F500/F680) determined from the sound and caries tooth samples are listed in Table 8. 1. It was observed that both the F500/F635 and F500/F680 ratios of caries tooth have values lower than those of sound tooth. The F500/F680 ratio shows a maximum variation of 48% between sound and enamel caries and 82% between sound and dentinal caries, whereas between enamel and dentinal caries lesions, this ratio has a variation of 64%.

8.3.3 Discrimination using FRS ratio Scatter plots

A reference standard consisting of fluorescence spectral intensity ratio scatter plot was developed to facilitate discrimination between different types of caries. Fig.8. 2 (a-b) shows the scatter plots of the FRS ratios F500/F635 and F500/F680 in 65 patients, with their lesions diagnosed as enamel and dentinal caries, along with the control data from 25 sites of sound teeth. The fluorescence intensity ratios (Table 8.1) used in this classification has low independent Student t-test values of $p < 0.001$. Cut-off lines were drawn between sound tooth and enamel caries, sound tooth and

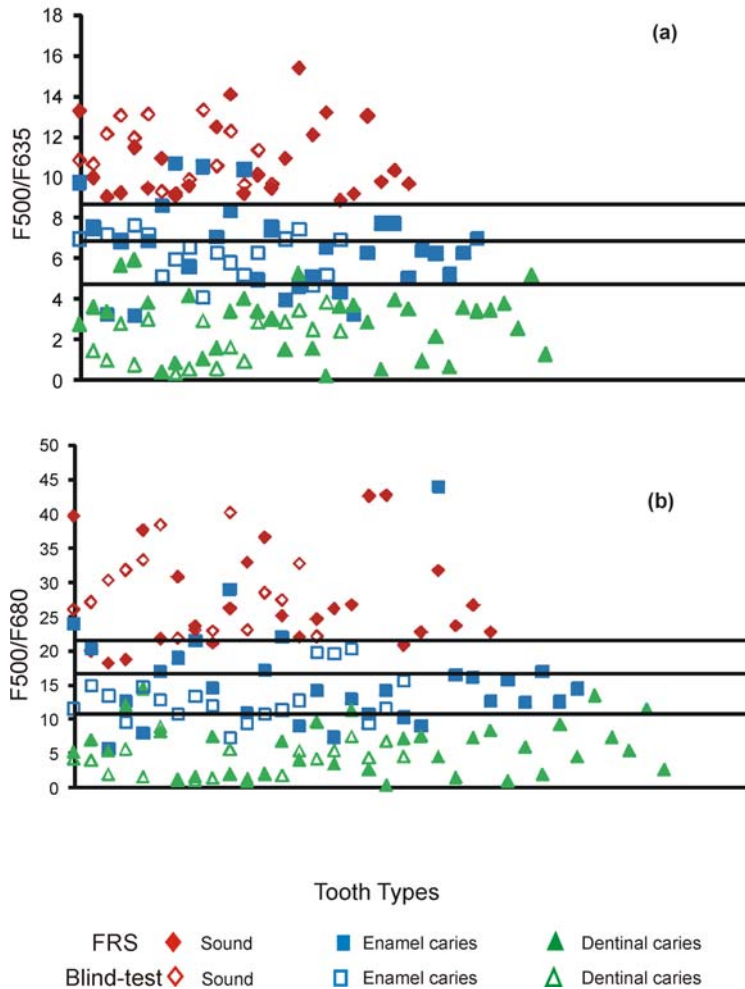


Fig. 8.2(a-b) FRS scatter plots of fluorescence intensity ratios a) F500/F635 and b) F500/F680 from 65 patients, diagnosed as enamel caries and dentinal caries along with the ratios from 25 sound tooth. The solid symbols represent data points of FRS whereas the hollow symbols represent the results of blind test carried out in 40 patients.

dentinal caries, enamel and dentinal caries data points, at values that correspond to the average ratio values of the respective groups. For example, to differentiate the sound tooth from enamel caries, the cut off line was drawn at 8.69 (the mean ratio of

the sound tooth and enamel caries lesion data points). The classification sensitivity, specificity, positive predictive value and negative predictive value for discriminating each category were calculated based on the cut-off values, by validation with visual-tactile and radiographic observation results.

For F500/F635 and F500/F680 ratios, by selecting a cut-off at the mean value of sound tooth and dentinal caries values (6.87 and 16.67) respectively, a sensitivity and specificity of 100% were achieved for discriminating these categories, with a positive and negative predictive value of 1. In Fig.8.2a, by selecting 8.69 as the cut-off value in the F500/F635 scatter plot to discriminate sound tooth from enamel caries, a sensitivity and specificity of 87% and 100% respectively were obtained, with a positive predictive value of 1 and negative predictive value of 0.86. In this study, only 4 out of the 30 enamel caries lesions were misclassified as sound. For discriminating enamel from dentinal caries, a sensitivity and specificity of 89% and 80% respectively, were achieved for the same ratio by using 4.73 as the cut-off value, with a corresponding positive predictive value of 0.84 and negative predictive value of 0.86. Here, only 4 out of 35 dentinal caries lesions were misclassified as enamel and 6 out of 30 enamel caries lesions were misdiagnosed as dentinal caries. Furthermore, an overall sensitivity and specificity of 85% and 90% respectively, were achieved for discriminating sound tooth from enamel caries, whereas a sensitivity and specificity of 100% was obtained to discriminate sound tooth from dentinal caries. Table 8.2 illustrates independent and overall sensitivity, specificity, PPV and NPV of FRS ratios, F500/F635 and F500/F680 for classifying different stages of tooth caries.

8.4 DISCUSSION

Until now visual inspection alone or its combination with radiography is considered as the gold standard for caries detection. However, x-rays are ionizing and hazardous in nature and cannot detect caries until they are well advanced. Hence development of diagnostic algorithms or reference standards based on LIF spectral ratios would be of great help for the real-time, non-invasive detection of tooth caries in the clinic.

8.4.1 LIF spectral features

The mean LIF spectra from sound and caries tooth shows characteristic features based on the absorption and scattering properties of light by cariogenic substances and fluorophores in the tooth. The reduction in the fluorescence intensity of the caries lesion could also be attributed to the changes in the physical structure and chemical composition during the disintegration of tooth enamel leading to caries or due to the

import of exogenous molecules during the caries process. This clearly supports the progressive rise of fluorescence spectral intensity in the red wavelength region with caries progression, and the consequent decrease in the autofluorescence emission around 500 nm.

Normally, tooth enamel is composed of millions of prisms or rods with waveguide properties that facilitate deep penetration when illuminated with visible light. In the case of dental caries, the prism structure is damaged and the waveguide properties are lost so that the irradiated light cannot penetrate deeply. This leads to a reduction in the fluorescence intensity in caries lesion (Ando et al, 2001).

The broad autofluorescence emission around 500 nm in sound tooth is due to the emission from natural enamel and dentin (Konig et al, 1998) and emissions observed at 635 and 680 nm are due to endogenous porphyrins and metalloporphyrins, in particular protoporphyrin IX (PpIX), meso-porphyrin and copro-porphyrin synthesised by bacteria (Konig et al, 1998; Hibst et al, 2001). PpIX concentration is reported to be higher in Gram-negative oral bacteria and its level increases as the dental biofilm becomes more mature, which is responsible for the red fluorescence in teeth (Walsh and Shakibaie, 2007). Pretty et al (2005) reported that the fluorescence due to porphyrins in certain oral plaque species, particularly Gram-negative anaerobes, is more abundant in late than early plaque (Marsh and Martin, 1999). Similarly, Buchalla (2005) reported that caries lesions fluoresce at 624, 650 and 690 nm, as due to porphyrins, more efficiently when excited in the wavelength range between 400 and 420 nm.

Konig et al (1993) observed that the autofluorescence emission in the red spectral region of carious lesions with 407 nm krypton ion laser excitation, is caused by the oral microorganisms such as *Prevotella intermedia*, *Actinomyces odontolytics*, *Corynebacterium species* and *Candida albicans*, which are able to synthesise high levels of endogenous metal-free fluorescent porphyrins. They also found that lactic acid bacteria, such as lactobacilli and streptococci, did not show typical porphyrin fluorescence in the red wavelength region. Thus the maturity of dental plaque, rather than the presence of cariogenic streptococci, is the basis for the red fluorescence when excited with near-UV light (Coulthwaite et al, 2006).

8.4.2 LIF intensity ratios

As compared to the mean fluorescence spectral intensity ratios of sound tooth given in Table 8. 1, the caries tooth belonging to different categories has lower ratios.

Both LIF ratios showed 100% sensitivity and specificity for detecting dentinal caries ($p < 0.001$). Nevertheless, by selecting suitable cut-off value, both FRS ratios could detect enamel caries with an average sensitivity of 85% and specificity of 90%.

8.4.3 Validation of FRS ratio

The best standard for validating detection accuracy in a clinical setting should be one that is derived from actual patient data. Blind-test for validation of FRS used data from 40 patients with the results correlated by clinical and radiographic findings (Fig.8.2a-c). The corresponding sensitivity, specificity, PPV and NPV for differentiating different stages of tooth caries are given in Table 8.2. It is found that both FRS ratios discriminates sound tooth from enamel and dentinal caries with 100% sensitivity and specificity. An overall sensitivity of 100% and specificity of 93% was achieved in discriminating enamel from dentinal caries lesions with a positive predictive value of 0.95 and negative predictive value of 1.00.

Table 8.2 Independent and overall sensitivity, specificity, PPV and NPV of FRS ratios, F500/F635 and F500/F680 for classifying different stages of tooth caries.

| Type | LIF ratios | Sound vs Enamel caries | | | | Sound vs Dentinal caries | | | | Enamel vs Dentinal caries | | | |
|--------------------|------------|------------------------|-----------------|---------|---------|--------------------------|-----------------|---------|---------|---------------------------|-----------------|---------|---------|
| | | Sensitivity (%) | Specificity (%) | PPV (%) | NPV (%) | Sensitivity (%) | Specificity (%) | PPV (%) | NPV (%) | Sensitivity (%) | Specificity (%) | PPV (%) | NPV (%) |
| FRS results | F500/F635 | 87 | 100 | 1.00 | 0.86 | 100 | 100 | 1.00 | 1.00 | 89 | 80 | 0.84 | 0.86 |
| | F500/F680 | 83 | 80 | 0.83 | 0.80 | 100 | 100 | 1.00 | 1.00 | 86 | 73 | 0.79 | 0.82 |
| | Overall | 85 | 90 | 0.92 | 0.83 | 100 | 100 | 1.00 | 1.00 | 88 | 77 | 0.82 | 0.84 |
| Blind-test results | F500/F635 | 100 | 100 | 1.00 | 1.00 | 100 | 100 | 1.00 | 1.00 | 100 | 90 | 0.91 | 1.00 |
| | F500/F680 | 100 | 100 | 1.00 | 1.00 | 100 | 100 | 1.00 | 1.00 | 100 | 70 | 0.77 | 1.00 |
| | Total | 100 | 100 | 1.00 | 1.00 | 100 | 100 | 1.00 | 1.00 | 100 | 80 | 0.84 | 1.00 |

LIF: Laser-Induced fluorescence, FRS: Fluorescence reference standard; PPV: Positive predictive value; NPV: Negative predictive value
independent t-test : $P < 0.01$

Validation of the diagnostic method usually takes place under clinical conditions, if follow-up treatment is planned. Nevertheless, if no operative intervention is intended, validation of the results is difficult for want of proper gold standard. Visual inspection

appears to have very low specificity and high sensitivity for detecting enamel caries and the opposite is true for dentinal caries of primary and permanent teeth. This shows that changes in enamel are easily identified by visual examination, while several dentinal caries might be covered up by mineralized enamel (Rodrigues et al, 2008; Valera et al, 2008; Ie and Verdonschot, 1994). Instead, visual inspection combined with radiography classified 82% of caries correctly (Bader et al, 2004). Recently in an *in vitro* study, Valera et al (2008) compared visual inspection, radiographic examination and use of DIAGNOdent device as well as their combinations for occlusal caries detection and found that visual and radiographic examination resulted in a specificity of 99%, whereas visual inspection alone resulted in 100% specificity. Therefore, we used a combination of visual-tactile and radiographic examinations as the gold standard for caries diagnosis in this study.

In a recent study, Alkurt et al (2008) reported LIF to be more reliable to assess actual lesion depth than visual inspection or bitewing radiography. Similarly, in a clinical study with permanent and primary molar teeth, Costa et al (2007) observed that laser fluorescence measurements yielded results similar to visual examination. In another study, Huth et al (2008) reported that LIF shows good discrimination between sound and carious tooth with area under the curve (AUC) of 0.92 and 0.78 for discriminating between enamel and dentin caries. Reis et al (2006) reported that no significant difference was observed between LIF measurements and visual inspection under both *in vitro* and *in vivo* conditions.

Attrill and Ashley (2001) compared LIF, visual examination and radiography and found that LIF was the most precise method (sensitivity of 77-80%) for detection of occlusal caries extending into dentine in extracted primary molars. In another study, Lussi, et al (2001) reported a sensitivity and specificity of 92% and 86%, respectively for detecting occlusal dentin caries using DIAGNOdent device as compared to visual inspection and bite-wing radiography. When carious enamel was used as threshold, sensitivity was about 96%. Anttonen, et al (2003) observed a sensitivity of 92% and specificity of 82% by selecting a cut-off point of 30 for occlusal caries detection in children. Similarly, the study conducted by Heinrich-Weltzien, et al (2005) revealed sensitivity values of 93%; however the specificity was lower (63%) when compared to the other reports. In another study, Olmez et al (2006) reported that LIF has higher sensitivity and specificity as compared to visual inspection and bitewing radiography for occlusal caries detection. However, Burin et al (2005) assessed the efficiency of LIF, visual examination and bitewing radiography and found that visual inspection was as valid as LIF, which should be considered a better adjunct than bitewing

radiography for caries diagnosis.

In comparison, the results of this clinical study showed improvements in discrimination between sound and carious tooth and between different stages of caries. It may be noted that both FRS ratios gave 100% sensitivity and specificity for discriminating sound tooth from enamel (incipient) caries and dentinal (advanced) caries. As regards differentiation of enamel caries from dentinal caries, the F500/F635 ratio showed 100% sensitivity and 90% specificity. Furthermore, the sensitivity and specificity shown in Table 8.2 for blind tests are also higher than the earlier reports (Lussi et al, 2001; Anttonen et al, 2003; Rodrigues et al, 2008; Huth et al, 2008; Angnes et al, 2005).

The investigation shows that diagnostic algorithms based on fluorescence intensity ratio of the emission peaks can localize and discriminate caries lesions from sound tooth. With the help of FRS threshold, the F500/F635 and F500/F680 ratio algorithms classified caries lesions from sound tooth with an average sensitivity and specificity of more than 90% with a positive predictive value of 0.96 and a negative predictive value of 0.92. This study relies on the assumption that the gold standard (a combination of visual-tactile and radiographic examination) provides diagnosis with 100% of sensitivity and specificity (i.e., 0% false-positives and false-negatives).

8.5 CONCLUSIONS

The blind-test results of this clinical study illustrate that information provided by non-invasive LIF spectroscopy has excellent potential to detect dental caries in its early stage. The FRS ratio diagnostic algorithm based on tissue autofluorescence was found to be sensitive and specific in discriminating different stages of tooth caries and in detecting early changes in tooth enamel that lead to caries formation. Therefore, LIF spectroscopy could function as a tool to dentists for early detection of tooth caries, in particular those not visible to the eye, hidden under restorations and beneath the exposed enamel surfaces in a fast and sensitive manner. Both FRS ratios (F500/F635 and F500/F680) were found suitable to understand caries progression from sound to enamel and dentinal caries with 100% sensitivity and specificity with PPV of and NPV of 1.00. Our results confirm that classification of tooth caries from fluorescence signatures, with 404 nm diode laser excitation allows precise visualisation and quantification of both the intrinsic green fluorescence of dental hard tissues as well as the red fluorescence of bacterial origin. The potential of LIF spectroscopy to detect secondary caries has not been tested and would be interesting.

Chapter 9

Application of Curve-fitting to Diagnose Dental
Caries *in vivo*

9.1 INTRODUCTION

This section discusses the advantage of analyzing the LIF spectra by curve-fitting for distinguishing different stages of tooth caries. Towards this, LIF emission spectra were recorded in the 400-800 nm spectral range on a miniature fiber-optic spectrometer from 105 patients, with excitation at 404 nm from a diode laser. The spectral results were correlated with visual-tactile examinations. It was noticed that caries tooth have lower fluorescence intensities as compared to sound tooth and the intensity decreases with the progression of caries. The LIF emission of sound tooth shows a broad emission around 500 nm whereas two additional peaks are seen at 635 and 680 nm in carious tooth. In order to locate the exact peak positions of the constituent bands and their relative contributions in the overall spectrum, LIF spectra were analyzed by curve-fitting using Gaussian spectral functions. Thus, it was possible to determine the variance in curve-fitting parameters such as peak center, Gaussian curve area, peak amplitude, FWHM and their ratios for different stages of tooth caries. A comparative evaluation of these ratios with those derived from raw LIF spectral data was made and the results are presented. Further, the diagnostic performance of LIF spectroscopy in a clinical setting was evaluated in terms of receiver operating characteristic (ROC) curve.

9.2 STUDY MATERIAL, PROTOCOL AND DATA PROCESSING

The study population, ethical issues and acquisition parameters were mentioned earlier (Chapter 8). The recorded LIF spectra shows a sharp rising edge in the short wavelength side (400-450 nm), which is due to the usage of the 420 nm long-wavelength pass filter (Schott UG420) for blocking the back-scattered laser light from entering the spectrometer. In order to correct the influence of this filter, the recorded LIF spectra is corrected using the spectral transmittance of the filter in the 350-800 nm wavelength region (Fig.9.1). Fig. 9.2

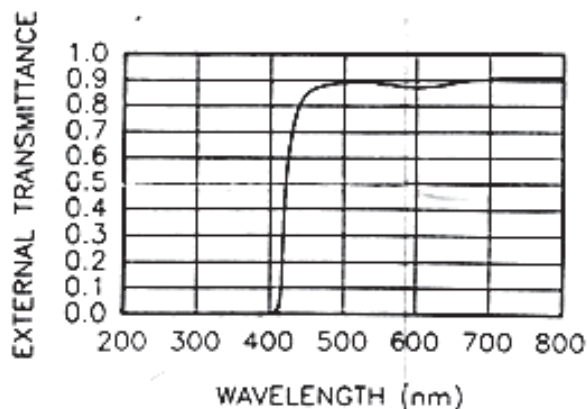


Fig. 9.1 External transmittance curve of Schott filter UG420.

represents the *in vivo* LIF spectra recorded with the UG420 filter and the corrected fluorescence spectra of sound tooth.

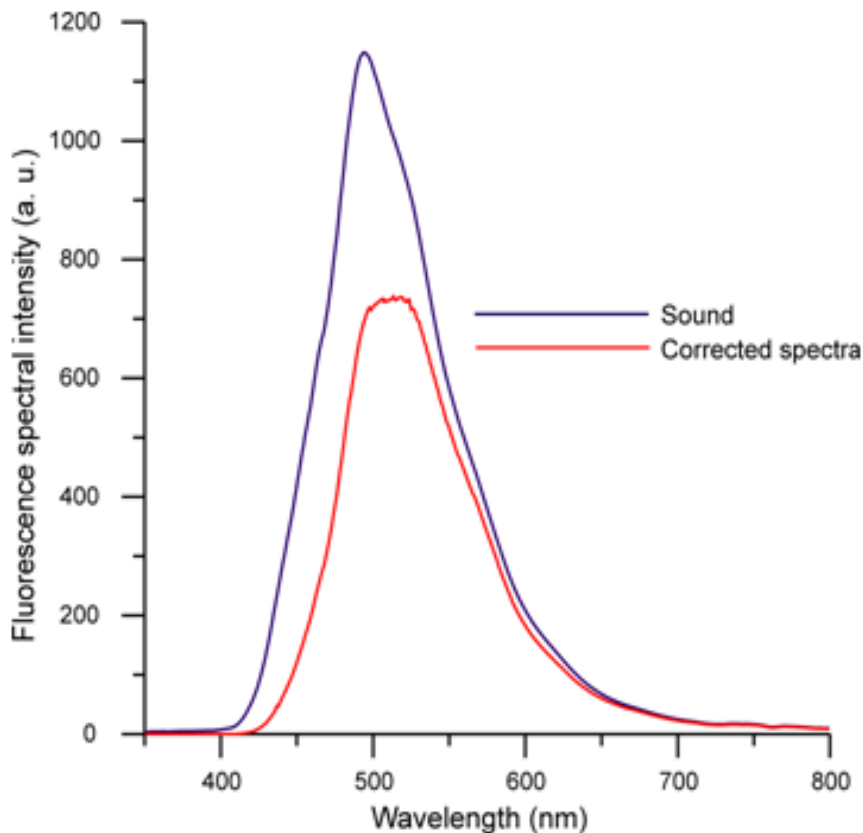


Fig. 9.2 Mean *in vivo* LIF spectra of a sound tooth and the corresponding filter transmittance corrected spectra.

The corrected LIF spectra were analyzed by curve-fitting using Gaussian spectral functions to determine the peak positions of the constituent bands and their relative contribution in the overall spectrum using Origin software (details given in Chapter 3). Various band intensity ratios were then determined from the constituent peak amplitudes and Gaussian curve areas and correlated with those derived from raw spectral data. An independent Student's t-test was performed on the Gaussian amplitude and area ratios, F490/F635 and F490/F675, to assess the statistical significance of the fluorescence ratios in discriminating different stages of tooth caries.

The diagnostic performance achieved by curve-fitting was determined in terms of ROC curve. The resultant ROC curve displays variation in sensitivity and specificity along the diagnostic range. The use of gold standard is a prerequisite for the assessment of ROC curve.

9.3 RESULTS

9.3.1 LIF spectral features

Fig. 9.3a) shows the corrected LIF spectra recorded from sound tooth, enamel caries and dentinal caries and Fig. 9.3b) that after normalization to the peak intensity. As compared to sound tooth, caries tooth exhibit lower fluorescence intensity. The LIF spectrum of sound tooth consists of a broad auto-fluorescence around 500 nm with a long tail extending towards the red region possibly due to an emission peak around 550 nm. But, in caries tooth, two additional peaks are seen at 635 and 680 nm. In addition, caries tooth exhibit an apparent red shift in the emission maxima.

9.3.2 Curve-fitting analysis

The mean LIF spectra from sound, enamel and dentinal caries tooth were analyzed by curve-fitting using Gaussian spectral functions. Fig. 9.4 (a-c) shows the peak fitted spectrum and the constituent emission bands. It was seen that curve fitting of sound tooth with the help of three Gaussian

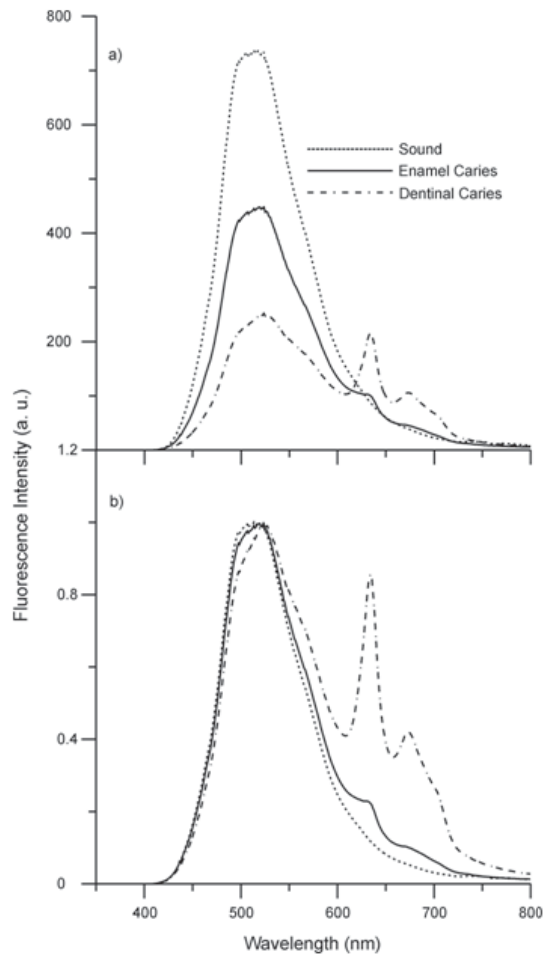


Fig.9.3. a) Mean corrected LIF spectra from sound and caries lesions belonging to different stages and b) normalized to maximum fluorescence intensity. Sound spectra represent the mean of 15 measurements each in 40 samples, whereas enamel caries spectra is of 15 × 50 measurements and the dentinal caries spectra is of 15 × 55 measurements.

Table 9.1 Curve-fitted parameters of the mean in vivo LIF spectra from sound tooth, enamel caries and dentinal caries.

| Tooth | Peak Centre (nm) | FWHM (nm) | Area | Amplitude | χ^2 | r^2 |
|-----------------|------------------|-----------|--------|-----------|----------|-------|
| Sound tooth | 491.85 | 21.9 | 3058.1 | 111.42 | 105.6 | 0.998 |
| | 513.21 | 66.618 | 47084 | 563.92 | | |
| | 561.37 | 108.35 | 30673 | 225.88 | | |
| Enamel caries | 505.31 | 56.865 | 29481 | 413.66 | 19.8 | 0.999 |
| | 532 | 17.758 | 744.31 | 33.442 | | |
| | 563.13 | 56.669 | 15612 | 219.81 | | |
| Dentinal caries | 625.8 | 31.21 | 1923 | 49.162 | 22.1 | 0.997 |
| | 655.62 | 93.343 | 5316.1 | 45.442 | | |
| | 507.19 | 58.331 | 14294 | 195.52 | | |
| | 550.82 | 45.464 | 2019.1 | 35.434 | | |
| | 573.15 | 85.074 | 12989 | 121.82 | | |
| | 633.05 | 15.361 | 2382.8 | 123.77 | | |
| | 674.67 | 67.785 | 7480.3 | 88.05 | | |

peaks gives a good fit (correlation coefficient $r^2 = 0.998$). In the case of carious tooth, five Gaussian peaks were required to give a good fit of the mean LIF spectra. Table 9.1 shows the peak position of the various bands, their Gaussian curve areas, full width at half intensity maximum (FWHM) and the χ^2 and r^2 values of fitting. It is seen that the 491.85 nm peak shifts towards the red region by 14 nm in enamel and 15 nm in dentinal caries. Further this peak appears broadened with a shoulder peak around 513.21 nm, which shifts towards the red region by 19 nm to 532 in enamel caries and by 38 nm to 551.75 nm in dentinal caries. Another notable feature is the broadening of the 560 nm peak by 12 nm; with concurrent decrease in Gaussian curve area and peak amplitude in dentinal caries. Besides, the 625.8 nm and 655.62 nm peaks seen in enamel caries shift towards the red region by 7.3 nm and 19.1 nm in dentinal caries. For the 625.8 nm and 655.62 nm peaks seen in enamel caries, the curve fitted amplitude and area values show an increasing trend with increase in the stage of caries. During caries progression from enamel to dentinal stage, the increase in the 625.8 nm peak amplitude and area is 60% and 20%, while the corresponding increase in the 655.62 nm peak amplitude is 48% and 29%, respectively. However, for sake of simplicity these peaks will be designated as 490, 513, 560, 635 and 675 nm peaks.

9.3.3 Curve-fitted and Raw LIF ratios

Table 9.2 shows the fluorescence ratios (F490/F635 and F490/F675) calculated

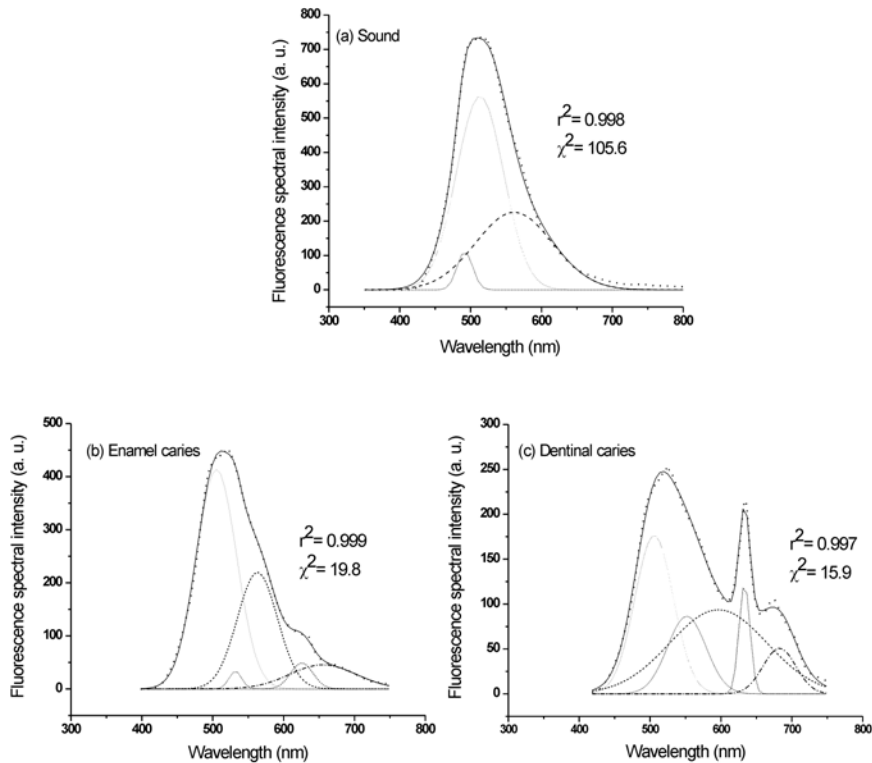


Fig. 9.4(a-c) Curve-fitted LIF spectrum showing the constituent bands from (a) sound and (b) enamel and (c) dentinal caries tooth. The dots on the LIF spectrum relate to the data points, the solid line is the curve-fitted line and the dotted and dashed lines show the constituent bands.

from curve-fitted peak amplitudes, Gaussian curve areas and raw spectral data for different stages of caries. The fluorescence intensity of the LIF spectra at the peak wavelength determined by curve-fitting was used to evaluate the raw fluorescence intensity ratio. As compared to the ratios determined from raw spectral data, the fluorescence ratios calculated from Gaussian area curves and curve-fitted amplitudes show increased variation with the extend of caries. For example, the raw LIF spectral ratio F490/F635 involving the two main peaks, which has a variation of 60% between enamel and dentinal stage of caries, showed an enhanced variation of 81.2% when curve-fitted peak amplitude values are used for determination of this ratio. Similarly,

the curve-fitted amplitude and area F490/F675 ratios showed variances of 75.6% and 65.6% during caries progression from enamel to dentin as compared to 60% change noted in the raw F490/F675 ratio. Fig. 9.5(a-c) shows the fluorescence ratios derived from curve-fitted spectral amplitude, curve-fitted spectral area and raw LIF spectral data for these two stages of caries.

Table 9.2 *In vivo* LIF ratios determined from Gaussian curve-fitted amplitude, area and raw spectral data.

| Ratios | Curve-fitted amplitude | | Curve-fitted area | | Raw LIF spectrum | |
|-----------|------------------------|-----------------|-------------------|-----------------|------------------|-----------------|
| | Enamel caries | Dentinal caries | Enamel caries | Dentinal caries | Enamel caries | Dentinal caries |
| F490/F635 | 8.41 | 1.58 | 15.33 | 5.99 | 5.19±0.3 | 2.04±0.2 |
| F490/F675 | 9.1 | 2.22 | 5.55 | 1.91 | 11.59±1.08 | 4.61±0.9 |

9.3.4 Diagnostic performance of LIF spectroscopy

The ability of LIF spectroscopy to discriminate different types of caries lesions from sound tooth can be assessed from the ROC curve, where the sensitivities are plotted against the 1-specificities as in Fig.9.6 a-c. In general, a value for the area under ROC curve close to 0.9 indicates good discrimination between the two classes studied. The receiver-operator characteristic areas under the curve (ROC-AUCs) was 1.0 ($p < 0.001$) for discriminating sound from dentinal caries and 0.97 for distinguishing sound from enamel caries (Table 9.3). For the distinction between enamel and dentinal caries, the ROC-AUC was 0.86.

9.4 DISCUSSION

The broad autofluorescence peak around 500 nm in sound tooth is due to emission from natural enamel, particularly hydroxyapatite (Alfano and Yao, 1981; Konig et al, 1998) and emissions at 635 and 680 nm are from endogenous porphyrins, particularly protoporphyrin IX (PpIX), meso-porphyrin and copro-porphyrin in bacteria (Konig et al, 1998; Hibst et al, 2001 and Subhash et al, 2005).

The mean LIF spectra from sound and caries tooth shows characteristic features based on the absorption and scattering properties of light by carious substances and differences in the content of fluorophores. As reported earlier (Ando et al, 2001; Borisova et al, 2004 and Subhash et al, 2005), the caries tooth exhibits lower fluorescence intensities than sound tooth. The reduction in the fluorescence intensity of the caries

lesion could be attributed to the changes in the physical structure and chemical composition during the disintegration of tooth enamel leading to caries or due to import of exogenous molecules during the caries process. This clearly supports the progressive rise of the fluorescence spectral intensity in the red wavelength region and decrease around 500 nm with the caries progression (Borisova et al, 2006). Moreover, porphyrin peaks that are prominent in caries tooth can also be used for discriminate different stages of caries.

Further, by curve-fitting using Gaussian spectral functions, it was possible to resolve the LIF spectra of sound tooth into three constituent peaks centered at 491.85, 513.21 and 561.37 nm whereas two additional peaks were required, respectively at 625.8 and 655.62 nm and at 633.05 and 674.67 nm in enamel and dentinal caries, to fit the spectral data. Since the correlation coefficients of curve-fitting were very close to unity, and the residuals of fitting were few and scattered uniformly over the fitted curve, it is to be assumed that the peak wavelength positions identified by the curve-fitting algorithm are fairly accurate. There are marked variations not only in the peak emission bands but also in the peak amplitude, FWHM width, and the Gaussian curve area during caries development. The variation in peak position, intensity and FWHM width of the 490 nm band is noteworthy. Therefore, shift in peak position of the 490 nm peak between enamel and dentinal caries, and the appearance of the new peak at 635 and 675 nm would be useful indicators of the extent or stage of tooth caries. In comparison, in an earlier study using 337

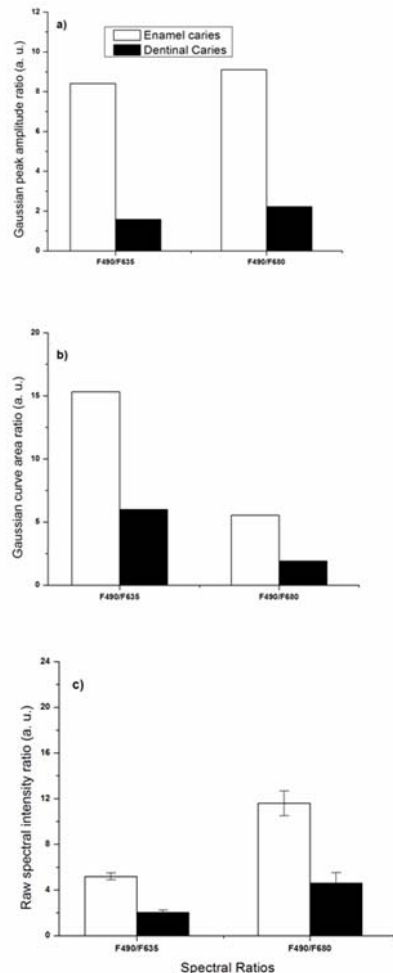


Fig. 9.5 Fluorescence ratios derived from **a)** curve-fitted spectral amplitude, **b)** curve-fitted spectral area and **c)** raw LIF spectral data from different stages of caries lesions.

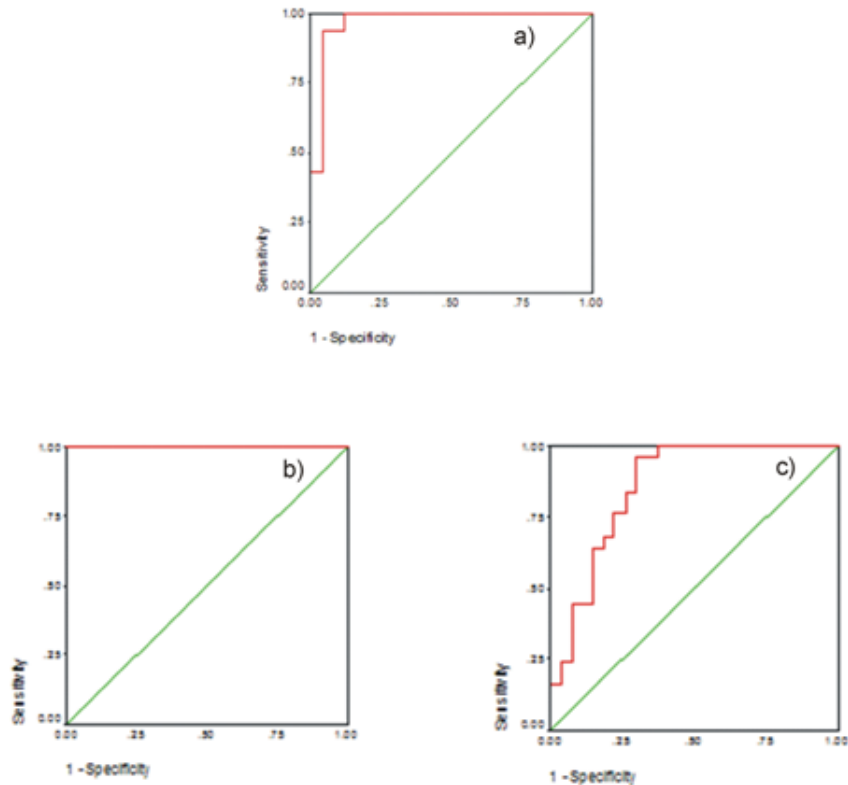


Fig.9.6 Receiver operating characteristics curves (ROC) for discriminating different stages of caries lesions using LIF spectroscopy **a)** the discrimination cut-off between sound and enamel caries, **b)** the discrimination cut-off between sound and dentinal caries and **c)** the discrimination cut-off between enamel and dentinal enamel and dentinal caries lesions.

nm nitrogen laser, it was found that the curve-fitting of the sound tooth shows four peaks centered at 403.80, 434.20, 486.88, and 522.45 nm. Further, the 522 nm peak is seen red-shifted by 32 and 8 nm in dentin and pulp level caries. A new peak at 636.78 nm was also seen in the case of pulp level caries (Subhash et al, 2005).

Significant differences in the Gaussian amplitude and area ratios (F490/F635 and F490/F675) were observed during caries progression (Table 9.2). As compared to ratios derived from raw LIF spectra, marginal increase in sensitivities was seen with curve-fitting. Among the various ratios, the curve-fitted Gaussian peak amplitude ratio,

F490/F635 appears to be more suited to distinguish different stages of tooth caries. All these fluorescence intensity ratios used to classify the sound from caries tooth had a low independent Student t-test value, $p < 0.001$. In contrast, in an earlier study, curve-fitted Gaussian area ratio F435/F525 was reported to be suitable for discrimination between different stages of tooth decay (Subhash et al, 2005). Using a 405 nm diode laser excitation, Ribeiro et al (2005) also reported significant differences in the spectral ratios of the integrated fluorescence in wavelength region between 480-500 nm and 620-640 nm for sound tooth and all smooth surface non-cavitated caries ($p < 0.001$).

Table 9.3 Results of ROC analysis in the discrimination of enamel and dentinal caries from sound tooth.

| Lesion Type | Receiver Operating Characteristics Curve | | |
|-------------------------|--|------------|--------|
| | AUC | 95% CI | p |
| Sound - Enamel caries | 0.97 | 0.92-1.000 | <0.001 |
| Sound – Dentinal caries | 1.0 | 1.0-1.0 | <0.001 |
| Enamel– Dentinal caries | 0.86 | 0.75-0.96 | <0.001 |

CI: Confidence Interval; p: Significance of difference to the diagonals; AUC: Area under the Curve

Shi et al (2000) found that the *in vitro* diagnostic accuracy of DIAGNOdent measurements in terms of area under the ROC curve was significantly higher (0.96) than for conventional radiography (0.66). In an *in vitro* study, Ferreira-Zandona et al (1998) observed a sensitivity of 49% and specificity of 67% with ROC value of 0.78 for detecting demineralization in occlusal pits and fissures. Angnes et al (2005) reported that that visual inspection was the most valid method for caries diagnosis followed by laser fluorescence in terms of ROC-AUC, sensitivity and specificity. In a recent study by Huth et al (2008) it was observed that the LF device's discrimination performance for different caries depths was moderate to good with AUC of 0.92 for discrimination between sound and carious tooth and 0.78 for discrimination between enamel and dentin caries. In another study, Olmez et al (2006) observed that LF shows higher sensitivity and specificity as compared to visual inspection and bitewing radiography for occlusal caries detection. However, Burin et al (2005) assessed the efficiency of LF, visual examination and bitewing radiography and found that visual inspection was as valid as LF device, which should be considered as a better adjunct than bitewing radiography for caries diagnosis.

In comparison, the results of this *in vivo* study showed that the diagnostic performance of LIF spectroscopy in discriminating different stages of caries can be improved with curve-fitting using Gaussian spectral functions. Further, it was possible to discriminate dentinal caries from sound tooth with an AUC of 1.0, while the AUC's were 0.97 and 0.86, respectively for discrimination between enamel caries and sound tooth, and between enamel and dentinal caries.

The benefit of ROC analysis is that it displays the diagnostic performance more systematically than sensitivity and specificity, which depends on the cut-off point. This analysis also provides an overall validity for the methods employed. From a mathematical point of view, the ROC analysis gives a better picture, since it does not consider any given threshold. However, in clinical practice, clinicians usually have to consider a cut-off point at which the treatment options fall from non-invasive to invasive approach. Therefore, the sensitivity and specificity values are still valuable tools for comparison of diagnostic methods.

9.5 CONCLUSIONS

LIF ratios showed significant changes depending on the nature and extent of caries and the detection capability was enhanced when contributions from constituent bands derived by curve-fitting of the LIF spectra using Gaussian spectral functions were considered. Further, it can be presumed that LIF with excitation by a 404 nm diode laser has the potential to diagnose different stages of caries. Studies have shown that tooth decay or caries not only affect the fluorescence spectral intensities, but also alter the spectral shape as evidenced by the appearance of new peaks, peak shifts, and variations in curve-fitted peak area, intensity and bandwidth. Moreover, the ratios determined from curve-fitted spectral parameters showed better sensitivity to tissue transformations as compared to the ratios derived from raw spectral data. Among the two ratios studied, F490/F635 ratio determined from curve fitted amplitude was found to be more suited to understand caries progression and to discriminate sound from caries tooth. The LIF spectroscopy's diagnostic performance for detecting and discriminating different stages of tooth caries as evidenced by ROC analysis indicates that it can be used as an adjunct tool in the diagnosis of dental caries.

Chapter 10

Diffuse Reflectance Spectroscopy for *in vivo*
Detection of Caries

10.1 INTRODUCTION

Diffuse reflectance (DR) spectral features in the ultraviolet–visible (UV–VIS) wavelength range, which depends on tissue absorption and scattering, reflects the intrinsic physiological and structural properties of lesion. As this technique uses white light illumination such as that of a tungsten-halogen lamp, it is cost-effective, and shows great potential to provide near real-time, non-destructive, and quantitative characterization of tooth caries. Therefore, a clinical trial was carried out to assess the capability of DR spectroscopy for detecting tooth caries *in vivo*. This chapter presents the results of the clinical trial conducted at the Government Dental College, Trivandrum in 24 patients. Diffuse reflectance reference standard (DRRS) scatter plots of the reflectance intensity ratios R500/R700, R600/R700 and R650/R700 were used to differentiate sound from non-cavitated caries lesions. The sensitivity, specificity, PPV and NPV of the DRRS ratios in detecting tooth caries are calculated and presented. Further, the diagnostic performance of DR spectroscopy in a clinical setting was evaluated in terms of receiver operating characteristic (ROC) curve.

10.2 STUDY MATERIAL AND PROTOCOL

24 patients, aged between 20 and 50 years with clinically suspected with non-cavitated caries were included in this study. An experienced clinician selects the tooth lesion for spectral measurement in each patient and records its visual-tactile imprint as per the protocol described earlier (Chapter 8). The visual criteria included the absence of any tooth discoloration whereas the tactile criteria are the smoothness and hardness felt without a catch by dental probe during its passage over the suspicious surface. The study population included 225 sites of sound (clear enamel-intact tooth surfaces), and 360 sites of non-cavitated caries lesions (white spot, dull, brown spot).

Ethical issues and acquisition parameters were as mentioned in Chapter 8. DR spectrum is recorded from selected sites on a miniature fiber-optic spectrometer, with white light illumination from the tungsten halogen lamp of the dental light (Confident Dental Equipments Ltd, India, 20W) in the patient examination chair. The fiber-optic handpiece for DR light collection from lesion uses a 400 microns dia. optical fiber. DR intensity ratios are calculated from the recorded mean spectra by measurement of spectral intensities at 500, 600, 650 and 700 nm over an interval of ± 10 nm. In-order to discriminate sound from non-cavitated caries lesions, diffuse reflectance reference standard (DRRS) ratio scatter plots of the DR intensity ratios R500/R700,

R600/R700 and R650/R700 were developed using the spectral data obtained from 24 patients. An independent Student *t*-test was performed on the DRRS ratios to discriminate sound from caries tooth, and to determine the statistical significance of the developed model for detection of dental caries. For determining the diagnostic accuracies of DR incaries discrimination, ROC curves of sensitivity versus 1-specificity were plotted.

10.3 RESULTS

10.3.1 DR spectral features

Significant variation in the DR intensities was seen between sound and caries tooth. Fig.10.1a, b shows the mean DR spectra recorded from sound and caries tooth and that after normalization. As seen in Fig 10.1a the DR intensity of caries tooth is markedly lower than that of sound tooth. However, beyond 700 nm the spectral intensity decreases further (spectra not shown). The standard deviation in the recorded spectra is shown at 500, 600 and 650 nm wavelength positions in the mean DR spectra of sound and caries lesions. The DR spectrum shows a broad reflectance dip between 540 and 580 nm, which might be due to hemoglobin absorption. The normalized spectrum shows a reduction in relative intensity with caries formation in the spectral window below 600 nm whereas the trend reverses beyond 625 nm. The reflectance intensity ratios (R500/R700, R600/

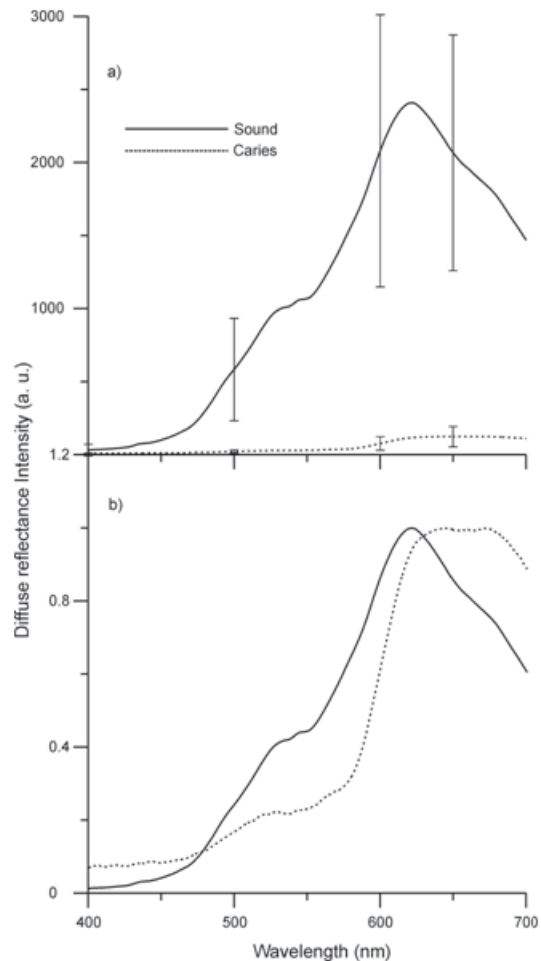


Fig.10. 1 Mean DR spectra recorded from (a) sound and caries tooth and (b) the DR spectra normalized to the maximum intensity. Sound spectra represent the mean of 15 measurements each in 15 samples, whereas non-cavitated caries lesions spectra are of 15×24 measurements.

R700 and R650/R700) determined from the recorded mean spectra is presented in Table 10.1. Among these ratios, R600/R700 ratio shows the maximum decrease of 93.1% from sound to non-cavitated caries lesions, while R650/R700 and R500/R700 shows decreases of 46.2% and 10.8%, respectively.

Table 10.1 Mean DR spectral ratios determined *in vivo* from sound and non-cavitated caries tooth.

| DR ratios | Sites (n) | R500/R700 | R600/R700 | R650/R700 |
|-----------|-----------|-----------|-----------|-----------|
| Sound | 225 | 0.43±0.03 | 1.41±0.1 | 1.49±0.01 |
| Caries | 360 | 0.18±0.1 | 0.75±0.2 | 1.18±0.1 |

10.3.2 Discrimination with DRRS ratio

The DR spectral ratio of caries tooth is always lower than that of sound tooth. Fig.10. 2 (a-c) shows the scatter plots of the DRRS ratios R500/R700, R600/ R700, and R650/R700 from 24 patients. Cut-off lines were drawn between sound and caries tooth at values that correspond to the average ratio values of the respective groups. The classification sensitivity and specificity for discriminating each group were calculated based on the cut- off values, by confirmation with visual-tactile findings. The DR intensity ratios have shown a low independent Student t-test values of $p < 0.01$.

For R500/R700 ratio, by selecting a cut-off at the mean of sound (0.43) and non-cavitated caries (0.18) tooth, a sensitivity of 83% and specificity of 100% were achieved for discrimination, with a positive predictive value of 1 and negative predictive value of 0.79. In Fig.8.2b, by selecting 1.08 as the cut-off value to discriminate sound tooth from caries lesions, a sensitivity and specificity of 92% and 100% were obtained, respectively for R600/R700 with a positive predictive value of 1 and negative predictive value of 0.88. Among the study population, only 2 of the 24 caries lesions were misclassified as sound. Table 10.2 illustrates independent and overall sensitivities, specificities, PPV and NPV of DRRS ratios, R500/R700, R600/ R700, and R650/R700 for tooth caries detection.

10.3.3 Caries Discrimination using ROC curve

ROC curves were plotted with sensitivity against 1-specificity to graphically

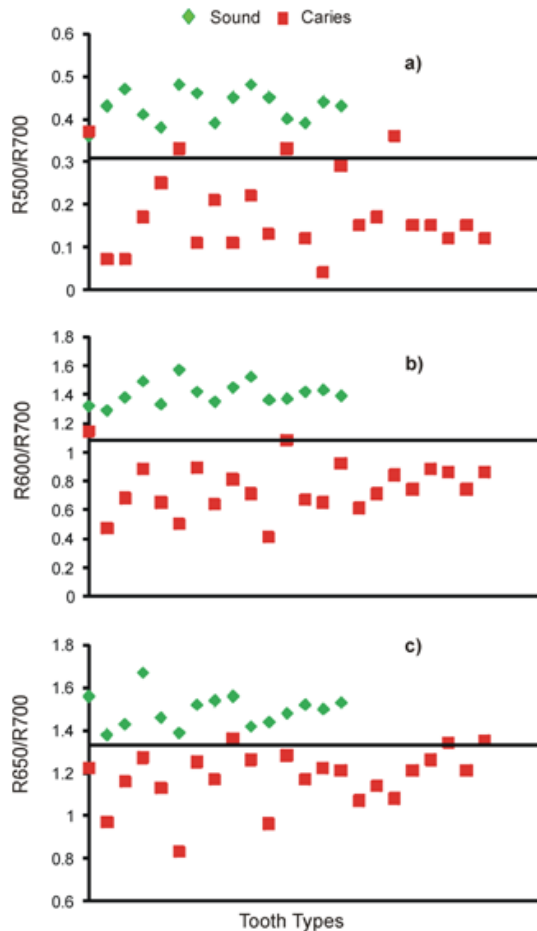


Fig. 10.2(a-c) DRRS developed from sound and caries tooth of 24 patients for a) R500/R700, b) R600/R700 and c) R650/R700 ratios.

scattering coefficient reflects the size and density of scattering centers in tissue. In this *in vivo* study, we observed significant differences between the DR spectra of sound and caries tooth. The spectrum of sound tooth is a combination of diffused reflection from the enamel and dentine layers (Uzunov et al, 2003). With increase in demineralization, angular distribution of diffuse light is altered, which in turn reduces the maximum DR intensity (Tuchin and Altshuler, 2007). If successful separation is

illustrate the capability of DR spectroscopy for discriminating non-cavitated caries from sound tooth (Fig.8.3). The plot shows an AUC of 0.95 (CI: 0.92 to 1.0), confirming the diagnostic ability of the DR spectroscopy to discriminate between sound and non-cavitated caries lesions.

10.4 DISCUSSION

DR spectroscopy refers to the detection of both the diffuse and specular components of reflectance. We have explored the use of DR spectroscopy in the visible spectral range for diagnosis of tooth caries. A set of diffuse reflectance spectra between 400 and 700 nm measured from sound and caries tooth were analyzed using DRRS ratio and ROC analysis.

DR spectrum reflects the absorption and scattering properties of tissue. The absorption coefficient is directly related to the concentration of physiologically relevant absorbers in the tissue. Tissue absorption in the visible spectral region is due to natural absorbers such as hemoglobin, bilirubin, melanin, and water. The

done using specific wavelength or scattering angle, surface diffuse component can be used as a tool for detecting tooth demineralization and pre-caries (white spots).

Table 10.2 Sensitivity, specificity, PPV and NPV of R500/R700, R600/ R700, and R650/R700 ratios for tooth caries detection.

| DR ratios | Sound vs Non-cavitated Caries | | | |
|-----------|-------------------------------|-------------|------|------|
| | Sensitivity | Specificity | PPV | NPV |
| R500/R700 | 83 | 100 | 1.00 | 0.79 |
| R600/R700 | 92 | 100 | 1.00 | 0.88 |
| R650/R700 | 88 | 100 | 1.00 | 0.83 |

DR: Diffuse reflectance; PPV: Positive predictive value; NPV: Negative predictive value

The chromophores present in caries, with strong absorption in the blue-green spectral region, have resulted in decreased DR spectral intensity in the 400–600 nm range (Fig. 10.1). These spectral changes in caries might be due to the import of exogenous molecules during caries developmental process, as evidenced by the presence of increased absorption in the short wavelength region. The concentration of these exogenous molecules increases due to the presence of food particles, blood cells and bacterial activity. Thus carious lesion is a complex structure of different absorbers; with each contributing to the reflectance spectra and hence, cannot be easily explained in terms of reflectance properties alone.

The mean DR ratios from caries tooth were always found to be lower than that of sound tooth (Table 10. 1). In our measurements, maximum variation of 93% was seen between sound and enamel caries for the R600/R700 ratio. Earlier measurements by Uzunov et al (2003) showed significant decrease in the reflectance spectral ratios by 158% and 32.4% respectively, for the R500/ R900 and R750/R900 ratios between sound and deep cavitation tooth. Similarly in an earlier *in vitro* study, it was observed that the diffuse reflectance spectral ratio, R500/R700, was suitable to distinguishes between different stages of caries tooth (Subhash et al, 2005).

Borisova et al (2007) observed significant decrease in reflected light intensity between caries and non-carious lesions in the blue region. They also developed an algorithm with diagnostic accuracy of 86% for differentiating precarious stage from sound tooth, and also obtained 100% diagnostic accuracy for determination of deep

cavitation. In another study, Lussi, et al (2001) reported a sensitivity and specificity of 92% and 86%, respectively for detecting occlusal caries using DIAGNOdent device as compared to visual inspection and bite-wing radiography. Similarly Shi et al (2001) achieved a sensitivity and specificity of 94% and 100%, respectively for detecting smooth surface caries with the QLF method; but achieved a lower sensitivity (78-82%) for detecting occlusal caries using DIAGNOdent device. They found that the *in vitro* diagnostic accuracy of DIAGNOdent measurements in terms of area under the ROC curve was significantly higher (0.96) than that of conventional radiography (0.66). Another study by Ferreira-Zandona et al (1998) reported a sensitivity of 49% and specificity of 67% with a ROC value of 0.78 for detecting demineralization in occlusal pits and fissures.

In contrast, the DRRS ratios, R600/R700 and R650/R700 have given a specificity of 100% and sensitivity of 92% and 88% respectively. On the other hand, the R500/R700 ratio has a specificity of 100%, but the sensitivity was lower (83%). Nevertheless, DRRS ratios show potential to detect tooth caries with an average sensitivity of 88% and specificity of 100% with PPV value of 1.00 and NPV value of 0.83. All these ratios have low independent Student t-test, $p < 0.01$, for detection of tooth caries. The results presented show the significance of using the scatter plots to detect tooth caries from the diffuse reflectance. Further, an AUC of 0.95 was obtained to discriminate non-cavitated caries lesions from sound tooth using DR spectroscopy.

10.5 CONCLUSIONS

Diffuse reflectance characterizes some of the optical features exploited in fluorescence spectroscopy, notably absorption due to various biological chromophores, and tissue scattering properties. The primary advantage of this technique is that DR signals are several orders magnitude greater than the weak

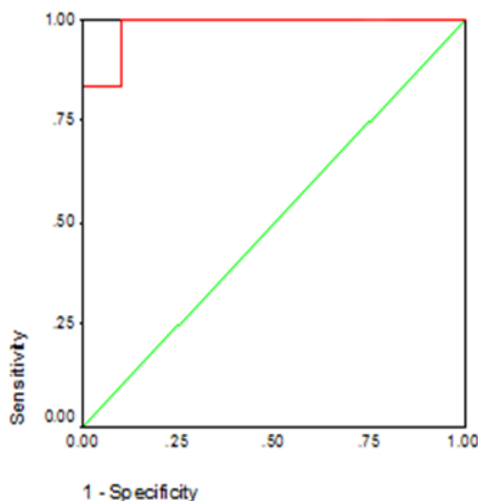


Fig.10.3 Receiver operating characteristics curves (ROC) for discriminating caries lesions from sound tooth using DR spectroscopy.

endogenous fluorescence of tissues. In addition, the present system uses the halogen light of the patient examination chair enabling savings on cost. Therefore, if DR measurements are capable of discriminating sound and non-cavitated carious lesions at comparable accuracies of fluorescence measurements, there would be a considerable increase in cost-effectiveness. On the basis of the results obtained in the present study, the non-invasive DR spectroscopic technique appears to have the potential for detecting tooth caries *in vivo*, but with comparatively lower sensitivities and specificities as compared to fluorescence techniques. Among the various ratios studied, R600/R700 ratio appears to be more suited. Nevertheless, the present studies were able to discriminate sound from caries lesions with an overall sensitivity of 88% and specificity of 100% and a detailed trial to discern various types of cavitations including incipient stages could prove its effectiveness in a clinical setting.

Chapter 11

Discussion and Conclusion

This chapter reviews the entire study presented in this thesis and summarizes the benefits of optical spectroscopic techniques and their limitations related to the early detection of dental caries. A comparison of the diagnostic accuracies of the LIF and DR spectroscopic techniques to identify incipient changes in tooth enamel and to discriminate between tooth erosion and caries is also presented in this chapter. An assessment of the future prospective of optical techniques in the field of dentistry is described on the basis of the current work.

Dental caries is the most widespread oral disease in the world. In spite of our improved knowledge of the caries process and the availability of effective intervention, caries lesions still develop to the point where tooth structure is compromised and invasive intervention and restoration are required. Appropriate diagnosis of carious lesions at their earlier stages is a major factor in the prevention and management of dental caries. It is also clear that reliable and detailed information about the extent and severity of existing caries will enhance the likelihood of a successful treatment outcome. However, visual examination alone is inadequate to detect early carious lesions. Further, biochemical composition and/or structural changes associated with tooth caries disturb optical properties of dental hard tissues. Hence, optical diagnostic techniques appear to be a more suited for early diagnosis of tooth caries, which in turn improves disease management (Chapter 1).

Dental hard tissues are receptive to photonics based applications. When light interacts with tooth, it undergoes the processes of elastic scattering, absorption and fluorescence, before leaving the tooth surface. Dental caries is accompanied by the decalcification of mineral components and dissolution of the organic matrix of hydroxyapatite, which in turn affect the absorption and scattering properties of dental hard tissues. Further, increased fluorescence seen in carious lesions is due to endogenous porphyrin production by several oral microorganisms. Therefore, general information about the structure, biologic processes of tissue and physical properties of light will help to understand and control the outcome of its interaction with biological systems for diagnostic purposes (Chapter 2).

Recent years have seen an increase in research activity directed towards the development of several diagnostic methods, particularly in the assessment of early caries lesions. Quite a few optical spectroscopy systems have been developed and are available for commercial purposes. This study uses a compact laser-induced fluorescence and reflectance spectroscopy (LIFRS) system to non-invasively detect caries formation and demineralization changes in tooth by point monitoring. The LIFRS

system consists of two light sources that could be switched for alternate recording of fluorescence and diffuse reflectance spectra. The LIFRS system uses either nitrogen (337 nm) or a diode (404 nm) laser for the excitation of fluorescence and has a tungsten halogen lamp for diffuse reflectance measurements. The light from either of these sources is coupled through optical fibres to the specimen under investigation through a fiber-optic hand-piece. The resultant LIF or DR spectra collected from the specimen is recorded on a miniature fibre-optic spectrometer, connected to the USB port of the laptop computer (Chapter 3).

In the present study, the LIFRS system was used under both *in vitro* and *in vivo* conditions for detection and characterization of different stages of caries lesions. Before being tested in a clinical environment, extensive *in vitro* studies were carried out on extracted tooth samples to test the applicability of LIFRS system for detecting dental caries. During *in vitro* studies, tooth autofluorescence was measured using both the 337 nm nitrogen laser and the 404 nm diode laser to identify the appropriate excitation regimen in UV-visible range for caries diagnosis and data processing algorithm were developed. Further, the potential of LIFRS system for detecting demineralization and remineralization changes in tooth samples were evaluated.

LIF and diffuse reflectance (DR) signatures of sound/healthy and carious tooth are of interest in caries detection. It was observed that carious lesions showed lower fluorescence and DR intensities as compared to sound tooth. With excitation at 337nm, the LIF spectrum of sound tooth consists of two broad bands with maxima around 490 and 440 nm, with a satellite peak at 405 nm. In pulp level caries an additional peak appears at 630 nm (Chapter 4). In addition, during caries progression, variations can be seen in the fluorescence emission spectral shape with respect to the extent of caries. In order to determine the peak positions of the constituent bands and their relative contributions in the overall spectrum, the LIF spectrum was analyzed by a curve-fitting program using Gaussian spectral functions. The deconvoluted peaks were found centered at 403.80, 434.20, 486.88, and 522.45 nm in sound tooth. But, in dentin and pulp level caries the 522 nm peak was seen red-shifted by 32 and 8 nm, respectively. The exact source for the appearance of this peak is not clear, but it could be due to various factors like the presence of exogenous molecules/fluorophores in the tooth or changes in chemical composition during the disintegration process or from bacteria metabolism products. With respect to detection accuracy, fluorescence ratios determined from curve-fitted amplitudes and Gaussian curve areas showed higher contrast between different stages of caries or tooth decay as compared to raw LIF ratios. The ratios involving the 435 nm emission peak, such as F405/F435,

F435/F525, and F435/F490, appeared more suitable for sighting the evolutionary changes during caries formation.

With 404 nm excitation, the sound tooth shows only the 500 nm autofluorescence peak, with a long tail extending towards the red region, whereas, two additional peaks are seen at 635 and 680 nm in the case of caries tooth (Chapter 7). Further, the fluorescence intensity of the 635 and 680 nm peaks increases with the extent of caries and could be used as a marker for discriminating different stages of caries lesions. The enhancement in these autofluorescence peak intensities in particular at 635 nm, seen in the normalized LIF spectra was found to be most sensitive for detection of early changes in tooth enamel and distinguishing different stages of tooth decay (Chapter 8). Further, by curve-fitting, LIF spectra from sound tooth were resolved into three constituent peaks centered at 491.85, 513.21 and 561.37 nm but two additional peaks were seen at 625.8 and 655.62 nm in enamel caries and at 633.05 and 674.67 nm in dentinal caries (Chapter 9). In addition, Gaussian peak amplitude ratio, F490/F635 was found to be more suited to distinguish between different stages of tooth caries.

The potential of LIFRS system to detect early stages of dental erosion was tested. It was observed that both LIF and DR spectral intensity increases gradually with tooth erosion. While examining sectioned slices of sound enamel and dentin, with curve-fitting carried out using Gaussian spectral functions, broad bands seen at 440 and 490 nm in enamel were resolved into four peaks centered at 409.1, 438.1, 492.4 and 523.1 nm, whereas in dentin the peaks were observed at 412.0, 440.1, 487.8 and 523.4 nm. The transformation from the enamel layer to the dentin layer of tooth can be visualized from the sudden increase/decrease in ratios. The fluorescence spectral ratio, F410/F525, derived from curve-fitted Gaussian peak amplitudes and curve areas were found to be more sensitive to erosion as compared to the DR spectral ratio R500/R700 and the raw LIF spectral ratio (Chapter 5). Likewise, the LIFRS system was used to detect early demineralization and remineralization changes in tooth enamel. Both the LIF and DR spectral intensities show a decreasing trend during cyclic de- and re-mineralization and this trend gets reversed during continuous remineralization. Curve-fitted parameters such as peak center, FWHM, Gaussian amplitude and curve area were found to vary with de/re-mineralization changes in tooth enamel. Variations seen in Gaussian curve area and amplitude of the deconvoluted peaks at 410 and 525 nm of LIF spectra were found to be more suited for detecting mineralization changes in tooth as compared to the raw LIF and DR spectral characteristics (Chapter 6).

Even though, analysis of LIF spectra by curve-fitting with Gaussian spectral functions increases the detection accuracy for caries diagnosis, it is a tedious and time consuming process. Further, caries lesions reveal characteristic fluorescence emission peaks within the red wavelength region, from porphyrin derivatives. Diode laser excitation at 404 nm induces red fluorescence more effectively than 337 nm nitrogen laser excitation. Also, differences between the fluorescence intensity of sound and carious tooth were marked with excitation at 404 nm than at 337 nm.

Receiver operating characteristic (ROC) analysis was used to compare the diagnostic performance of 337 nm nitrogen laser and 404 nm diode laser excitation for discrimination between different stages of dental caries using SPSS software (Version 10, SPSS Inc., Chicago, IL, USA) and the results are given in Table 11.1. Both techniques showed high area under the curve (AUC) for discriminating sound from non-cavitated and cavitated caries lesions. Further, the AUC obtained for discrimination between non-cavitated and cavitated caries lesions was good (0.82) with 404 nm excitation. As compared to 337 nm excitation, results obtained with excitation at 404 nm were found to be more sensitive in discriminating different stages of caries lesions.

Table 11.1 A comparison of 337 and 404 nm LIF in caries discrimination with ROC-AUC analysis.

| Lesion Type | LIF spectral intensity | | | | | |
|----------------------------------|--|-----------|--------|--------|-----------|--------|
| | Receiver Operating Characteristics Curve | | | | | |
| | 337 nm | | | 404 nm | | |
| | AUC | 95% CI | p | AUC | 95% CI | p |
| Sound – Non-cavitated Caries | 0.91 | 0.88-0.93 | <0.001 | 0.86 | 0.83-0.89 | <0.001 |
| Sound – Cavitated Caries | 0.96 | 0.91-1.0 | <0.001 | 0.98 | 0.96-1.0 | <0.001 |
| Non-cavitated - Cavitated Caries | 0.59 | 0.49-0.68 | <0.001 | 0.82 | 0.79-0.85 | <0.001 |

CI: Confidence Interval; p: Significance of difference to the Diagonals; AUC: Area under the Curve.

During clinical trials, LIF and DR spectra were recorded from sound tooth and clinically or radiographically proven carious lesions belonging to different stages. It may also be noted that different stages of caries lesions were occasionally seen in the same tooth. It was observed that the position of peaks in the LIF spectra of sound enamel region and sound tooth determined by curve-fitting are different. This could

be avoided by measuring sound enamel spectra from sound tooth, not from sound area of caries affected tooth, as the laser beam can penetrate to the caries affected lesions underneath and show the spectra of carious tooth. Further this will lead to false positive results with lower specificities.

The clinical trial were carried out in 105 patients at the Government Dental College, Trivandrum. Fluorescence reference standard (FRS) scatter plots were developed based on spectral ratio F500/F635, F500/F680 to discriminate different stage of caries from sound tooth. The FRS ratio scatter plots showed better sensitivity and specificity as compared to clinical and radiographic examination. Among these FRS ratios, the F500/F635 ratio appeared to be more suited for detecting early tooth caries. Also the blind-test conducted in a population of 40 patients confirmed the reliability of the developed FRS ratio in discriminating different stages of caries lesions with 100% sensitivity and specificity (Chapter 8). However, the clinical trials were carried out in patients who had already developed symptoms of caries such as pain and sensitivity to foods. Therefore the diagnostic accuracies achieved may not always be attainable in random population. The advantage of using spectral ratios is that it eliminates systemic errors due to changes in excitation energy/ light levels, detection system configuration and spectral response.

The DR ratios were also used for detecting dental caries, both under *in vitro* and *in vivo* conditions (Chapter 4 & 10). Among the various ratios studied, R500/R700 and R600/R700 ratios appear to be more suited for detecting tooth caries. The studies conducted have shown that DR ratios have the ability to discriminate sound from carious lesions with a sensitivity of 88% and specificity of 100%. The major advantages of this technique is that diffuse reflectance signals are several orders of magnitude greater than the weak endogenous fluorescence signals of tooth and that one could use the inbuilt tungsten halogen lamp of the dentist's examination chair to record the DR spectra. Therefore, if DR measurements were capable of discriminating sound from carious lesions at similar accuracies to that of fluorescence measurements, there would be a considerable increase in cost-effectiveness.

Many research groups have used optical techniques to detect dental caries, (Attrill and Ashley, 2001; Alwas-Danowska et al, 2002; Virajsilp et al, 2005; Reis et al, 2006; Alkurt et al, 2008), to discriminate between different stages of caries (Uzunov et al, 2003; Borisova et al, 2007), to discriminate between tooth caries and demineralization, (Borisova et al, 2004), and to detect remineralization in carious lesions (Arends and Gelhard, 1983; Fausto et al, 2003; Jones and Fried, 2006). Jone et al, 2006). An ideal

Table 11.2 Comparative evaluation of the diagnostic accuracies of the present study with the results obtained by different groups using optical spectroscopy for caries detection.

| Research Group | Diagnostic Method | Sites | Sensitivity | Specificity |
|-------------------------------|---|--|-------------|-------------|
| Hall et al, 1996 | QLF | Smooth surface, in vitro | 0.75 | 0.90 |
| Lussi et al, 1999 | DIAGNOdent | Permanent teeth, occlusal surfaces, in vitro | 0.76-0.84 | 0.79-0.87 |
| Shi et al, 2001 | QLF | Smooth surface, in vitro | 0.76 | 0.92 |
| Shi et al, 2000 | DIAGNOdent | Permanent teeth, occlusal surfaces, in vitro | 0.78-0.82 | 1 |
| Francescut and Lussi, 2003 | DIAGNOdent | Permanent teeth, occlusal surfaces, in vitro | 0.73 | 0.65 |
| Costa et al, 2002 | DIAGNOdent | Permanent teeth, occlusal surfaces, in vitro | 0.79 | 0.89 |
| Bamzahim et al, 2002 | DIAGNOdent | Permanent teeth, occlusal surfaces, in vitro | 0.8 | 1 |
| Lussi et al, 2001 | DIAGNOdent | Permanent teeth, occlusal surfaces, in vivo | 0.92 | 0.86 |
| Heinrich-Weltzien et al, 2002 | DIAGNOdent | Permanent teeth, occlusal surfaces, in vivo | 0.93 | 0.63 |
| Anttonen et al, 2003 | DIAGNOdent | Permanent teeth, occlusal surfaces, in vivo | 0.92 | 0.69 |
| Rocha et al, 2003 | DIAGNOdent | Deciduous teeth, occlusal surfaces, in vivo | 0.73 | 0.95 |
| Bamzahim et al, 2005 | DIAGNOdent | Secondary caries, in vivo | 0.6 | 0.81 |
| Huth et al, 2008 | DIAGNOdent pen | Permanent teeth, occlusal surfaces, in vivo | 0.88 | 0.85 |
| Rodrigues et al, 2008 | DIAGNOdent | Permanent teeth, proximal surfaces, in vivo | 0.89 | 0.82 |
| Rodrigues et al, 2008 | DIAGNOdent | Permanent teeth, occlusal surfaces, in vitro | 0.2-0.69 | 0.72-0.94 |
| Angnes et al, 2005 | DIAGNOdent | Permanent teeth, occlusal surfaces, in vivo | 0.81 | 0.54 |
| Present study (Chapter 8) | LIF spectroscopy, fluorescence reference standard (FRS) ratio scatter plots | Permanent teeth, in vivo | 1 | 1 |
| Present study (Chapter 10) | DR spectroscopy, DR spectral ratio scatter plots | Permanent teeth, in vivo | 0.88 | 1 |

diagnostic method should offer high sensitivity and high specificity (Ekstrand et al, 1997). The real challenge for a diagnostic method lies in its ability to identify caries lesions in its incipient stage. The efficiency of laser fluorescence for caries detection

was investigated and compared with conventional methods. Some of these diagnostic modalities show promising results to discriminate sound from caries lesions with good enough sensitivity and specificity. Table 11.2 gives a comparison of the diagnostic accuracies of the LIF and DR spectroscopic studies presented in this thesis with the results obtained by other research groups for caries detection, both *in vitro* and *in vivo*.

The diagnostic performances of LIF and DR spectroscopy for caries detection were evaluated in terms of the area under ROC curve, sensitivity and specificity. For both LIF and DR spectroscopy, detection of caries lesions was successful with ROC-AUC values between 0.93 and 0.98. Sensitivity, specificity and AUC (A_z) obtained for LIF ratios F500/F635 and F500/F680 (Chapter 8) and DR ratios R500/R700, R600/R700 and R650/R700 (Chapter 10) to detect caries lesions are shown in Table 11.3. In general, an area under the ROC curve >0.9 indicates good classification between the two classes. Moreover, AUC obtained using LIF ratios F500/F635 was 0.98, while for F500/F680 it was 0.97. In comparison, the DR ratio R600/R700 gave an AUC value of 0.97 to discriminate sound from carious lesions. But the sensitivity was higher than that of DRS or detecting caries with LIF. Nonetheless, the results of statistical analysis evaluating the diagnostic performance showed LIF-FRS ratio as a better diagnostic parameter as compared to DRRS ratio.

Table 11.3 Comparison of LIFS and DRS in diagnosing dental caries in terms of sensitivity, specificity and area under the ROC curve (A_z).

| | Methodology | Sensitivity | Specificity | ROC-AUC (A_z) |
|------|-------------|-------------|-------------|-------------------|
| LIFS | F500/F635 | 100 | 100 | 0.98 |
| | F500/F680 | 100 | 100 | 0.97 |
| DRS | R500/R700 | 83 | 100 | 0.93 |
| | R600/R700 | 92 | 100 | 0.97 |
| | R650/R700 | 88 | 100 | 0.94 |

The advantage of ROC analysis is that it demonstrates the diagnostic performance more methodically than sensitivity and specificity, which are determined by only one cut-off point. This analysis also provides an overall validity of the methods employed. Therefore from a mathematical point of view, the ROC analysis is the best one although it does not consider any given threshold. However, in clinical practice clinicians usually have to consider a cut-off point in which the treatment options falls from non-invasive

to invasive approach and this makes sensitivity and specificity values of the diagnostic method is still valuable.

The advantages of using a diode laser at 404 nm as against other lasers at longer emission such as argon ion laser (488 nm) or diode laser (655 nm), for obtaining caries sensitive fluorescence signatures have been clearly brought out. The major disadvantage of DIAGNOdent is the unsuitability of the 655 nm laser emission of this device for excitation of the chemical constituents of teeth like the protoporphyrin, or the altered tooth substances and bacterial metabolism products that cause tooth decay. It may further be noted that fluorescence of caries lesions is due to changes in organic content of the lesion rather than mineral loss. Further, the use of a diode laser emitting at 404 nm which matches with the absorption band of PpIX, confirms the enhanced capability and accuracy for LIF spectroscopy to detect different stages of caries lesions. Moreover, this facilitates visualisation and quantification of both the intrinsic green fluorescence and red fluorescence of bacterial origin from dental tissues.

Our studies have shown that the developed LIFRS system has the potential to measure autofluorescence and diffuse reflectance spectra from tooth and can be used as a suitable tool for non-invasive and real time diagnosis of dental caries. Furthermore, these techniques could also be a useful to detect dental erosion and to monitor de- and re-mineralization changes in tooth. If properly used and correctly interpreted, this device would improve caries detection and diagnosis and therefore, the selection of proper restorative intervention. However, for optimal application of the technique, tooth surface should be properly cleaned before measurement because the spectra could be influenced by the plaque, calculus and stains. Further, the probe tip should be kept in close contact with tooth surfaces in order to reduce stray light from entering the detection system. In conclusion, studies with the LIFRS system has shown that it has the potential to be further developed into a cost effective portable system for clinical use in view of the recent developments of low cost LED's emitting in the near UV region.

Besides, more clinical studies based on relatively larger samples need to be carried out to detect caries lesions present in pits and fissures and around restoration. Because, secondary caries occur as a result of restoration failure and detection by conventional methods is oftendifficult. In addition, there is little information about the use of optical techniques in tooth with enamel hypoplasia, fluorosis or discoloration, which might influence the fluorescence spectral intensity. Therefore, more research is required in this direction, as well.

References

1. Albin S, Byvik CE, Buoncristani AM. Laser induced fluorescence of dental caries, In *Laser Surgery: Characterization and Therapeutics* 1988; SPIE vol. 907: 96-99.
2. Alfano RR, Yao SS. Human teeth with and without dental caries studied by visible luminescent spectroscopy. *J Dent Res* 1981; 54: 67.
3. Alexander H. Device for identifying caries, plaque, bacterial infection, concretions, tartar and other fluorescent substances on teeth. US Patent 6,561,802. May 13, 2003.
4. Aljehani A, Bamzahim M, Yousif MA, Shi XQ. In vivo reliability of an infrared fluorescence method for quantification of carious lesions in orthodontic patients. *Oral Health and Preventive Dentistry* 2006; 4: 145-150.
5. Aljehani A, Yang LF, Shi XQ. In vitro quantification of smooth surface caries with DIAGNOdent and the DIAGNOdent pen. *Acta Odontol Scand* 2007; 65: 60-63.
6. Al-Khateeb S, Ten Cate JM, Angmar-Mansson B, de Josselin De Jong E, Sundstrom G, Exterkate RAM, Oliveby A. Quantification of formation and remineralization of artificial enamel lesions with a new portable fluorescence device. *Adv Dent Res*. 1997a; 11: 502-506.
7. Al-Khateeb S, Oliveby A, de Josselin De Jong E, Angmar-Mansson B. Laser fluorescence quantification of remineralization in situ of incipient enamel lesions: influence of fluoride supplements. *Caries Res*. 1997b; 31: 132-140.
8. Al-Khateeb S, Forsberg C, de Josselin de Jong E, Angmar-Mansson B. A longitudinal laser fluorescence study of white spot lesions in orthodontic patients. *Am J Orthod Dentofac Orthop* 1998; 113: 595-602.
9. Alkurt MT, Peker I, Arisu HD, Bala O, Altunkaynak B. In vivo comparison of laser fluorescence measurements with conventional methods for occlusal caries detection. *Lasers Med Sci* 2008; 23: 307-312.
10. Alwas-Danowska HM, Plasschaert AJM, Suliborski S, Verdonschot EH. Reliability and validity issues of laser fluorescence measurements in occlusal caries diagnosis. *J Dent* 2002; 30:129-134.

11. Anderson P, Elliott JC. Rates of mineral loss in human enamel during in-vitro demineralization perpendicular and parallel to the natural surface. *Caries Research* 2000; 34: 33-40.
12. Ando M, Eggertsson H, Isaacs R, Analoui M, Stookey G. Comparative studies of several methods for the early detection of fissure lesions. In *Early detection of dental caries II*, eds. Stookey GK. Indianapolis: Indiana University, School of dentistry 2000; 279-299.
13. Ando M, van der Veen MH, Schemehorn BR, Stookey GK. Comparative study to quantify demineralized enamel in deciduous and permanent teeth using laser- and light- induced fluorescence techniques. *Caries Res.* 2001; 35: 464-470.
14. Angmar-Mansson B, ten Bosch JJ. Advances in methods for diagnosing coronal caries: A review. *Adv Dent Res.* 1993; 7: 70-79.
15. Angnes V, Angnes G, Batisttella M, Grande RHM, Loguercio AD. Clinical effectiveness of laser fluorescence, visual inspection and radiography in the detection of occlusal caries. *Caries Res* 2005; 39: 490-495.
16. Anttonen V, Seppa L, Hausen H. Clinical study of the use of the laser fluorescence device DIAGNOdent for detection of occlusal caries in children. *Caries Res* 2003; 37: 17-23.
17. Arcoria C, Miserendino LJ. In *Laser in Dentistry*, Eds. Miserendino LJ and Pick RM, Quintessence Publ. Co, Inc, Chicago, et al., 1995; 76.
18. Arends J, ten Cate JM. Tooth enamel remineralization. *J Cryst Growth.* 1981; 53: 135-147.
19. Arends J, Gelhard T. In *Demineralization and Remineralization of the teeth*. Eds., Leach S and Edgar W, IRL Press, Oxford, UK, 1983; 1-16.
20. Arends J, Ruben JL, Inaba D. Major topics in quantitative microradiography of enamel and dentin: R parameter, mineral distribution visualization, and hyper-remineralization. *Adv. Dent. Res.* 1997; 11: 403-414.
21. Ashley PF, Blinkhorn AS, Davies RM. Occlusal caries diagnosis: An invitro histological validation of the electronic caries monitor [ECM] and other methods. *J Dent* 1998; 26(2): 83-88.
22. Altshuler GB, Erofeev AV. In *Laser in Dentistry*, Eds. Miserendino LJ and Pick RM, Quintessence Publ. Co, Inc, Chicago, et al., 1995; 283.

23. Altshuler GB. J. Optical model of the tissues of the human tooth. *J Opt Technol* 1995; 62: 516-520.
24. Altshuler GB, Grisimov VN, Ermolaev VS, Vityaz IV. Human tooth as an optical device. *SPIE Proc Holography Interferometry Opt Pattern Recognition Biomed* 1991; 1429: 95-104.
25. Altshuler GB, Grisimov VN. Effect of waveguide light propagation in human tooth. *Dokl Acad Sci USSR* 1990; 3: 1245-1248.
26. Attrill DC, Ashley PF. Occlusal caries detection in primary teeth: a comparison of DIAGNOdent with conventional methods. *Br. Dent. J.* 2001; 190: 440-443.
27. Avery JK and Chiego, Jr DJ. In *Essentials of Oral Histology and Embryology: A Clinical Approach*. Mosby, Canada, 2006.
28. Bader JD, Shugars DA. A systematic review of the performance of a laser fluorescence device for detecting caries. *J Am Dent Assoc* 2004; 135: 1413-1426.
29. Balooch M, Demos SG, Kinney JH, Marshall GW, Balooch G, Marshall SJ. Local mechanical and optical properties of healthy and transparent root dentin. *J Mater Sci Mater Med* 2001; 12: 507-514.
30. Bamzahim M, Shi XQ, Angmar-Mansson B. Occlusal caries detection and quantification by DIAGNOdent and Electronic Caries Monitor: in vitro comparison. *Acta Odontol Scand* 2002; 60: 360-364.
31. Bamzahim M, Shi XQ, Angmar-Mansson B. Secondary caries detection by DIAGNOdent and radiography: a comparative in vitro study. *Acta Odontol Scand* 2004; 62: 61-64.
32. Bamzahim M, Aljehani A, Shi XQ. Clinical performance of DIAGNOdent for detection of secondary carious lesion. *Acta Odontol Scand* 2005; 63: 26-30.
33. Barnes CM. Dental hygiene participation in managing incipient and hidden caries. *Dent Clin N Am* 2005; 49: 795-813.
34. Bath-Balogh, M and Fehrenbach, MJ, In *Dental Embryology, Histology, and Anatomy*. Philadelphia, PA: WB Saunders, 2006.
35. Baysan A. In *Minimally Invasive Dentistry: The management of caries*, Eds. Wilson NHF, Quintessence Publ. Co, Ltd, London, et al., 2007; 29-33.

36. Bhaskar SN. In Orban's oral histology and embryology, Tenth Edition, Mosby, 2000.
37. Bissonnette R, Zeng H, McLean DI, Schreiber WE, Roscoe DL, Lui H: Psoriatic plaques exhibit red autofluorescence that is due to protoporphyrin IX. *J Invest Dermatol* 1998; 111: 586– 590.
38. Bjelkhagen H, Sundstrom , Angmar-Mansson B. Early detection of enamel caries by luminescence excited by visible laser light. *Swed Dent J* 1982; 6: 1-7.
39. Booij M, ten Bosch JJ. A fluorescent compound in bovine dental enamel matrix compared with synthetic dityrosine. *Archs Oral Biol* 1982; 27: 417-421.
40. Borisova EG, Uzunov TT, Avramov LA. Early differentiation between caries and tooth demineralization using laser-induced autofluorescence spectroscopy. *Lasers Surg Med* 2004; 34: 249-253.
41. Borisova E, Uzunov T, Avramov L. Laser-induced autofluorescence study of caries model in vitro. *Lasers Med Sci* 2006; 21(1): 34-41.
42. Borisova E, Uzunov T, Valkanov S, Avramov L. Light diffuse reflectance for detection and differentiation of teeth caries lesions. *SPIE Proc.* 2007; 6535.
43. Boulnois JL. Photophysical processes in recent medical laser developments: A review, *Lasers Med Sci* 1986; 1: 47-66.
44. Brazier J: A note on ultra-violet red fluorescence of anaerobic bacteria in vitro. *J Appl Bacteriol* 1986; 60: 121–126.
45. Buchalla W. Comparative fluorescence spectroscopy shows differences in noncavitated enamel lesions. *Caries Res* 2005; 39: 150-156.
46. Bulher CM, Ngaotheppitak P, Fried D. Imaging of occlusal dental caries (decay) with near-IR light at 1310 nm. *Optics Exp.* 2005; 13: 573-582.
47. Burin C, Burin C, Loguercio AD, Grande RH, Reis A. Occlusal caries detection: a comparison of a laser fluorescence system and conventional methods. *Pediatr Dent* 2005; 27:307–312.
48. Chance B, Cohen P, Jobsis F, Schoener B. Intracellular oxidation-reduction states in vivo, *Science* 1962; 137: 499-508.
49. Costa AM, Yamaguti PM, De Paula LM, Bezzerra AC. In vitro study of laser diode 655 nm diagnosis of occlusal caries. *ASDC J Dent Child* 2002; 69: 249-253.

50. Costa AM, Bezzerra AC, Fuks AB. Assessment of the accuracy of visual examination, bite-wing radiographs and DIAGNOdent on the diagnosis of occlusal caries. *European Archives of Paediatric Dentistry* 2007; 8: 118–122.
51. Coulthwaite L, Pretty IA, Smith PW, Higham SM, Verran J. The microbiological origin of fluorescence observed in plaque on dentures during QLF analysis. *Caries Res* 2006; 40: 112-116.
52. Creanor SL, Russell JL, Strang DM, Stephen KW, Burchell CK. The prevalence of clinically undetected occlusal dentine caries in Scottish adolescents. *Br Dent J* 1990; 169: 126-129.
53. Darling C, Huynh G, Fried D. Light scattering properties of natural and artificially demineralized dental enamel at 1310-nm. *J Biomed Opt.* 2006; 11(3): 034023 (1-11).
54. Dawes C. What is the critical pH and why does a tooth dissolve in acid?. *J Can Dent Assoc.* 2003; 69: 722 - 724.
55. Dederich DN. Laser tissue interaction. *Alpha Omegan* 1991; 84: 33-36.
56. De Josselin de Jong E, Sundstrom F, Westerling H, Tranaeus S, ten Bosch JJ, Angmar-Mansson B. A new method for in vivo quantification of changes in initial enamel caries with laser fluorescence. *Caries Res.* 1995; 29(1): 2-7.
57. Drakaki E, Borisova E, Makropoulou M, Avramov L, Serafetinides AA, Angelov I. Laser-induced autofluorescence studies of animal skin used in modelling of human cutaneous tissue spectroscopic measurements. *Skin research and technology* 2007; 1-10.
58. Eibofner E, Klotz M, Lussi A, Bareiss M. Method and device for determination of caries in teeth. US Patent 6,102,704. August 15, 2000.
59. Eisenberg J. Phenomena observed by subjecting dental tissues to ultra-violet rays corresponding to approximately 3590AU. *Dent Cosmos* 1933; 5: 284.
60. Ekstrand KR, Ricketts DN, Kidd EA. Reproducibility and accuracy of three methods for assessment of demineralization depth of the occlusal surface: an in vitro examination. *Caries Res* 1997; 31: 224–231.
61. Ekstrand KR, Ricketts DN, Kidd EAM. Occlusal caries: pathology, diagnosis and logical management. *Dent Update* 2001; 28: 380–387.
62. Ekstrand KR. Improving clinical visual detection- potential for caries clinical trials. *J. Dent. Res.* 2004; 83: C67-71.

63. Elderton RJ. Longitudinal study of dental treatment in the General Dental service in Scotland. *Br Dent J* 1983; 155: 91–96.
64. Emami Z, Al-Khateeb S, de Josselin de Jong E, Sundstrom F, Trollsas K, Angmar-Mansson B. Mineral loss in incipient caries lesions quantified with laser fluorescence and longitudinal microradiography: A methodologic study. *Acta Odontol Scand.* 1996; 54: 8-13.
65. Farrell TJ, Patterson MS, Wilson B. A diffusion theory model of spatially resolved, steady-state diffuse reflectance for the non-invasive determination of tissue optical properties in vivo. *Med Phys* 1992; 19: 879-888.
66. Fausto MM, Jose N, Danilo AD. Evaluation of the effectiveness of laser fluorescence in monitoring in vitro remineralization of incipient caries lesions in primary teeth. *Caries Res.* 2003; 37: 442-444.
67. Featherstone JDB, O'Reilly MM, Shariati M, Brugler S. In *Factors relating to demineralization and remineralization of the teeth*, S. A. Leach, Ed., IRL Press, Oxford, UK, 1986.
68. Featherstone JD. The caries balance: the basis for caries management by risk assessment. *Oral Health Prev Dent* 2004; 2: 259-264.
69. Fejerskov O. Concepts of dental caries and their consequences for understanding the disease. *Community Dent oral Epidemiol* 1997; 25: 5-12.
70. Ferreira Zandona AG, Analoui M, Beiswanger BB, Isaacs R, Kafrawy A, Eckert G, Stookey G. An in vitro comparison between laser fluorescence and visual examination for detection of demineralization in occlusal pits and fissures. *Caries Res* 1998; 32: 210-218.
71. Ferreira Zandona AG, Isaacs R, Van der Veen MH, Stookey G. Indiana pilot clinical study of quantitative light fluorescence. In *Early detection of dental caries II*, eds. Stookey GK. Indianapolis: Indiana University, School of dentistry 2000; 219-230.
72. Francescut P, Lussi A. Correlation between fissure discoloration, DIAGNOdent measurements and caries depth: an in vitro study. *Pediatr Dent* 2003; 25: 559-564.
73. Fried D, Glena RE, Featherstone JDB, Seka W. Nature of light scattering in dental enamel and dentin at visible and near-infrared wavelengths. *Appl Opt* 1995; 34: 1278-1285.

74. Fried D. In *Biomedical Photonics Handbook*, Ed. Tuan Vo-Dinh, CRC Press, Boca Raton, 2003; 50-51.
75. Fujimoto D, Akiba K, Nakamura N. Isolation and characterization of a fluorescent material in bovine Achilles tendon collagen. *Biochem Biophys Res Comm*. 1977; 76: 1124-1129.
76. Gillenwater A, Jacob R, Richards-Kortum R. Fluorescence spectroscopy: A technique to improve the early detection of aerodigestive tract neoplasia. *Head & Neck* 1998; 556-562.
77. Gupta PK, Ghosh N, Patel HS. In *Fundamentals and applications of Biophotonics in Dentistry*, Eds. Kishen A and Asundi A, Imperial College Press, London, 2007; 135-136.
78. Hafstrom-Bjorkman U, Sundström F, ten Bosch JJ. Fluorescence in dissolved fractions of human enamel. *Acta Odontol Scand* 1991; 49: 133–138.
79. Hale GM, Querry MR. Optical constants of water in the 200 nm to 200 μm wavelength region. *Appl Opt* 1973; 12: 555-563.
80. Hall AF, DeSchepper E, Ando M, Stookey GK. Dye-enhanced laser fluorescence method. Presented at 1st Annual Indiana Conference. Indianapolis, Indiana University Press 1996a; 156-171.
81. Hall AF, DeSchepper E, Ando M, Stookey GK. In vitro studies of laser fluorescence for detection and quantification of mineral loss from dental caries. *Adv Dent Res*. 1997; 11: 507-514.
82. Heinrich –Weltzien R, Weerheijm KL, Kuhnisch J, Oehme T, Stosser L. Clinical evaluation of visual, radiographic and laser fluorescence methods for detection of occlusal caries. *ASDC J Dent Child* 2002; 69: 127-132.
83. Heinrich –Weltzien R, Kuhnisch J, Ifland S, Tranaeus S, Angmar-Mansson B, Stosser L. Detection of initial caries lesions on smooth surfaces by quantitative light-induced fluorescence and visual examination: an in vivo comparison. *Eur J Oral Sci* 2005; 113: 494-498.
84. Hibst R, Gall R. Development of diode laser-based fluorescence caries detector. *Caries Res*. 1998; 32: 294.
85. Hibst R, Paulus R. Caries detection by red excited fluorescence investigations on fluorophores. *Caries Res* 1998; 32: 294.

86. Hibst R, Paulus R. Caries detection by red excited fluorescence: Investigations on fluorophores. *Caries Res* 1999; 33: 295.
87. Hibst R, Paulus R: A new approach on fluorescence spectroscopy for caries detection. *SPIE* 1999; 3593: 141–147.
88. Hibst R, Paulus R. Molecular basis of red excited caries fluorescence. *Caries Res* 2000; 34: 323.
89. Hibst R, Paulus R. Method and device for the recognition of caries, plaque, concretions or bacterial infection on teeth. US Patent 6,186,780. February 13, 2001.
90. Hibst R, Paulus R, Lussi A. Detection of occlusal caries by laser fluorescence: basic and clinical investigations. *Med Laser Appl* 2001; 16: 205-213.
91. Hintze H, Wenzel A, Danielsen B, Nyvad B. Reliability of visual examination, fiber-optic transillumination, bite-wing radiography and reproducibility of direct visual examination following tooth separation for the identification of cavitated carious lesions in contacting approximal surfaces. *Caries Res.* 1998; 32(3): 204-209.
92. Hunt AM. A description of the molar teeth and investing tissues of normal guinea pigs. *J Dent Res* 1959; 38(2): 216-31.
93. Hunter RS, Harold RW. The measurement of appearance, Wiley & Sons ed. 2 New York, 1987; 29-35.
94. Huth KC, Neuhaus KW, Gyax M, Bucher K, Crispin A, Paschos E, Hickel R, Lussi A. Clinical performance of a new laser fluorescence for detection of occlusal caries lesions in permanent molars. *J Dent* 2008; 36: 1033-1040.
95. Huysmans MC, Longbottom C, Pitts NB, Los P, Bruce PG. Impedance spectroscopy of teeth with and without approximal caries lesions: an in vitro study. *J Dent Res* 1996; 75: 1871-1878.
96. Ie YL, Verdonschot EH. Performance of diagnostic systems in occlusal caries detection compared. *Community Dent Oral Epidemiol* 1994; 22: 187-191.
97. Jones RS, Fried D. Remineralization of Enamel caries can decrease optical reflectivity. *J Dent Res.* 2006; 85(9), 804-808.
98. Jones RS, Darling CL, Featherstone JDB, Fried D. Remineralization of in vitro dental caries assessed with polarization-sensitive optical coherence tomography. *J Biomed Opt.* 2006; Jan/Feb 11(1): 014016(1-9).

99. Karlstrom S. Physical, physiological and pathological studies of dental enamel, with special reference to the question of its vitality. A.-B Fahlcrantz' Boktryckeri; Stockholm 1931; 182.
100. Kidd EAM, Joyston-Bechal S. Essentials of dental caries: the disease ad its management. Bristol. Wright, 1987.
101. Kidd EAM, Ricketts DNJ, Pitts NB. Occlusal caries diagnosis: A changing challenge for clinicians and epidemiologists. J Dent 1993; 21: 323-331.
102. Kidd EAM. The diagnosis and management of the early carious lesion in permanent teeth. Dent. Update 1994; 11: 69 -81.
103. Kidd EAM, Joyston-Bechal S: Essentials of dental caries: the disease ad its management. Oxford University Press Inc., New York, 1997.
104. Kidd EA & Fejerskov O. What constitutes dental caries? Histopathology of carious enamel and dentin related to the action of cariogenic biofilms. J Dent Res 2004; 83(Spec C): 35–38.
105. Kienle A, Forster FK, Diebolder R, Hibst R. Light Propagation in Dentin: Influence of Light Propagation on Anisotropy. Phys Med Biol 2003; 48: N7-N14.
106. King NM, Shaw L. Value of bitewing radiographs in detection of occlusal caries, Community Dent and Oral Epidemiol 1979; 7(4): 218-221.
107. Ko CC, Tantbirojin D, Wang T, Douglas WH. Optical scattering power for characterization of mineral loss”, J. Dent. Res. 2000; 79; 1584-1589.
108. Konig K, Hibst R, Meyer H, Flemming G, Schneckenburger H. Laser-induced autofluorescence of carious regions of human teeth and caries-involved bacteria. SPIE 1993; 2080: 170–180.
109. Konig K, Schneckenburger H. Laser-induced autofluorescence for medical diagnosis. J Fluoresc 1994; 4: 17-40.
110. Konig K, Flemming G, Hibst R. Laser-induced autofluorescence spectroscopy of dental caries. Cell Mol Biol 1998; 44: 1293-1300.
111. Konig K, Schneckenburger H, Hibst R. Time-gated in vivo autofluorescence imaging of dental caries. Cell Mol Biol (Noisy-le-grand) 1999; 45: 233-239.
112. Koort HJ, Frentzen M. YAG-lasers in restorative dentistry: A histological investigation. In Laser Surgery: Advanced Characterization, Therapeutics and

- Systems III, Eds. Anderson PR, Katzir A, SPIE Proc 1992 a; 1643: 403-411.
113. Kortum G. *Reflectance Spectroscopy*, Springer, New York - Berlin - Heidelberg, 1969.
 114. Kuhnisch J, Heinrich–Weltzien R, Tranaeus S, Angmar-Mansson B, Stosser L. Confounding factors in clinical studies using QLF. *Int Poster J Dent Oral Med* 2003; 5(2): 177.
 115. Kuhnisch J, Ifland S, Tranaeus S, Angmar-Mansson B, Hickel R, Stosser L, Heinrich –Weltzien R. Estabilishing quantitative light-induced fluorescence cut-offs for the detection of occlusal dentine lesions. *Eur J Oral Sci* 2006; 114: 483-488.
 116. Lakowicz JR. *Principles of fluorescence spectroscopy*. Plenum Press, New York, 1983.
 117. Lennon AM, Buchalla W, Switalski L, Stookey GK. Residual caries detection using visible fluorescence. *Caries Res* 2002; 36: 315–319.
 118. LeGeros RZ. *Calcium phosphates in oral biology and medicine*. Karger, Basel-Munchen-Paris. 1991.
 119. Levy G, Rizoiu IM. In *Laser in Dentistry*, Eds. Miserendino LJ and Pick RM, Quintessence Publ. Co, Inc, Chicago, et al., 1995; 300.
 120. Lizarelli RFZ, Bregagnolo DDS, Lizarelli RZ, Palhares JMC and Villa GEP. A comparative in vitro study to diagnose decayed dental tissue using different methods. *Photomedicine and Laser Surgery* 2004; 22: 205-210.
 121. Loesche WJ. Role of *Streptococcus mutans* in human dental caries. *Microbiol Rev.* 1986; 50(4): 353-380.
 122. Longbottom C, Huysmans MC, Pitts NB, Los P, Bruce PG. Detection of dental decay and its extent using a. c. impedance spectroscopy. *Nat Med* 1996; 2: 235-237.
 123. Lussi A, Imwinkelried S, Pitts NB, Longbottom C, Reich E. Performance and reproducibility of a laser fluorescence system for detection of occlusal caries in vitro. *Caries Res* 1999; 33: 261-266.
 124. Lussi A, Megert B, Longbottom C, Reich E, Francescut P. Clinical performance of a laser fluorescence device for detection of occlusal caries lesions. *Eur J Oral Sci.* 2001; 109: 14-19.

125. Lussi A, Francescut P. Performance of conventional and new methods for detection of occlusal caries in deciduous teeth. *Caries Res* 2003; 37: 2-7.
126. Lussi A, Hibst R, Paulus R. DIAGNOdent: an optical method for caries detection. *J Dent Res* 2004; 83: C80–C3.
127. Lussi A, Hellvig E. Performance of a new laser fluorescence device for the detection of occlusal caries in vitro. *J Dent* 2006; 34: 467-471.
128. Marsh P, Martin MV. *Oral Microbiology*, ed 4, Oxford, Wright 1999; 61-63.
129. Marthaler TM. Caries status in Europe and predictions of future trends. *Caries Res* 1990; 24: 381-396.
130. Marthaler TM. Changes in dental caries 1953-2003. *Caries Res* 2004; 28: 173-181.
131. Masychev VI, Sokolovsky AA, Kesler G, Alexandrov MT. Early dental caries detection by method of PNC-diagnostics: Comparison with visual and X-ray methods. *SPIE* 2000; 3910: 269–280.
132. Matsumoto H, Kitamura S, Araki T. Autofluorescence in human dentine in relation to age, tooth type and temperature measured by nanosecond time-resolved fluorescence microscopy. *Arch Oral Biol* 1999; 44: 309–318.
133. Metz CE. Basic principles of ROC analysis. *Sem Nucl Med* 1978; 8: 283-298.
134. Muller MG, Gergakoudi I, Zhang Q, Wu J, Feld MS. Intrinsic fluorescence spectroscopy in turbid media: disentangling effects of scattering and absorption. *Appl Opt* 2001; 40: 4633-4646.
135. Nagasawa A. Research and development of laser in dental and oral surgery. In *New Frontiers in Laser Medicine and Surgery*, Eds. K. Atsumi. Elsevier, Amsterdam- Oxford, 1983; 233-241.
136. Naseem S. Oral and dental diseases: Causes, prevention and treatment strategies: Burden of diseases. *National Commission on Macroeconomics and Health*. 2005; 275-298.
137. Newbrun E. Problems in caries diagnosis. *Int Dent J* 1993; 43: 133–142.
138. Nichols MG, Hull EL, Foster TH. Design and testing of a white-light, steady-state diffuse reflectance spectrometer for determination of optical properties of highly scattering systems. *Appl. Opt.* 1997; 36(1): 93–104.

139. Ng SY, Ferguson MWJ, Payne PA, Slater P. Ultrasonic studies of unblemished and artificially demineralized enamel in extracted human teeth: a new method for detecting early caries. *J Dent* 1988; 16: 201-209.
140. Olmez A, Tuna D, Oznurhan F. Clinical evaluation of DIAGNOdent in detection of occlusal caries in children. *J Clin Pediatr Dent* 2006; 30:287–291 312.
141. Pinelli C, Serra MC, Loffredo LCM. Validity and reproducibility of a laser fluorescence system for detecting the activity of white-spot lesions on free smooth surfaces in vivo. *Caries Res* 2002; 36: 19-24.
142. Pretty IA, Edgar WM, Higham SM. Detection of in vitro demineralization of primary teeth using quantitative light-induced fluorescence (QLF). *Int. J of Paediatr. Dent.* 2002; 12: 158- 167.
143. Pretty I.A, Pender N, Edgar WM, Higham SM. The in vitro detection of early enamel de- and re-mineralization adjacent to bonded orthodontic cleats using quantitative light-induced fluorescence. *Eur J Orthod.* 2003; 25: 217-223.
144. Pretty IA, Smith PW, Edgar WM, Higham SM. Detection of in vitro on demineralization adjacent to restorations using quantitative light induced fluorescence (QLF). *Dental Materials* 2003; 19: 368-374.
145. Pretty IA, Edgar WM, Smith PW, Higham SM. Quantification of dental plaque in the research environment. *J Dent* 2005; 33: 193-207.
146. Ramanujam N. Fluorescence spectroscopy of neoplastic and non-neoplastic tissues. *Neoplasia* 2000; 2: 89-117.
147. Reis A, Mendes FM, Angnes V, Angnes G, Grande RH, Loguercio AD. Performance of methods of occlusal caries detection in permanent teeth under clinical and laboratory conditions. *J Dent* 2006; 34: 89-96.
148. Ribeiro A, Rousseau C, Girkin J, Hall A, Strang R, Whitters CJ, Creanor S, Gomes ASL. A preliminary investigation of a spectroscopic technique for the diagnosis of natural caries lesions. *J Dent* 2005; 33: 73-78.
149. Richards-Kortum R, Sevick-Muraca E. Quantitative optical spectroscopy for tissue diagnosis. *Annual Review of Physical Chemistry* 1996; 47: 555-606.
150. Roberson T, Heymann HO, Swift EJ. *Sturdevant's Art & Science of Operative Dentistry* St Louis, Missouri, Mosby, 2002.
151. Rocha RO, Ardenghi TM, Oliveira LB, Rodrigues CRMD and Ciamponi AL. In

- vivo effectiveness of laser fluorescence compared to visual inspection and radiography for detection of occlusal caries in primary teeth. *Caries Res* 2003; 37: 437-441.
152. Rodrigues JA, Diniz MB, Josgrilberg EB, Cordeiro RCL. In vitro comparison of laser fluorescence performance with visual examination for detection of occlusal caries in permanent and primary molars. *Lasers Med Sci* 2008; DOI 10.1007/s10103-008-0552-4.
 153. Rodrigues JA, Hug I, Lussi A. The influence of zero value subtraction on the performance of a new laser fluorescence device for approximal caries detection. *Lasers Med Sci* 2008; DOI 10.1007/s10103-008-0549-z.
 154. Rock WP, Kidd EAM. The electronic detection of demineralization in occlusal fissures. *Br Dent J* 1988; 164: 243-247.
 155. Ross G. Caries diagnosis with the DIAGNOdent Laser: A user's product evaluation. *Ont Dent* 1999; 76(2): 21-24.
 156. Sanchez-Figueras A Jr. Occlusal pit-and-fissure caries diagnosis: a problem no more. A science-based approach using laser-based fluorescence device. *Compend Contin Educ Dent* 2003; 24: 3-11.
 157. Sarkissian A, Le AN. Fiber optic fluorescence microprobe for endodontic diagnosis. *Journal of dental education* 2005; 69: 633-638.
 158. Sawle RF, Andlaw RJ. Has occlusal caries become more difficult to diagnose? A study comparing clinically undetected lesions in molar teeth of 14-16 year old children in 1974 and 1992. *British Dent J* 1988; 164: 209-211.
 159. Schneiderman A, Elbaum M, Shultz T, Keem S, Greenebaum M, Driller J. Assessment of dental caries with digital imaging fiber-optic transillumination (DIFOTI): in vitro study. *Caries Res.* 1997; 31: 103-110.
 160. Sheehy EC, Brailsford SR, Kidd EAM, Beighton D, Zoitopoulos L. Comparison between visual examination and a laser fluorescence system for in vivo diagnosis of occlusal caries. *Caries Res* 2001; 35: 421-426.
 161. Shiny ST, Rupananda JM, Mini J, Subhash N. Investigation of in vitro dental erosion by optical techniques. *Lasers Med Sci.* 2008; 23: 319-329.
 162. Shi XQ, Welander U, Angmar-Mansson B. Occlusal caries detection with KaVo DIAGNOdent and radiography: an in vitro comparison. *Caries Res.* 2000; 34: 151-158.

163. Shi XQ, Tranaeus S, Angmar-Mansson B. Comparison of QLF and DIAGNOdent for quantification of smooth surface caries. *Caries Res.* 2001a; 35: 21-26.
164. Stokes GG, *Über die andung der brechbarkeit des lichtes.* *Philos Trans R Soc,* 1852; 107: 11.
165. Stubel H, *Die fluorezone tierische gewebe in ultravioletten licht.* *Pflingers Arch Ges Physiol* 1911; 142: 1.
166. Stookey GK. The evolution of caries detection. *Dimensions of Dental Hygiene* 2003; 12: 5.
167. Subhash N, Mazzinghi P, Agati G, Fusi F, Lercari B. Analysis of laser induced fluorescence line shape of intact leaves: Application to UV stress detection. *Photochem Photobiol* 1995; 62: 711-718.
168. Subhash N, Mohanan CN. Curve fit analysis of chlorophyll fluorescence spectra: Application to nutrient stress detection in sunflower. *Remote Sens Environ* 1997; 60: 347-356.
169. Subhash N, Shiny ST, Rupananda JM, Mini J. Tooth caries detection by curve fitting of laser-induced fluorescence emission: A comparative evaluation with reflectance spectroscopy. *Lasers Surg Med* 2005; 37: 320-328.
170. Sundstrom F, Fredriksson K, Montan S, Hafstrom -Bjorkman U, Strom J: Laser-induced fluorescence from sound and carious tooth substance: Spectroscopic studies. *Swed Dent J* 1985; 9: 71–80.
171. Summit, James B, William J, Robbins, Richard S, Schwartz. *Fundamentals of operative dentistry: A contemporary approach*, 2nd edition, Quintessence Publishing Co, Inc. 2001.
172. Takamori K., Hokari N, Okumura Y, Watanabe S. Detection of occlusal caries under sealants by use of laser fluorescence system. *J Clin Laser Med Surg* 2001; 19: 267-271.
173. Ten Bosch J. Light scattering and related methods in caries diagnosis. In: *Early detection of dental caries.* Ed. Stookey GK, Indianapolis: Indiana University School of Dentistry, 1996; 81-90.
174. Ten Cate JM. In vitro studies on the effects of fluoride on de- and remineralization. *J Dent Res.* 1990; 69: Spec No. 614-619.

175. Ten Cate AR. Oral Histology: Development, Structure, and Function, 5th edn., St Louis, Mosby, 1998.
176. The World Oral Health report, 2003.
177. Thylstrup A and Fejerskov O. Text book of clinical cariology (2nd edition), Munksgaard, Copenhagen, 1994.
178. Tuchin VV, Altshuler GB. In Fundamentals and Applications of Biophotonics in Dentistry, Eds. Kishen A and Asundi A, Imperial College Press, London, 2007; 256.
179. Utzinger U, Brewer M, Silva E, Gershenson D, Bast RC Jr, Follen, Richards-Kortum R. Reflectance spectroscopy for in vivo characterization of ovarian tissue. *Lasers Surg Med* 2001; 28(1): 56–66.
180. Uzunov TT, Borisova EG, Kamburova KP, Avramov LA. Reflectance spectroscopy of human teeth in vitro. BPU-5: Fifth General conference of the Balkan Physical Union SP16-003 1775-1778, 2003.
181. Valera FB, Pessan JP, Valera RC, Mondelli J, Percinoto C. Comparison of visual inspection, radiographic examination, laser fluorescence and their combinations on treatment decisions for occlusal surfaces. *American J Dent* 2008; 21: 25–29.
182. Van der Veen MH and ten Bosch JJ. Autofluorescence of bulk sound and in vitro demineralised human root dentin. *Eur J Oral Sci* 1995; 103: 375-381.
183. Verdonschot EH, Bronkhorst EM, Burgersdijk RCW, Konig KG, Schacken MJM, Truin GJ. Performance of some diagnostic systems in examinations for small occlusal carious lesions. *Caries Res* 1992; 26: 59-64.
184. Verdonschot EH, Bronkhorst EM, Burgersdijk RCW, Konig KG, Schaeken MJM, Truin GJ. Performance of some diagnostic systems in examinations for small occlusal carious lesions. *Caries Res* 1992a; 26: 59-64.
185. Verdonschot EH, Wenzel A, Truin GJ, Konig KG. Performance of electrical resistance measurements adjunct to visual inspection in the early diagnosis of occlusal caries. *J Dent* 1993; 21: 332-337.
186. Verdonschot EH, Angmar-Mansoon B, ten Bosch JJ, Deery CH, Huysmans MCDNJM, Pitts NB, Waller E. Developments in caries diagnosis and their relationship to treatment decisions and quality of care. *Caries Res.* 1999; 33: 32-40.

187. Virajsilp V, Thearmontree A, Aryatawong S, Paiboonwarachat D. Comparison of proximal caries detection in primary teeth between laser fluorescence and bitewing radiography. *Pediatr Dent* 2005; 27:493–499.
188. Von Fraunhofer J. Dissolution of dental enamel in soft drinks. *General Dentistry* 2004; 52(4): 308-312.
189. Wagnieres G, Star W, Wilson B. In vivo fluorescence spectroscopy and imaging for oncological applications. *Photochemistry and Photobiology* 1998; 68(5): 603-632.
190. Walsh LJ, Shakibaie F. Ultraviolet-induced fluorescence: shedding new light on dental biofilms and dental caries. *Australasian dental practice*, 2007; 56-60.
191. Walters C, Eyre DR. Collagen cross links in human dentin: increasing content of hydroxypyridinum residues with age. *Calcif Tissue Int.* 1983; 35: 401-405.
192. Weerheijm KL, van Amerongen WE, Eggink CO. The clinical diagnosis of occlusal caries: A problem. *J Dent Child* 1989; 56: 196-200.
193. Weerheijm KL, Groen HJ, Bast AJJ, Kieft JA, Eijkman MAJ, van Amerongen WE. Clinically undetected occlusal dentine caries: A radiographic comparison. *Caries Res* 1992a; 26: 305-309.
194. Weerheijm KL, Grujthuysen RJM, van Amerongen WE. Prevalence of hidden caries. *J dent Child* 1992b; 59: 408-412.
195. Weersink RA, Hayward JE, Diamond KR, Patterson MS: Accuracy of non-invasive in vivo measurements of photosensitizer uptake based on a diffusion model of reflectance spectroscopy. *Photochem Photobiol* 1997; 66: 326-335.
196. Wendlandt WW, Hecht HG. *Spectroscopie de reflectance*. Interscience (J. Wiley) New York, 1966; 21.
197. Wenzel A, Fejerskov O. Validity of diagnosis of questionable caries lesions in occlusal surfaces of extracted third molars. *Caries Res* 1992; 26: 188-194.
198. Whaites E, In *Minimally Invasive Dentistry: The management of caries*, Eds. Wilson NHF, Quintessence Publ. Co, Ltd, London, et al., 2007; 38.
199. White DJ, Featherstone JDB. A longitudinal microhardness analysis of fluoride dentifrice effects on lesion progression in vitro. *Caries Res.* 1987; 21: 502-512.
200. White SC and Pharoah MJ. *Oral radiology principles and interpretation*. 5th edition. St Louis, Mosby, 2004.

201. Wigdor H, RizoIU IM, Levy G. Light interaction with dental hard tissues spectrophotometry. Presented at the American Society for Laser Medicine and Surgery, New Orleans, April 1994; 18-20.
202. World Health Organisation, Dental Health published in World Health, 1981. In Chakraborty M, Saha JB, Bhattacharya RN, Roy A, Ram R. Epidemiological correlates of dental caries in an urban shun of West Bengal. Indian J of Pub Hlth 1997; 41(2): 56.
203. Yanagisawa T, Miake Y. High-resolution electron microscopy of enamel-crystal demineralization and remineralization in carious lesions. J. Electron Microsc. 2003; 52, 605–613.
204. Yassin OM. In vitro studies of the effect of a dental explorer on the formation of an artificial carious lesion. J Dent Children 1995; 62: 111-117.
205. Young DA. New caries detection technologies and modern caries management: merging the strategies. Gen Dent. 2002; 50(4): 320-331.
206. Zero D T. Dental caries process. Dent Clin North Am. 1999; 43: 635-664.
207. Zezell DM, Ribeiro AC, Bachmann L, Gomes ASL, Rousseau C, Girkin J. Characterization of natural carious lesions by fluorescence spectroscopy at 405-nm excitation wavelength. J Biomed Opt 2007; 12(6): 064013 (1-6).
208. Zijp JR, ten Bosch JJ. Angular dependence of He–Ne laser light scattering by bovine and human dentine. Arch Oral Biol 1991; 36: 283-289.
209. Zijp JR and ten Bosch JJ. Theoretical model for the scattering of light by dentin and comparison with measurements. Appl Opt 1993; 32: 411-415.
210. Zijp JR and ten Bosch JJ. Anisotropy of volume-backscattered light. Appl Opt 1997; 36: 1671-1680.
211. Zonios G, Perelman L, Backman V, Manoharan R, Fitzmaurice M, Van Dam J, Feld MS: Diffuse reflectance spectroscopy of human adenomatous colon polyps in vivo. Appl Opt 1999; 38: 6628-6637.